

**APPLICATION OF CHITOSAN COMPOSITES FOR THE REMOVAL
OF ORGANIC DYES**

TAN JIA HUI


**A project report submitted in partial fulfilment of the
requirements for the award of Bachelor of Engineering
(Honours) Chemical Engineering**

**Lee Kong Chian Faculty of Engineering and Science
Universiti Tunku Abdul Rahman**

May 2021

DECLARATION

I hereby declare that this project report is based on my original work except for citations and quotations which have been duly acknowledged. I also declare that it has not been previously and concurrently submitted for any other degree or award at UTAR or other institutions.

Signature : 

Name : Tan Jia Hui

ID No. : 1604779

Date : 12 April 2021

APPROVAL FOR SUBMISSION

I certify that this project report entitled "**APPLICATION OF CHITOSAN COMPOSITES FOR THE REMOVAL OF ORGANIC DYES**" was prepared by **TAN JIA HUI** has met the required standard for submission in partial fulfilment of the requirements for the award of Bachelor of Engineering (Honours) Chemical Engineering at Universiti Tunku Abdul Rahman.

Approved by,

Signature

:



Supervisor

:

Dr Pang Yean Ling

Date

:

15 April 2021

Signature

:



Co-Supervisor

:

Ir Dr Chong Woon Chan

Date

:

15 April 2021

The copyright of this report belongs to the author under the terms of the copyright Act 1987 as qualified by Intellectual Property Policy of Universiti Tunku Abdul Rahman. Due acknowledgement shall always be made of the use of any material contained in, or derived from, this report.

© 2021, Tan Jia Hui. All right reserved.

ACKNOWLEDGEMENTS

I would like to thank all those who had provided assistance and support to me throughout my final year project. I would like to express my sincere gratitude to my research supervisor, Dr Pang Yean Ling for her guidance, motivation, valuable advice and tremendous patience who had led me to the successful completion of this project.

Next, I would also like to express my gratitude to my beloved family and friends who had helped me and given me encouragement throughout the period in completing the project. Lastly, I would also like to give special thanks to my fellow friends for the useful advice and information to complete my project.

ABSTRACT

Recently, chitosan has received particular attention from researchers to be used as a potential biosorbent for the removal of organic dyes. It is a biodegradable, inexpensive and renewable biopolymer derived from food waste. It consists of carboxyl ($-\text{COOH}$), hydroxyl ($-\text{OH}$), amine ($-\text{NH}_2$) and amide ($-\text{NHCOCH}_3$) functional groups on its surface that are responsible to remove organic dyes. However, pure chitosan has some limitations that exhibit lower biosorption capacity, surface area and thermal stability than chitosan composites. Many research studies have been carried out to improve the physicochemical properties of pure chitosan by modifying it with the addition of reinforcement materials to synthesise chitosan composites. Therefore, this study incorporates multiple journals to reveal the performance of various chitosan composites synthesised by other researchers to remove organic dyes. The reinforcement materials used for the synthesis of chitosan composites were classified as carbon-based materials, metal oxide and other biopolymer. Tripolyphosphate and epichlorohydrin were the two commonly used crosslinking agents to combine pure chitosan with the reinforcement materials. This study was conducted in five steps: i) review planning; ii) the searching process of basic literature; iii) publication screening and selection; iv) data extraction; v) data analysis and report writing. The physicochemical properties of chitosan composites were studied through scanning electron microscopy (SEM), energy dispersive X-ray (EDX), surface area analysis, Fourier transform infrared (FTIR) spectroscopy, X-ray diffraction (XRD) and thermogravimetric (TGA). The characterisation results revealed that the chitosan composites possessed a heterogeneous surface with a larger surface area ($> 1.81 \text{ m}^2/\text{g}$) and became more amorphous than pure chitosan ($> 0.141 \text{ m}^2/\text{g}$). The chitosan composites also had a higher thermal stability with less than 40 % weight loss at each stage of the thermal degradation process. Besides, the FTIR results showed that the presence of additional functional groups on the chitosan surface could facilitate the interaction with dye molecules and improve the biosorption capacity. Therefore, chitosan composites exhibited better physicochemical properties than pure chitosan. Lastly, the behaviour of the biosorption process for various chitosan composites was compared and analysed through the kinetic models, isotherm

models and thermodynamic parameters. The findings with a high coefficient of determination (R^2) value suggested that most of the biosorption processes were better defined by the pseudo-second-order (PSO) kinetic model and Langmuir isotherm model. This indicated that monolayer chemisorption of organic dyes occurred on the homogenous surface of chitosan composites. Based on the biosorption thermodynamic results, most of the biosorption processes were endothermic, feasible, spontaneous at the low temperature range between 288 K and 320 K. Therefore, chitosan composites have been proved as a promising biosorbent for the removal of organic dyes.

TABLE OF CONTENTS

| | | |
|--|------------------------------------|------------|
| DECLARATION | | i |
| APPROVAL FOR SUBMISSION | | ii |
| ACKNOWLEDGEMENTS | | iv |
| ABSTRACT | | v |
| TABLE OF CONTENTS | | vii |
| LIST OF TABLES | | ix |
| LIST OF FIGURES | | x |
| LIST OF SYMBOLS / ABBREVIATIONS | | xii |
| | | |
| CHAPTER | | |
| 1 | INTRODUCTION | 15 |
| 1.1 | Water Pollution in Malaysia | 15 |
| 1.2 | Textile Industry | 16 |
| 1.3 | Problem Statement | 19 |
| 1.4 | Research Objectives | 20 |
| 1.5 | Scope and Limitation of the Study | 20 |
| 1.6 | Outline of the Report | 21 |
| 2 | LITERATURE REVIEW | 23 |
| 2.1 | Biopolymers | 23 |
| 2.1.1 | Classification of Biopolymers | 25 |
| 2.1.2 | Types of Biopolymers | 26 |
| 2.1.3 | Modification of Chitosan | 28 |
| 2.2 | Chitosan Composites | 31 |
| 2.2.1 | Chitosan/Zeolite | 32 |
| 2.2.2 | Chitosan/Carbon-based Materials | 32 |
| 2.2.3 | Chitosan/Zinc Oxide (Chitosan/ZnO) | 33 |
| 2.2.4 | Chitosan/Other Biopolymers | 34 |
| 2.3 | Removal Methods of Organic Dyes | 35 |
| 2.3.1 | Biological Treatment | 35 |

| | | | |
|----------|-------|--|------------|
| | 2.3.2 | Chemical Treatment | 37 |
| | 2.3.3 | Physical Treatment | 38 |
| 2.4 | | Biosorption in Water Remediation | 40 |
| 2.5 | | Parameter Studies | 42 |
| | 2.5.1 | Effect of Solution pH | 42 |
| | 2.5.2 | Effect of Biosorbent Dosage | 44 |
| | 2.5.3 | Effect of Initial Dye Concentration | 45 |
| | 2.5.4 | Effect of Contact Time | 47 |
| | 2.5.5 | Effect of Temperature | 48 |
| | 2.5.6 | Comparison Performance for Various Types of Chitosan Composites | 49 |
| 3 | | METHODOLOGY AND WORK PLAN | 53 |
| | 3.1 | Literature Review Methodology | 53 |
| | 3.2 | Review Planning | 53 |
| | 3.3 | Overall Research Flow | 54 |
| | 3.4 | Screening and Selection of Literatures | 55 |
| | 3.5 | Data Extraction | 55 |
| | 3.6 | Data Analysis and Report Writing | 56 |
| 4 | | RESULTS AND DISCUSSION | 57 |
| | 4.1 | Characterisation Studies of Chitosan Composites | 57 |
| | 4.1.1 | Scanning Electron Microscopy (SEM) | 57 |
| | 4.1.2 | Energy Dispersive X-ray (EDX) | 59 |
| | 4.1.3 | Surface Area Analysis | 62 |
| | 4.1.4 | Fourier Transform Infrared (FTIR) | 65 |
| | 4.1.5 | X-ray Diffraction (XRD) | 75 |
| | 4.1.6 | Thermogravimetric (TGA) | 79 |
| | 4.2 | Biosorption Kinetics | 82 |
| | 4.3 | Biosorption Isotherms | 89 |
| | 4.4 | Biosorption Thermodynamics | 95 |
| 5 | | CONCLUSIONS AND RECOMMENDATIONS | 100 |
| | 5.1 | Conclusions | 100 |
| | 5.2 | Recommendations for Future Work | 101 |
| | | REFERENCES | 102 |

LIST OF TABLES

| | | |
|------------|---|----|
| Table 1.1: | Degree of Fixation and Percentage Loss in Effluent for Various Types of Dyes (Choudhury, 2016). | 18 |
| Table 2.1: | Advantage and Limitations of Different Wastewater Treatment Methods (Crini and Lichtfouse, 2019). | 36 |
| Table 2.2: | Filtration Scope of Different Membrane Filtration Processes (Upadhye and Joshi, 2012). | 39 |
| Table 2.3: | Removal Efficiency of Cationic Dyes Using Various Types of Chitosan Composites under Different Operating Conditions. | 50 |
| Table 2.4: | Removal Efficiency of Anionic Dyes Using Various Types of Chitosan Composites under Different Operating Conditions. | 51 |
| Table 4.1: | Elemental Composition of Chitosan Composites Before and After Biosorption of Dyes. | 60 |
| Table 4.2: | Surface Properties of Various Chitosan Composites. | 63 |
| Table 4.3: | Functional Groups of Chitosan with The Respective Wavelength (Kumari, et al., 2015; Li, et al., 2016; Quesada, et al., 2020). | 67 |
| Table 4.4: | Summarisation of FTIR Spectra of Various Types of Chitosan Composites. | 68 |
| Table 4.5: | TGA Data for Chitosan Composite at Different Thermal Degradation Stages. | 80 |
| Table 4.6: | Kinetic Constants of PFO and PSO Kinetic Models for Biosorption of Various Dyes onto Chitosan Composites. | 85 |
| Table 4.7: | Intraparticle Diffusion Model Parameters for Biosorption of Dyes by Chitosan Composites. | 89 |
| Table 4.8: | Adsorption Isotherm Parameters of Langmuir and Freundlich Isotherm Model for Biosorption of Various Dyes by Different Types of Chitosan Composites. | 93 |
| Table 4.9: | Thermodynamic Parameters for Biosorption of Dyes Using Various Type of Chitosan Composites. | 97 |

LIST OF FIGURES

| | | |
|-------------|--|----|
| Figure 1.1: | River Water Pollution Trend in Malaysia between 2012 and 2017 (Department of Environment, 2017). | 16 |
| Figure 2.1: | Classification of Biopolymers Based on the Type of Monomers, Biodegradability, Raw Materials, and Backbones (Younes, 2017). | 25 |
| Figure 2.2: | Cellulose Chemical Structure (Shukla, et al., 2013). | 26 |
| Figure 2.3: | Chitin Chemical Structure (Shukla, et al., 2013). | 28 |
| Figure 2.4: | Chitosan Chemical Structure (Shukla, et al., 2013). | 28 |
| Figure 2.5: | Polymer Grafting Methods (Banerjee, Paira and Mandal, 2014). | 29 |
| Figure 2.6: | Types of Mechanisms in Biosorption (Abdel Maksoud, et al., 2020). | 41 |
| Figure 2.7: | Effect of Initial Dye Concentration on Biosorption Capacity of Chitosan/Kaolin-clay Composite at Constant Time (Jawad, et al., 2020). | 46 |
| Figure 2.8: | Effect of Contact Time on Biosorption Efficiency of Cationic Dyes at Constant Initial Dye Concentration of 2.3 mg/L (Muinde, et al., 2020). | 47 |
| Figure 3.1: | Overall Literature Review Methodology Flow Chart. | 54 |
| Figure 4.1: | SEM Micrographs of (a) Pure Chitosan (Jawad and Abdulhameed, 2020a), (b) ACCHPS Composite with Unloaded Dyes and (c) ACCHPS Composite with Loaded Dyes (Idohou, et al., 2020). | 58 |
| Figure 4.2: | SEM Micrographs of (a) Chitosan/Cellulose (Wang, et al., 2018), (b) Chitosan/PVA (Anitha, Kumar and Kumar, 2016) and (c) Chitosan/MWCNTs Composites (Salam, Makki and Abdelaal, 2011). | 59 |
| Figure 4.3: | FTIR Spectra of (a) Silica, (b) Chitosan and (c) Chitosan/Silica Composite (Bahalkeh, et al., 2020). | 66 |
| Figure 4.4: | TGA Graph of Chitosan, ZnO Nanoparticle and Chitosan/ZnO Composite (Nguyen, Nguyen and Nguyen, 2020). | 81 |

Figure 4.5: Linear Graph of Intraparticle Diffusion Model for Biosorption of Reactive Blue 5 by Chitosan/Quartzite Composite (Wang, et al., 2018).

LIST OF SYMBOLS / ABBREVIATIONS

| | |
|------------------|--|
| ΔS° | entropy change, J/(mol·K) |
| ΔH° | enthalpy change, kJ/mol |
| ΔG° | Gibb's free energy change, kJ/mol |
| C | y-intercept of the graph that related to the boundary layer thickness, mg/g |
| C_e | equilibrium concentration of dyes, mg/L |
| $C_{e,m}$ | mass of dyes molecules adsorbed per unit mass of chitosan composite at equilibrium, mg/g |
| C_o | concentration of dyes at initial process, mg/L |
| C_s | equilibrium concentration of dyes remaining in aqueous solution, mg/L |
| D | average crystallite size, nm |
| d_p | average pore diameter |
| K | Scherrer's constant |
| k_1 | rate constant of PFO model, min ⁻¹ |
| k_2 | rate constant of PSO model, g/(mg·min) |
| K_c | equilibrium constant |
| K_F | Freundlich constant related to the adsorption capacity, (mg/g)(L/g) ^{1/n} |
| K_L | Langmuir constant, L/mg |
| k_p | rate constant of intraparticle diffusion, mg/(g·min ^{0.5}) |
| n | heterogeneity factor |
| q_e | mass of dyes adsorbed per unit mass of chitosan composite at equilibrium condition, mg/g |
| q_{max} | maximum biosorption capacity, mg/g |
| q_t | mass of dyes adsorbed per unit mass of chitosan composite at any time t , mg/g |
| R_L | separation factor |
| S_{BET} | Brunauer–Emmett–Teller (BET) specific surface area |
| t | contact time, min |
| T | absolute temperature, K |
| V_p | total pore volume |

| | |
|--------------------------------|--|
| R | gas constant (8.314 J/(mol·K)) |
| θ | Bragg's angle, rad |
| 2θ | 2 teta |
| ACCHPS | activated carbon/chitosan/papaya seed |
| Al | alumina |
| Au | aura |
| BET | Brunauer–Emmett–Teller |
| C | carbon |
| Ca | calcium |
| CH ₃ COOH | acetic acid |
| chitosan/ZnO | chitosan/zinc oxide |
| –COO [–] | carboxylate ion |
| –COOH | carboxyl group |
| EDX | energy dispersive X-ray |
| Fe ₃ O ₄ | magnetite |
| FTIR | Fourier transform infrared |
| H ⁺ | hydrogen ion |
| H ₂ O | water |
| JCPDS | Joint Committee on Powder Diffraction Specifications |
| Mg | magnesium |
| MgO | magnesium oxide |
| MWCNTs | multiwalled carbon nanotubes |
| N | nitrate |
| Na | sodium |
| –NH ₂ | amine group |
| –NH ₃ ⁺ | positively charged amine group |
| –NHCOCH ₃ | amide group |
| O | oxygen |
| OH [–] | hydroxide ion |
| –OH | hydroxyl group |
| P | phosphate |
| PFO | pseudo-first-order |
| pH _{pzc} | point zero charge |

| | |
|--------------------------------|------------------------------|
| PSO | pseudo-second-order |
| PVA | polyvinyl alcohol |
| R^2 | coefficient of determination |
| S | sulphur |
| SEM | scanning electron microscopy |
| Si | silicon |
| $-\text{SO}_3^-$ | sulphonate group |
| TGA | thermogravimetric |
| Ti | titanium |
| XRD | X-ray diffraction |
| ZnO | zinc oxide |
| $\gamma\text{-Fe}_2\text{O}_3$ | maghemite |

CHAPTER 1

INTRODUCTION

1.1 Water Pollution in Malaysia

Water is an essential and valuable component for sustaining the life of all living organisms and developing a sustainable ecosystem. In Malaysia, approximately 97 % of the raw water supply for domestic, agricultural and industrial activities comes from rivers (Bidaisee, 2018). However, water pollution has now become one of the most critical challenges facing many countries in accordance with the growth of urbanisation and socio-economic development. The water quality is deteriorating due to the uncontrolled usage of various chemicals and improper discharge of effluents from the household and industrial sector into the river without adequate treatment.

As the population keeps growing, people are increasing the pressure on water resources as well as the demand for safe and clean water supply. The world's population is currently over 7.6 billion and expected to exceed 9.7 billion in 30 years. Meanwhile, water consumption will double every 20 years (Kaneda, Greenbaum and Kline, 2020). Approximately 2.6 billion people cannot obtain basic sanitation and over 2 billion people are short of clean water (Bidaisee, 2018).

Figure 1.1 illustrates the trend of river water quality in Malaysia throughout 2012 and 2017. A total of 477 rivers has been monitored annually over these six years. The number of clean rivers was decreased from 277 to 219 while the numbers of slightly polluted and polluted rivers were increased from 162 to 205 and 38 to 52, respectively. The increased number of slightly polluted and polluted rivers was mainly due to insufficient sewage treatment or effluent from agro-based and manufacturing industries (Department of Environment, 2017). Several studies have reported that the most common pollutants present in industrial wastewater are heavy metals, organic compounds and inorganic compounds. Textile dyes are among the major contributor to water pollution (Rasheed, et al., 2019).

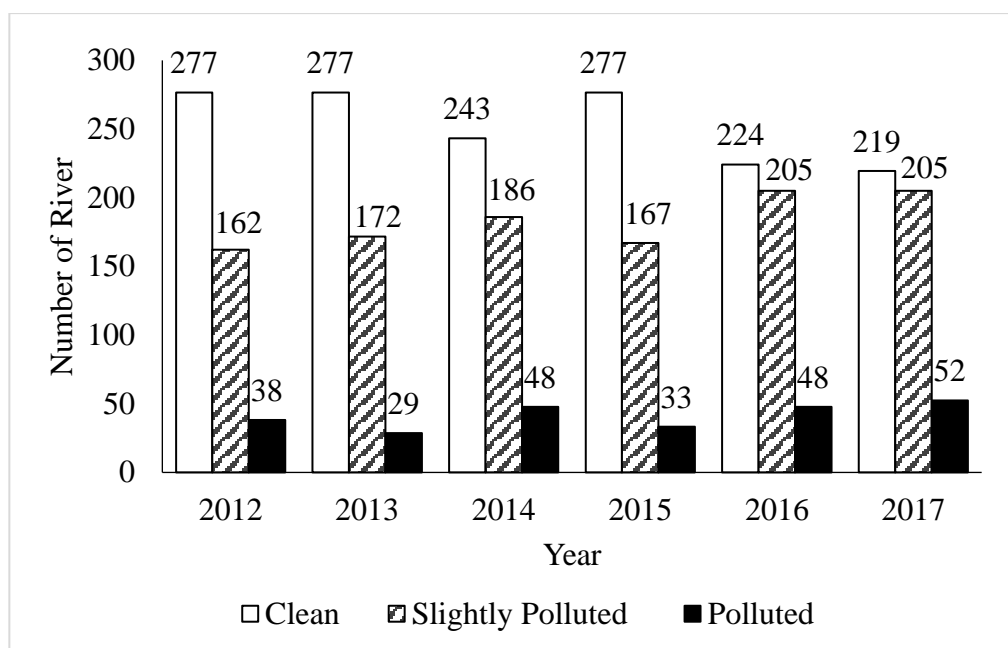


Figure 1.1: River Water Pollution Trend in Malaysia between 2012 and 2017 (Department of Environment, 2017).

1.2 Textile Industry

The textile industry is one of the fastest-growing sectors that has played an important role in Malaysia's economic development. Textiles and textile products were the nation's 13th largest export industries in 2018, accounting for about RM12 billion of Malaysia's total manufactured goods exports (Malaysian Investment Development Authority, 2018). However, the washing, dyeing, and finishing of textiles require high water consumption, which eventually generates a high discharge rate of wastewater containing a high amount of organic dyes. Approximate 100-300 m³ of water are utilised to generate one tonne of textile (The World Bank, 2014).

More than 10 000 types of dyes and pigments are employed in industry, and over 700 000 tonnes of synthetic dyes are generated every year (Berradi, et al., 2019). It is estimated that the textile industry consumes 90 % of the total production of dyes, while the remaining 10 % will be utilised in the leather, paper, plastic and chemical industry. During the dyeing and finishing operations, over 280 000 tonnes of dyes are lost to effluents every year (Yaseen and Scholz, 2019).

Dyes are organic compounds mainly used to provide colour and alter the crystal structure of the coloured substance. Dyes can be categorised into natural dyes or synthetic dyes. However, synthetic dyes are widely used in the textile industry due to their cost-effectiveness in synthesis and high retaining properties (Yaseen and Scholz, 2019). Dyes consist of two functional groups that mainly contribute to the colouring effect of dyes, namely chromophore and auxochrome. Chromophore is an electron-withdrawing group that controls the colour of dyes. The common chromophores are azo, nitroso, nitro, ethylene, carbon-nitrogen and carbonyl groups. In addition, auxochrome is an electron-donating substituent that can enhance the colour of the chromophore by making the system more soluble and improving the dye adherence to the fibre. The most significant auxochromes are amine ($-\text{NH}_2$), amide ($-\text{NHCOCH}_3$), carboxyl ($-\text{COOH}$), sulphonate ($-\text{SO}_3^-$), and hydroxyl ($-\text{OH}$) groups (Rangabhashiyam, Anu and Selvaraju, 2013).

Specifically, dyes can be classified into several types based on their applications characteristics and chemical structure such as acid, disperse, basic, metal-complex, direct, sulphur, reactive and vat dyes (Truskewycz, Shukla and Ball, 2016). During the dyeing and finishing processes, no single dye has a 100 % degree of fibre fixation. The amount of dye in the effluent is closely linked to the fixation rates of the various dyes and fibres. Table 1.1 shows the degree of fixation and the percentage of loss in the effluent for various types of dyes. It indicates that reactive dyes have the lowest degree of fixation on fibre which accounts for approximately 50-90 % of the dyes. During the dyeing and finishing processes, more than 50 % of the reactive dyes used may end up in the water bodies, resulting in highly coloured effluent due to their incomplete degree of fixation and exhaustion. Therefore, the problem of coloured industrial effluent primarily comes from the application of reactive dyes (Choudhury, 2016).

Among these dyes, azo dyes account for approximately 65-70 % of the total dye production (Pang and Abdullah, 2013). Azo dyes are the most common dyes utilised in the industrial process because they are easy to use, relatively cost-effective to produce and provide high colour intensity. The most common dyes are methyl orange, methylene blue and Rhodamine B.

Table 1.1: Degree of Fixation and Percentage Loss in Effluent for Various Types of Dyes (Choudhury, 2016).

| Dyes | Fibre Type | Loss in Effluent (%) | Degree of Fixation (%) |
|----------------------|-------------------|-----------------------------|-------------------------------|
| Acid | Polyamide | 5-20 | 80-95 |
| Disperse | Polyester | 0-10 | 90-100 |
| Basic | Acrylic | 0-5 | 95-100 |
| Metal-complex | Wool | 2-10 | 90-98 |
| Direct | Cellulose | 5-30 | 70-95 |
| Sulphur | Cellulose | 10-40 | 60-90 |
| Reactive | Cellulose | 10-50 | 50-90 |
| Vat | Cellulose | 5-20 | 80-95 |

Discharging of dye-containing effluents into water has drawn public attention due to its adverse effects on humans and the environment. Some of the dyes may cause skin, eyes, allergic dermatitis, and respiratory tract irritations if swallowed (Lellis, et al., 2019). Generally, the textile wastewater is characterised by a high value of colour intensity, biochemical oxygen demand, chemical oxygen demand, pH and suspended solids. The high colour intensity of dyes can block the light penetration through water bodies, reducing the photosynthetic activities of aquatic flora. As a result, the concentration of dissolved oxygen will be reduced and create an anaerobic condition in the river, thereby severely affecting the aquatic diversity.

Furthermore, organic dyes may undergo anaerobic reduction and generate aromatic amines due to the existence of azo- and nitro-compounds in their chemical structure. These aromatic amines are highly toxic and hazardous, which may induce cancer and tumours in humans and animals (Lellis, et al., 2019). Besides, dyes have high stability and low biodegradability owing to the complex aromatic ring structure. They can stay for a long time in the environment. Thus, the methods for their degradation have been gradually studied and developed.

1.3 Problem Statement

Recently, a vast amount of textile dyes has been detected in the surface water. The textile industry is found to be the major contributors to water pollution. These organic dyes have high toxicity and carcinogenicity, which can cause adverse effects on humans and the environment. Therefore, the adsorption process is widely employed to remove non-biodegradable organic dyes (Zhang, Zhou and Ou, 2012). Activated carbon is one of the most commonly used adsorbent material to adsorb these organic dyes from wastewater. However, it has some disadvantages, which create a need to search for an alternative adsorbent material.

In general, activated carbon is restricted by its costly supply chain. It is also non-biodegradable which might lead to environmental problems related to its waste disposal (Gautam, et al., 2014). As a result, the operating cost of the wastewater treatment will be increased due to the high cost of the adsorbent material. Besides, most of the existing adsorbents, including activated carbon will reach a saturation state and deactivate when the active sites of the adsorbents are fully occupied by pollutants. Therefore, regeneration is required before activated carbon can be reused. However, the regeneration process can lead to a reduction in the adsorption capacity of activated carbon (Raval, Shah and Shah, 2016). Hence, activated carbon is a not cost-effective adsorbent when treating a large volume of wastewater effluent.

In light of that, many researchers have focused on the evaluation of inexpensive and environmentally friendly alternative sorbents. Food wastes are renewable and inexpensive biopolymer that can be used for the production of biosorbents. According to the Food and Agriculture Organization of the United Nations, about 1.3 billion tonnes of food is lost or wasted annually (Tsang, et al., 2019). Inefficient food waste management may contribute to some negative environmental issues such as infectious diseases, land and water pollution. Hence, in order to handle such a large amount of food waste, the environmentally friendly approach is to recycle these wastes as secondary useful materials.

Several studies have found that food wastes appeared to be effective in removing organic dyes from wastewater (Ahmad and Danish, 2018; Massimi, et al., 2018). Food wastes are considered biopolymers that are rich in

carbohydrates, lipids and proteins. They consist of various functional groups such as -NH_2 , -OH and -COOH groups that make them emerge as efficient biosorbents. These functional groups could immensely contribute to the uptake of organic dyes through intermolecular interaction, hydrogen bonding and electrostatic attraction. Meanwhile, biosorption using food waste also can minimise solid waste management and landfill issues.

Among the biopolymers, chitosan has been reported in the literature as a promising biosorbent for the removal of dyes (Liu, et al., 2013; Zheng, et al., 2019). However, pure chitosan has some limitations such as low adsorption capacity, low regenerative and poor mechanical strength, thereby limiting its applications. Hence, a chemical or physical modification of chitosan can be carried out by introducing the reinforcement material in the chitosan matrix to synthesise chitosan composite. In this study, various chitosan composites were studied to analyse their physicochemical properties and biosorption behaviour to remove organic dyes.

1.4 Research Objectives

The purpose of this project is to conduct a review study on the application of chitosan composites as biosorbents for the removal of organic dyes. The objectives of this project are:

- i. To review the physicochemical properties of chitosan composites as biosorbents using various types of characterisation techniques.
- ii. To investigate the biosorption behaviour of various types of chitosan composites through biosorption kinetic, isotherm and thermodynamic studies.

1.5 Scope and Limitation of the Study

The scope of this study mainly involves the identification of biopolymers for the synthesis of chitosan composite as a hybrid biosorbent to remove organic dyes from wastewater. The chitosan derived from food waste as a potential biosorbent and its modification method for the synthesis of chitosan composite were identified through literature review. After that, the mechanism of biosorption process was studied to determine how the chitosan composites could be used to remove the organic dyes from aqueous solution. Meanwhile, the

parameter studies were conducted to determine the effect of solution pH, biosorbent dosage, initial dye concentration, contact time and temperature on the biosorption efficiency of organic dyes using chitosan composites as the biosorbents.

Next, the characterisation studies of chitosan composites were conducted through scanning electron microscopy (SEM), energy dispersive X-ray (EDX), surface area analysis, Fourier transform infrared (FTIR) spectroscopy, X-ray diffraction (XRD) and thermogravimetric (TGA). The chitosan composites were characterised to study their physicochemical properties that will affect the biosorption efficiency. Lastly, biosorption process behaviour for various chitosan composites was studied using the kinetic models, isotherm models and thermodynamic parameters.

Nevertheless, there are some limitations that must be taken into consideration during this study. For instance, all the information and experiment studies are retrieved and limited from the literature, so some of the desired information may be unavailable. Hence, this report will provide some own justification and analysis.

1.6 Outline of the Report

This report is divided into five chapters. Firstly, Chapter 1 starts with a general introduction of water pollution in Malaysia and the environmental impact of organic dyes discharged from the textile industry. The problem statement and objectives are also discussed in Chapter 1, with the aim of addressing the issues described in the problem statement. The scope of the study is also described in Chapter 1 to elaborate the objectives in more detail while informing the reader that the scope of the project is limited to certain events.

Secondly, Chapter 2 provides a literature review on the biopolymers derived from food waste and the modification methods to synthesise chitosan composite as the biosorbent. Besides, the removal method of organic dyes, the biosorption mechanism and the parameter effect on the removal efficiency of organic dyes are discussed in Chapter 2.

Next, Chapter 3 demonstrates the methodology to conduct the literature review study. In general, the literature review study is conducted in five significant steps: i) review planning; ii) literature searching process; iii)

publication screening and selection; iv) data extraction; v) data analysis and report writing.

In addition, Chapter 4 analyses and compares the results of the chitosan composites characterisation obtained from the selected literature. Furthermore, the results of biosorption kinetic, biosorption isotherms and biosorption thermodynamics among the chitosan composites are also discussed in Chapter 4. Finally, Chapter 5 concludes the findings obtained from this study and some recommendations are provided for the future research study.

CHAPTER 2

LITERATURE REVIEW

2.1 Biopolymers

Biopolymers can be described as natural polymers synthesised by living organisms through naturally synthesised enzymes and catalysed chain growth polymerisation in their growth cycle of biological cells (Sanchez-Vazquez, Hailes and Evans, 2013). Many materials such as microorganisms, plants, or trees that are commonly derived from biological sources can be described by the term "biopolymers". Materials chemically synthesised from biological raw materials such as starch, sugar, fat, resin, protein, and vegetable oil can also be called biopolymers (Hernández, Williams and Cochran, 2014). Biopolymers are mainly made up of a long chain of repeating monomer units that are covalently bonded to form larger molecules. There are three types of biopolymers: polysaccharides, polypeptides, and polynucleotides. They differ in terms of the monomers they consist of and the structure of the biopolymer formed. The monomer units of biopolymers are sugars, amino acids, and nucleotides.

Food wastes are considered a valuable renewable resource as they contain high-value components such as polysaccharides, proteins, and lipids. They can be converted into a variety of valuable products such as biochemical products and biofuels. Food wastes are also one of the primary sources of biopolymers. Recent studies have explored the application of food waste derived biochemical components extracted from lignocellulosic substrates such as succinic acid and 2, 3-butanediol as precursors for the production of biopolymers (Saratale, Jung and Oh, 2016; Ventrino, et al., 2017). Biopolymers also can be used as natural coagulants and flocculants in the wastewater treatment to remove non-biodegradable and highly stable water pollutants such as dyes, pharmaceutical compounds, and metal ions (Kanmani, et al., 2017).

Nowadays, biopolymers have been widely used in various sectors and have gradually replaced 30-90 % of petro-chemical polymers (Ventrino, et al., 2017). Due to their unique properties of biodegradability, biocompatibility, and renewability, they have been recognised as promising materials to replace petro-

chemical polymers (Tran, et al., 2017). Among these biopolymers, polysaccharides such as chitosan, cellulose, and lignin have received particular attention for the removal of organic dyes (Crini, et al., 2019). Polysaccharides are produced on a renewable basis and represent the largest group of polymers currently produced in the world. In fact, more than 150 million tonnes of polysaccharides are produced annually as compared to about 140 million tonnes of synthetic polymers (Poli, et al., 2011). Polysaccharides are polymers of amino sugars or glucose bonded by acetic bonds.

These biopolymers are widely used as biosorbents in the wastewater treatment plant because of their particular structure and physicochemical characteristics. They do not produce toxic by-products during the chemical process (Niaounakis, 2013). In addition, biopolymers consist of several functional groups in their chemical structure, such as $-OH$, $-NH_2$, and $-COOH$ groups in their polymer chain. Hence, biopolymers have high reactivity and excellent selectivity towards aromatic compounds and metals. They are able to interact with dyes through chemical or physical sorption.

Furthermore, it is well known that polysaccharides are biodegradable, available in abundance and have the ability to associate with various types of molecules through physical and chemical interactions (Crini, et al., 2019). Therefore, adsorption on polysaccharide derivatives can be a cost-effective method to separate and remove contaminants from the water bodies. It is also an environmentally friendly method to preserve the environment. Besides, the increasing number of publications on the adsorption of toxic compounds by these biopolymers indicates a recent concern in the development of new adsorbent polysaccharides-containing materials (Wang, et al., 2013). In this study, the type of biopolymers to be used as biosorbents for the removal of organic dyes is described and classified in the following sections. The selection of biopolymers to be used as biosorbents is considered from their morphology, adsorption capacity and modification methods.

2.1.1 Classification of Biopolymers

The classification of biopolymers can be made based on the type of monomers, biodegradability, raw materials and backbones, as shown in Figure 2.1. Firstly, biopolymers can be categorised into two main groups, which are biodegradable and non-biodegradable biopolymers. They are then alternatively categorised according to their origin, either being bio-based or non-bio-base biopolymers. Next, the biopolymer can also be classified based on their polymer backbone, including polyesters, polysaccharides, polycarbonates, polyamides and vinyl polymers. The three types of biopolymers can be further distinguished into polysaccharides, polypeptides and polynucleotides, depending on the type of monomers.

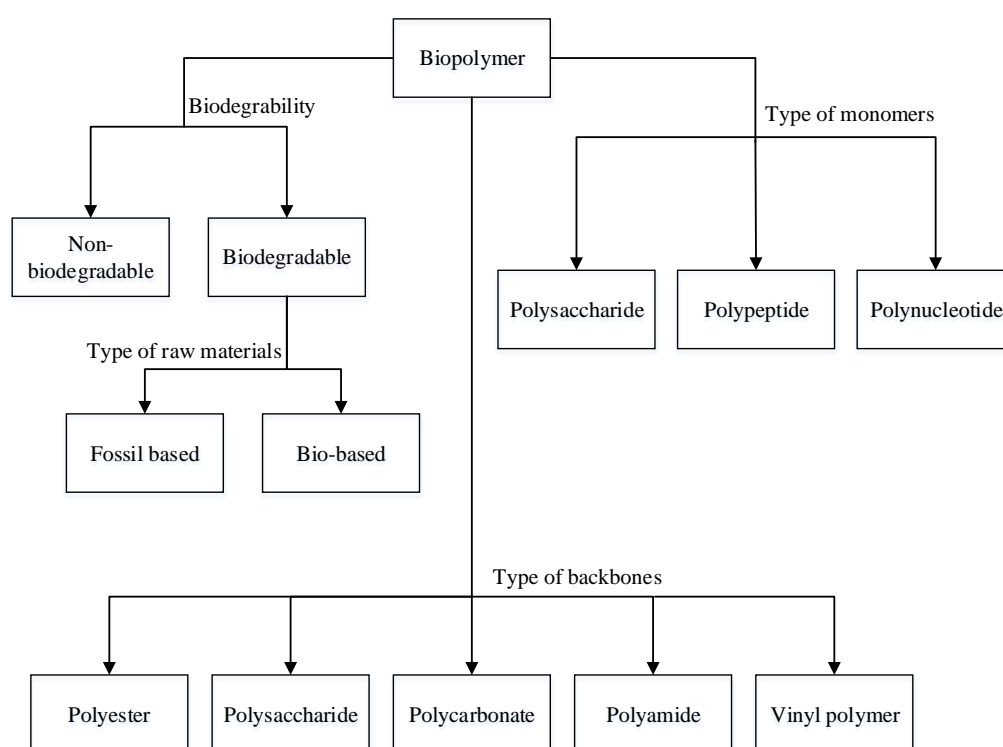


Figure 2.1: Classification of Biopolymers Based on the Type of Monomers, Biodegradability, Raw Materials, and Backbones (Younes, 2017).

Besides, the biopolymers can be further categorised based on the types of raw materials and their biodegradability. There are three categories of biopolymers: biodegradable bio-based biopolymers, non-biodegradable bio-based biopolymers, and biodegradable fossil-based biopolymers (Younes, 2017).

2.1.2 Types of Biopolymers

Among the biopolymers, cellulose and chitosan are the first and second most abundant biopolymers in the world that have been successfully employed for wastewater treatment. Cellulose is a structural polysaccharide made up of repeating β -D-glucose units arranged in a linear chain and linked by $\beta(1\rightarrow4)$ glycosidic bonds through the condensation process. Figure 2.2 illustrates the chemical structure of cellulose (Shukla, et al., 2013). The glycosidic bonds between β -D-glucose units make the structure of cellulose highly crystalline and stronger (Kanmani, et al., 2017).

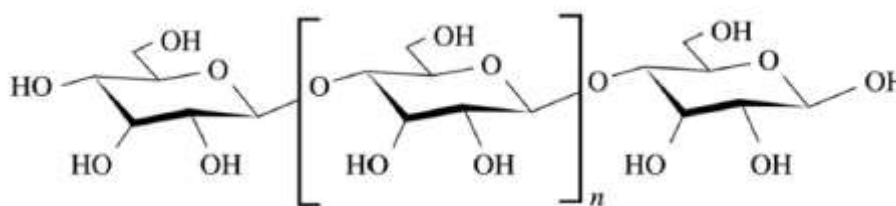


Figure 2.2: Cellulose Chemical Structure (Shukla, et al., 2013).

Approximately 33 % of the plants are made up of cellulose. Citrus peels, wheat straw, rice, and woody parts of vegetables are the richest cellulose source (Perez-Madriral, Edo and Aleman, 2016). An experiment study for the removal of dyes using orange peels as adsorbent has been carried out by Abdurrahman, Akter and Abedin (2013). The removal efficiency of orange peels achieved was 60-70 % at pH 7 with the optimum adsorbent dosage of 1.5 g. The high efficiency of dye removal was attributed to the high amount of surface functional groups such as $-\text{OH}$ and $-\text{COOH}$ groups available on the surface of cellulose. Thus, cellulose and its derivatives are proven can be used as biodegradable and low-cost natural adsorbents to adsorb organic compounds such as textile dyes and pharmaceutical compounds from aqueous solutions.

Chitin and chitosan are two promising biopolymers derived mainly from the exoskeleton of invertebrate animals and the cell walls of fungi. Chitin is a natural polysaccharide consist of a linear chain of 2-acetamido-2-deoxy-D-glucose joined by $\beta(1\rightarrow4)$ glycosidic bonds. Chitin is commonly obtained from commercial and marine sources such as crab shells, lobster shells, shrimp shells, oysters, squids, crawfish, cuttlefish and fungi (Sarode, et al., 2019). Chitin is dumped as a waste product from the seafood industry and approximately 1×10^{13}

kg of chitin is produced annually. Moreover, approximately 80 000 tonnes of chitin are synthesised based on marine by-products (Ghormade, Pathan and Deshpande, 2017).

Chitosan is the second most abundant biopolymer that is produced from chitin through the alkaline deacetylation process. Chitin deacetylation is a process that involves the reaction of chitin with 40-50 % sodium hydroxide solution to hydrolyse -NHCOCH_3 groups into -NH_2 groups. However, the degree of deacetylation can only achieve up to 98 % because complete deacetylation is difficult to achieve due to the heterogeneous process. Thus, chitosan is considered a partial deacetylated form of chitin (Rafique, et al., 2016). Generally, chitosan is formed from the units of D-glucosamine and a small amount of N-acetyl-D-glucosamine residue that joined by $\beta(1\rightarrow4)$ glycosidic bond (Al-Manhel, Al-Hilphy and Niamah, 2018). Each glucosamine unit consists of a free amino group, and this group can take on a positive charge which allows chitosan to be used as a coagulant agent and adsorbent for the removal of organic compounds. Its coagulation effect is more effective than mineral coagulants such as aluminium sulphate, polyethylene imide, and polyacrylamide in the removal of various pollutants from the aqueous solution (Obiora-Okafo and Onukwuli, 2017).

Figure 2.3 and Figure 2.4 show the respective chemical structures of chitin and chitosan (Shukla, et al., 2013). The chemical structure of chitosan is similar to chitin and cellulose, but -NH_2 groups only present in the structure of chitosan. Nevertheless, the solubility of chitosan in the aqueous acid medium is higher than its precursor polymer (chitin) and cellulose owing to the presence of -NH_2 groups and -OH groups that are responsible for adsorption. Chitin is not suitable used as a biosorbent for the adsorption of organic dyes as compared to chitosan due to its low solubility and low dispersion in water and other solvents. On the contrary, chitosan is soluble in dilute acidic solutions (Liu, et al., 2013). In order to improve the adsorption capacity of chitin for the removal of methylene blue dyes, Cao, et al. (2018) modified the chitin using chemical process through protonation, carboxylation, and grafting.

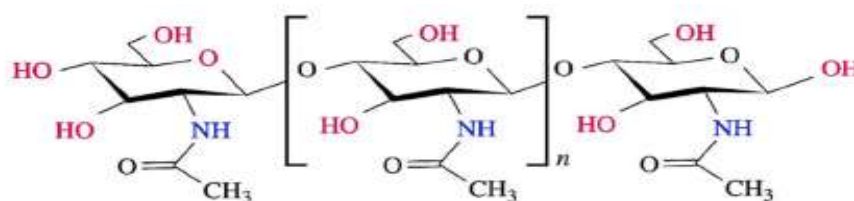


Figure 2.3: Chitin Chemical Structure (Shukla, et al., 2013).

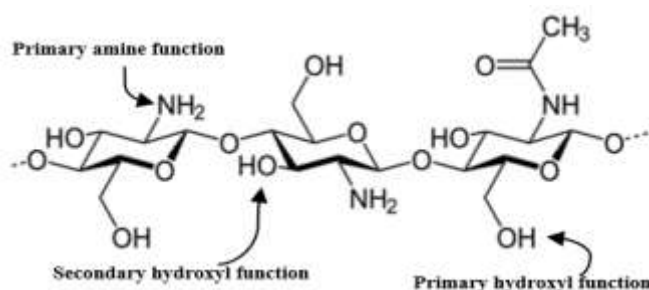


Figure 2.4: Chitosan Chemical Structure (Shukla, et al., 2013).

Chitosan has a long polymer chain and good polycation, aggregation and precipitation properties under neutral or alkaline pH conditions. The respective properties can promote the contact between polymer and organic dyes. Due to its high cationic charge density, chitosan can be used as coagulants and flocculants to remove the negatively charged colloidal organic and inorganic pollutants from water. With their regenerative ability and environmentally friendly properties, these properties allow them to be used in the adsorption process (Farias, et al., 2015). It is biodegradable, biocompatible, non-toxic and inexpensive. Many research studies have been carried out to investigate the adsorption capacity of chitosan and its composites to remove pollutants from wastewater. The application of chitosan in water treatment such as dye removal, heavy metal removal, and oil treatment of aqueous emulsion was studied (Elanchezhiyan, Muthu Prabhu and Meenakshi, 2018; Sarode, et al., 2019; Zheng, et al., 2019).

2.1.3 Modification of Chitosan

Among the biopolymers listed previously, chitosan was selected for further discussion in the following sections as it could be used as potential biosorbent to remove organic dyes. However, pure chitosan was reported to have poor physicochemical properties in terms of morphological properties, surface area,

functional groups and thermal stability, thereby reducing the biosorption capacity (Dehghani, et al, 2017). Therefore, chitosan can be modified using chemical and physical methods to overcome its limitations and improve the performance of chitosan. Modification of raw chitosan using chemical and physical methods is commonly employed to elevate the adsorption capacity of chitosan for the removal of organic dyes. Generally, the removal efficiency of organic dyes mainly depends on the physical and chemical properties of the adsorbent. There are several chitosan modification methods to improve the performance of chitosan on the adsorption efficiency, which are crosslinking, grafting and blending with other materials (Thakur, et al., 2015).

The grafting method is commonly used to promote the formation of chemical bonds between different types of polymers without mixing with other materials. This method can improve the physicochemical properties of chitosan by introducing additional functional groups such as $-NH_2$, $-NHCOCH_3$, $-COOH$ or thiol into crosslinked chitosan (Younes and Rinaudo, 2015). Besides, polymer grafting also can improve the polymerisation degree of biopolymer, polydispersity of main chain and side chains, graft density, graft distribution or graft uniformity (Thakur, Thakur and Gupta, 2013). In general, polymer grafting can be prepared using three methods: i) grafting by polymerisation of a macromonomer, ii) grafting from the surface or backbone of the polymer via reversible-deactivation radical polymerisation and iii) grafting a pre-synthesised polymer onto the surface or backbone of the polymer. Figure 2.5 shows the different methods for polymer grafting (Banerjee, Paira and Mandal, 2014).

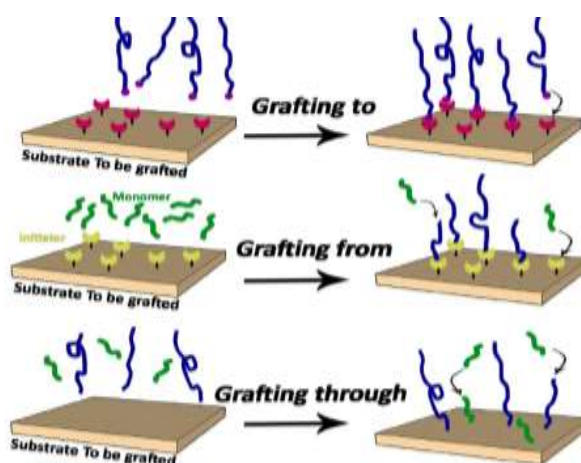


Figure 2.5: Polymer Grafting Methods (Banerjee, Paira and Mandal, 2014).

Kyzas, et al. (2013) grafted chitosan with polyacrylamide and also with polyacrylic acid to improve the adsorption capacity of chitosan. Grafting of functional groups such as $-\text{COOH}$, $-\text{OH}$, sulphate, phosphate and $-\text{NH}_2$ groups onto the biosorbent surface could increase the number of active sites of chitosan for the removal of organic dyes. For example, the surface of biosorbent was protonated by grafting $-\text{NHCOCH}_3$ functional groups on the chitosan surface. As a result, this could improve the adsorption capacity of chitosan towards the negatively charged dyes. Besides, grafting of $-\text{COOH}$ groups onto the surface of chitosan would result in more negative charges on the chitosan surface. Thus, this leads to the high adsorption capacity of chitosan towards cationic pollutants due to the strong interaction between cationic dyes and $-\text{COOH}$ functional groups.

Moreover, crosslinking is one of the effective approaches to modify polymer microstructures via chemical or physical methods. However, excessive crosslinking will reduce the mechanical stability of polymers and therefore crosslinking must be done in an appropriate and controlled manner (Rezazazemi, et al., 2014). Crosslinking reactions are commonly employed to prevent chitosan from dissolving in acidic media. At lower pH, chitosan will be dissolved in an acidic medium and lost its ability to bind as a solid adsorbent with adsorbates which can restrict its applications in wastewater treatment. Therefore, crosslinking reagents containing multifunctional groups such as aldehydes, anhydrides, and epoxides will be used to react with the functional groups on the surface of chitosan to increase the solubility of chitosan in solution (Wang and Chen, 2014). The common crosslinkers used in the research include glutaraldehyde, epichlorohydrin, glyoxal formaldehyde, ethylene glycol diglycidyl ether, and sodium tripolyphosphate (Nagireddi, Katiyar and Uppaluri, 2017).

Next, polymer blending is an economical and simple physical method of combining two or more materials, with or without any chemical bonds between their chains to develop a new material called polymer composite. However, it is provided that the concentration of polymer component in the blends should above 2 %. Polymer blending with other materials is widely used to improve the mechanical properties of biopolymers due to their recyclability and biodegradability (Kim, et al., 2012). The components involved in the blending

usually will have different physicochemical properties with each other. Therefore, blending also helps to overcome the shortage of reaction sites in the adsorption membrane structures of biopolymers. For example, Kumar and Kumar (2016) employed the polymer blending method to synthesise chitosan/polyvinyl alcohol (PVA) for the removal of Direct Red 80 dyes. Based on the results, chitosan/PVA could remove up to 89 % of Direct Red 80 dyes, while pure chitosan only could remove 54 % of dyes. The results indicated that blending PVA with chitosan could significantly improve the removal efficiency of dyes.

2.2 Chitosan Composites

Chitosan is a renewable, eco-friendly and biodegradable material that can be used as an alternative material for synthetic petroleum-based polymers. However, its mechanical strength, tensile strength, permeability, and thermal stability are lower than chitosan composites (Sanyang, et al., 2016). Therefore, the best way to increase the performance and stability of chitosan is to introduce reinforcement materials within the microregime or nanoregime (Abitbol, et al., 2016).

Chitosan composites are biopolymer-based materials made up of two or more different substances that combine together to produce a new material with better performance than a single constituent material. These composite materials consist of two main phases: the matrix phase with low modulus and high elasticity and the reinforcement phase with higher loading capacity (Díez-Pascual, 2019). The use of biopolymers alone may not be effective in removing the organic compounds from water. A suitable biopolymer composite should be inexpensive, available in abundant, efficient, eco-friendly, biocompatible, and reusable (Adewuyi, 2020). In general, chitosan composites can be synthesised through crosslinking reaction between the positively charged group of chitosan and negatively charged crosslinking agent in the ionic gelation process.

This section mainly focuses on the types of different materials that can be combined with chitosan to form chitosan composites in order to overcome its limitations. These materials are prepared by combining chitosan with other materials such as zeolites, carbon-based materials, zinc oxide (ZnO) and other biopolymers.

2.2.1 Chitosan/Zeolite

Zeolite mainly contains aluminate and silicate with three-dimensional framework structures. It can be employed to remove organic pollutants due to its excellent adsorption properties with outstanding ion exchange and secure modification capabilities (Wan Ngah, et al., 2012). Natural zeolite is an abundant, environmentally friendly, inexpensive, chemically, and mechanically stable hydrated alumina silicate material. It can be used to form composites with chitosan. Xie, et al. (2013) have employed chitosan/zeolite composites to remove cationic, anionic, and organic pollutants from aqueous solution with 31.6 mg/g adsorption capacity. Furthermore, Dehghani, et al. (2017) conducted an experimental study for the removal of methylene blue dye using pure chitosan and chitosan/zeolite composite. The results indicated that the dye removal efficiency using chitosan/zeolite was higher than pure chitosan. It was reported that 84.85 % of the methylene blue was removed by the chitosan/zeolite composite with a maximum adsorption capacity of 24.5 mg/g.

The chitosan/zeolite composite was synthesised through the bridging mechanisms and the formation of hydrogen bonds between the surface functional groups of chitosan with the –OH, silanol, and aluminol groups of zeolite (Wan Ngah, et al., 2012). Based on the SEM images produced by Metin, Çiftçi and Alver (2013), it was observed that pure chitosan had a lower specific surface area with a flak-like and smooth surface structure. However, the SEM image of chitosan/zeolite composite demonstrated a heterogeneous, irregular and rough surface as compared to pure chitosan. Besides, chitosan/zeolite possessed better thermal stability and experienced lower weight loss than pure chitosan during the thermal degradation process (Li and Huang, 2013). Therefore, the dye removal efficiency and thermal stability of chitosan were improved by immobilising zeolite in the chitosan matrix.

2.2.2 Chitosan/Carbon-based Materials

Carbon-based materials such as multiwalled carbon nanotubes (MWCNTs) and graphene oxide are attractive adsorbents for water treatment. The adsorption capacity can be improved by introducing MWCNTs into the chitosan matrix. This is because MWCNTs have high surface areas, functionalisation capability with different surface functional groups, and controllable size distribution. In

general, chitosan/MWCNTs composite had higher thermal and mechanical strength as compared to pure biopolymer (Khademian, et al., 2020).

Salam, Makki and Abdelaal (2011) added MWCNTs with average diameters of 60 to 100 nm in the chitosan matrix to synthesise a chitosan/MWCNTs composite. The MWCNTs were well dispersed on the surface of chitosan. Based on the SEM images, the membrane showed a porous morphology and sponge-like structure. Besides, TGA analysis showed that the thermal stability of chitosan/MWCNTs composite was higher than raw chitosan. The surface area of the MWCNTs was increased from 82.4 to 135.1 m²/g after the modification with chitosan. The excellent dispersion of MWCNTs in a chitosan matrix decreased the tangling and agglomeration of MWCNTs and greatly improved the adsorbent surface area.

Besides, graphene oxide has become a promising adsorbent material in wastewater treatment due to its excellent properties such as high surface areas and chemical stability. Graphene oxide consists of many functional groups, including –COOH, –OH, diol, epoxy, and ketone groups. These functional groups cause graphene oxide to have higher hydrophilic and able to compatible with other biopolymers (Kuilla, et al., 2010). The –COOH group of graphene oxide can react with the –NH₂ group of chitosan to form chitosan/graphene oxide composites. Huyen, et al. (2017) prepared chitosan/graphene oxide composites by lyophilisation for the removal of methylene blue. The results showed that the chitosan/graphene composites were found to be a suitable adsorbent for methylene blue with a maximum adsorption capacity of 662.25 mg/g. After the adsorption, chitosan/graphene oxide composites could be easily separated and recovered by filtration.

2.2.3 Chitosan/Zinc Oxide (Chitosan/ZnO)

There are many types of metal oxide nanoparticles such as ZnO, magnesium oxide (MgO), magnetite (Fe₃O₄) and maghemite (γ-Fe₂O₃) that can be used to form chitosan-based composites. However, ZnO is cheaper and has higher removal efficiency of organic pollutants than other metal oxides due to its higher semiconducting properties and high surface area. Therefore, ZnO is commonly used to combine with chitosan to form chitosan/ZnO nanocomposite (Nakkeeran, et al., 2018).

Chitosan/ZnO nanocomposite is a new hybrid material that can efficiently remove organic pollutants than pure chitosan. Introducing ZnO nanoparticles into the chitosan matrix can increase the number of active sites on the chitosan surface, resulting in an improvement of the adsorption performance. On the other hand, the modification of chitosan with ZnO nanoparticles can provide a surface strengthening effect and improve surface corrosion resistance. An experimental study for the removal of organic pollutants was carried out by Arafat, et al. (2015). The results showed that chitosan/ZnO nanocomposite could remove 95-99 % of organic pollutants by using 2 mg/L of the composite at the temperature of 50 °C and contact time of 60 minutes.

2.2.4 Chitosan/Other Biopolymers

Cellulose is a polysaccharide polymer that can be obtained abundantly from plants and it is relatively cheap. It can be introduced into a chitosan matrix to form a biopolymer composite. Sun, et al. (2009) carried out an experimental study to synthesise a chitosan/cellulose composite using ionic liquids to remove organic pollutants from aqueous solution. Based on the results, the adsorption capacity of chitosan/ cellulose composite was three times higher than the raw chitosan and cellulose. The chitosan/cellulose composite has a porous structure, larger surface areas, higher stability, and higher affinity for organic pollutants (Agarwal and Vaishali, 2017).

Besides, Li, et al. (2012) had incorporated polyvinyl alcohol (PVA) in the chitosan matrix to synthesise chitosan/PVA composite as a biosorbent to remove organic dyes. Although PVA has exceptional physicochemical properties, it is not suitable to be utilised as an individual adsorbent because of its low solubility in water and low adsorption capacity for organic dyes (Li, et al., 2012). However, chitosan can efficiently adsorb organic dyes due to the presence of a large amount of –OH and –NH₂ groups on its surface. Hence, it is suggested to combine the properties of both PVA and chitosan to prepare chitosan/PVA composites. The composites will have high mechanical stability, high performance of adsorption, and high chemical resistance in acidic and alkaline solution (Khademian, et al., 2020).

2.3 Removal Methods of Organic Dyes

There are several conventional methods in treating industrial wastewater before it can be discharged to the environment. These methods are divided into three categories, namely biological, chemical, and physical methods (Crini and Lichtfouse, 2019). Table 2.1 shows the benefits and limitations for each of the dye removal methods when treating the wastewater. Due to the presence of benzene ring on the chemical structure of organic dyes, the individual treatment process is inefficient to degrade organic dyes. Therefore, organic pollutant removal strategies must include a combination of different methods.

2.3.1 Biological Treatment

Biological treatment usually utilises microorganisms such as bacteria, fungi and enzymes to degrade organic dyes into harmless and simple molecule through either aerobic or anaerobic biological processes (Kanaujiya, et al., 2019). The aerobic biological process usually occurs in the presence of oxygen in which aerobic microorganisms break down biodegradable organic dyes into carbon dioxide, water and energy. In contrast, the anaerobic biological process utilises anaerobic microorganisms such as hydrogenic, acetogenic bacteria, methanogens, and sulphate-reducing bacteria to degrade organic pollutants into carbon dioxide, methane and energy in the absence of oxygen (Kanaujiya, et al., 2019). As compared to chemical and physical methods, biological treatment has been widely used in secondary wastewater treatment and has become an indispensable part of many wastewater treatment plants because of their simplicity, lower treatment cost, and environmentally friendly.

However, some organic pollutants with low biodegradability and high chemical stability cannot be effectively removed by biological treatment. Organic dyes are difficult to be biodegraded by biological treatment due to their complex polyaromatic structure and recalcitrant nature, making them highly stable in the water (Tomei, Mosca Angelucci and Daugulis, 2016). These organic compounds are resistant and toxic to microorganisms used in biological treatment. The resulting problems include sludge bulking, sludge uplift, and flocculation formation which are undesirable in many processes (Pang and Abdullah, 2013).

Table 2.1: Advantage and Limitations of Different Wastewater Treatment Methods (Crini and Lichtfouse, 2019).

| Treatment Methods | Advantages | Limitations |
|--------------------------------------|--|---|
| Biological Method | | |
| Aerobic Process | Low operating cost and simple design. | Longer detention times, high quantity of sludge generation and sensitive to toxic substance. |
| Anaerobic Process | Low operating cost and methane can be used as a fuel source. | Slow process, time-consuming and produces an unpleasant smell. |
| Chemical Method | | |
| Coagulation/ Flocculation | Short detention time and economical. | High quantity of sludge generation leads to the handling and disposal of the sludge problems. |
| Ozonation | No alteration of the volume of sludge and wastewater due to ozone is applied in a gaseous state. | Short half-life and expensive. |
| Physical Method | | |
| Ion Exchange | No adsorbent loss during regeneration. | Not effective for all types of organic pollutants. |
| Membrane Filtration | Efficient in removing all types of organic pollutants. | High maintenance and operating cost due to membrane fouling. |
| Adsorption | Efficient in removing a wide range of organic contaminants. | High cost. |

In addition, the anaerobic process is relatively slow and hence time-consuming. Sometimes, anaerobic decomposition results in the formation of gases such as hydrogen sulphide which creates an unpleasant odour (Sandra, et

al., 2017). Another limitation is the dependence of biological processes on various factors such as dissolved oxygen, water temperature, pH, nutrient adequacy, toxic substances, and organic loading rate.

2.3.2 Chemical Treatment

This method uses chemical reagents to convert more harmful organic pollutants into less harmful products such as carbon dioxide and water through chemical reactions. There are two types of chemical treatment: chemical precipitation and chemical oxidation. Coagulation and flocculation are processes involving the removal of colloidal and other suspended particles from wastewater using coagulants through chemical precipitation. Alum, ferrous sulphate and ferric chloride are the most common coagulants used for wastewater treatment (Mbaeze, Agbazue and Orjioke, 2017). Coagulants are used to destabilise the charged particles by charged neutralisation and promote the collision between neutralised particles to form larger flocs. After that, these flocs are removed by separation processes such as gravity sedimentation and filtration. However, coagulation and flocculation processes generate a large quantity of toxic sludge that requires proper handling and disposal of the sludge (Ariyanti, Maillot and Gao, 2018).

Chemical oxidation process such as ozonation is a simple and effective method to degrade non-biodegradable organic and inorganic pollutants that are toxic or inhibitory to microbial growth (Morali, Uzal and Yetis, 2016). Strong oxidising agents such as hydrogen peroxide, Fenton's reagents and ozone are commonly used in the chemical oxidation process (Bartolomeu, et al., 2018). Ozonation overcomes the limitations of the chemical and biological treatment methods by improving biodegradability, destroying phenolic compounds and reducing chemical oxygen demand (Quan, et al., 2017). This method can satisfactorily remove organic pollutants. Besides, one significant benefit of ozonation is that ozone is applied in gaseous state and will not increase the volume of sludge and wastewater. However, ozonation has a short half-life of about 20 minutes and it is relatively expensive (Hansen, et al., 2016). The stability of the process is influenced by pH, salt concentration, and temperature.

2.3.3 Physical Treatment

There are several physical treatments for the removal of organic pollutants such as ion exchange, membrane filtration, and adsorption. The ion exchange method is not widely used in industrial wastewater treatment because it cannot effectively remove a wide range of organic pollutants. The ion exchange method can only be used to remove undesirable anions and cations from wastewater. The removal of non-ionic pollutants is inadequate (Jiang, et al., 2015). When the exchange capacity of the ion exchange resin is saturated, the ion exchange resin needs to be regenerated before it can be reused. Nevertheless, this method is not cost-effective and costly. It requires the use of an expensive organic solvent to regenerate the spent ion-exchange resins (V́ctor-Ortega, Ochando-Pulido and Mart́nez-Ferez, 2017). The benefits of ion exchange treatment include the recovery of adsorbent after successful regeneration, recovery of the used solvent, and the effective removal of soluble organic pollutants.

Besides, there are many membrane filtration technologies such as microfiltration, nanofiltration, ultrafiltration, and reverse osmosis. Membrane filtration is the process in which wastewater passes through a semi-permeable membrane that filters out the organic pollutants based on the pore size of the membrane. This method is unable to reduce dissolved solids content, but it can effectively remove suspended solids. Table 2.2 shows the different types of membrane filtration processes used to remove the particular organic pollutants (Upadhye and Joshi, 2012). The nanofiltration method is suitable for the removal of dyes and pharmaceutical compounds due to the pore size of the membrane is smaller than these molecules (Abdel-Fatah, 2018). However, the main problem associated with these technologies is membrane fouling due to the accumulation of particles retained on the membrane pores. This causes the membrane to have a short lifetime and results in a high cost of membrane system. Thus, frequent cleaning and replacement of membranes are required to enhance their effectiveness in removing organic pollutants (Crini and Lichtfouse, 2019).

The adsorption process is known to be an effective method to remove the small size of organic pollutants from the wastewater by using adsorbents. The adsorption process is applicable to treat a large amount of wastewater. It has a simplicity of operation and thus does not require costly instruments. During the adsorption process, pollutant molecules in the liquid phase adhere to

the solid surface which is driven by the attractive force on the solid surface. The efficiency of adsorption mainly depends on the type of adsorbents. The adsorbent can be made selective by modification. Activated carbon is the most common type of adsorbent being used in the adsorption process due to its ability to adsorb a wide range of organic pollutants with high adsorption capacity (Akhtar, Amin and Shahzad, 2016). Although activated carbon can produce high water quality, it is costly and hard to be reactivated (Gautam, et al., 2014).

Table 2.2: Filtration Scope of Different Membrane Filtration Processes (Upadhye and Joshi, 2012).

| Process | Pore Size (Micro) | Molecular Weight (g/mol) | Examples |
|------------------------|------------------------------|---|--|
| Microfiltration | 0.001-2.0 | > 100 000 | Bacteria |
| Nanofiltration | 0.002-0.1 | 1 000-200 000 | Colloids, virus, protein, etc. |
| Ultrafiltration | 0.001-0.7 | 180-15 000 | Dyes, divalent ions, pharmaceutical compounds, pesticides. |
| Reverse Osmosis | < 0.001 | < 200 | Salts and ions. |

Recently, low-cost adsorbent materials are widely used in wastewater treatment because they are abundant in nature and have strong adsorption capacity after activation. Biosorption is also known as a subcategory of adsorption which uses biological raw materials as biosorbents to remove organic pollutants (Adewuyi, 2020). A variety of low-cost adsorbents derived from natural biological materials, agricultural wastes or by-products from industrial have been studied to treat industrial wastewater. Among these materials, agricultural by-products are suitable to be used as biological adsorbents because they are not only available in abundance but also cost-effective and have a relatively low impact on the environment. Compared with other wastewater

treatment methods, biosorption significantly reduces the costs in accordance with financial investment in the whole process (Vijayaraghavan, et, al., 2017).

2.4 Biosorption in Water Remediation

The biosorption process is a mass transfer process that moves substances from the liquid phase (water) to the solid phase (biosorbent). Biosorption can be referred to as the adsorption of sorbates such as atoms, molecules or molecular ions on the surface of solid biological sorbent (Fomina and Gadd, 2014). Biosorption continues until an equilibrium is reached where the amount of organic dyes adsorbed on the surface of the biosorbent is the same as the amount of organic pollutants left in the solution (Adewuyi, 2020). In general, it is a physicochemical and metabolism independent process to remove substances from solution by biological materials.

In recent years, the application of biological materials to adsorb and remove organic pollutants from water bodies has attracted a great deal of attention. It has become a hot topic among researchers due to the problems and shortcomings faced by the conventional methods in removing non-biodegradable organic pollutants. Biosorption is characterised by remarkable merits such as ease of modification of biosorbents, high efficiency, low operating and maintenance cost. Another significant benefit of this process is that it does not lead to the generation of intermediates (Ahmad and Danish, 2018). The process is reversible, and the adsorbent used can be regenerated by desorption for reuse.

This process can effectively remove organic pollutants even when organic pollutants are in low concentration. This is achieved through the binding of organic pollutants onto the vastly available active binding sites present on the surface of the biosorbent. The detailed biosorption mechanisms were discussed in the following subsection. The effects of the operating parameters such as pH, initial biosorbent dosage, initial dye concentration, and temperature were thoroughly studied.

The high efficiency of biosorption is a vital aspect that should be characterised to the biosorbent for the effective elimination of various water pollutants. The physicochemical features of the biosorbent vary due to the presence of the different functional groups with varying degrees present on its

surface. The most common functional groups present on the biosorbent surface are $-\text{NH}_2$, $-\text{COOH}$, $-\text{OH}$ and phosphate group. These respective functional groups can facilitate the sorption of water pollutants onto the biosorbent through multiple sorption mechanisms. Figure 2.6 illustrates the different types of mechanisms involved in the biosorption process. In fact, the interaction between organic pollutants and biosorbent surface occurs through electrostatic interaction, ion exchange, complexation, chelation and microprecipitation, physical and chemical adsorption (Abdel Maksoud, et al., 2020).

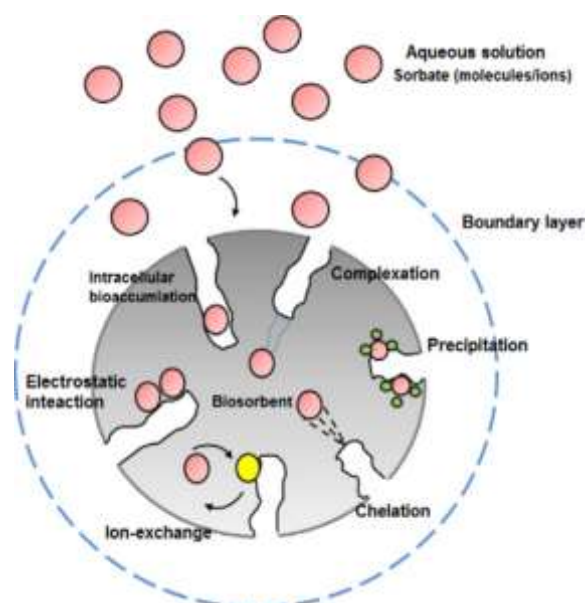


Figure 2.6: Types of Mechanisms in Biosorption (Abdel Maksoud, et al., 2020).

The biosorption interaction between sorbate and biosorbent mainly occurs in two different conditions: surface sorption and interstitial sorption. Surface sorption involves film diffusion. It occurs when sorbate moves through the bulk solution and diffuses across the liquid film boundary layer surrounding the biosorbent surface. The biosorbent provides numerous active sites for sorbate binding. After that, sorbate is adsorbed on the opposite charged of binding sites on the biosorbent surface (Michalak, Chojnacka and Witek-Krowiak, 2013). This phenomenon is strongly promoted by Van Der Waals forces, dipole interactions or hydrogen bonding (Joseph, et al., 2019). This process is followed by interstitial sorption. During interstitial sorption, it involves intraparticle diffusion. Sorbate further diffuses into the pores of the biosorbent and eventually attaches to the interior surface of the biosorbent. In

this process, film diffusion and intraparticle diffusion are considered as the rate-determining steps whereas the surface bonding takes place in a faster rate (Adewuyi, 2020).

2.5 Parameter Studies

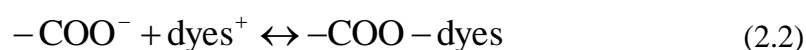
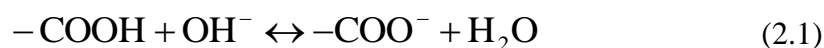
The biosorption efficiency is affected by many factors, including solution pH, biosorbent dosage, initial pollutant concentration, contact time and temperature. However, the effects of these parameters are studied individually while maintaining the rest at the constant condition.

2.5.1 Effect of Solution pH

The biosorption capacity of chitosan composite as the biosorbent is highly dependent on the pH of surface charge of chitosan composite and the type of organic dyes in the aqueous solution. The organic dyes can be classified into two types which are cationic dyes with positively charged and anionic dyes with negatively charged. It was reported that solution pH and point zero charge (pH_{pzc}) of chitosan composites was the most critical parameters affecting the biosorption capacity (Hassan, et al., 2019). They have a drastic impact on the surface charge of chitosan composite and ionisation of functional groups present on the chitosan composite surface.

pH_{pzc} can be defined as the pH value at which the net surface charge of chitosan composite is equivalent to zero (Li, et al., 2017). Under acidic conditions at low pH, hydrogen ions (H^+) are generated, while hydroxide ions (OH^-) are found under alkaline conditions at high pH. If the solution pH is more than pH_{pzc} , the surface of chitosan composite will be negatively charged due to the deprotonation of surface functional groups by OH^- at high pH condition. This will favour the biosorption of cationic dyes through electrostatic attraction. Nevertheless, the positively charged surface of chitosan composite will occur at solution pH beyond pH_{pzc} due to the protonation of surface functional groups. This eventually results in strong electrostatic repulsion between cationic dyes and chitosan composite, thus reducing the biosorption efficiency. Vice versa in the case of anionic dyes, the favourable biosorption condition is attributed to the electrostatic attraction between the negatively charged dyes with the positively charged surface of chitosan composite.

For instance, Kausar, et al. (2019) reported that the pH_{pzc} for chitosan/clay composite was at pH 7.0. The biosorption capacity of chitosan/clay composite for Rose FRN dyes increased until at pH 10. The results confirmed that the chitosan/clay composite was negatively charged since the optimal solution pH exceeded pH 7.0. Equation 2.1 shows that OH^- deprotonates the $-COOH$ group on the composite surface and carboxylate ion ($-COO^-$) with negatively charged and water (H_2O) are formed under alkaline condition. Moreover, the biosorption mechanism for the removal of cationic dyes at high pH could be well explained by Equation 2.2. The negative surface charge of chitosan composites could facilitate electrostatic interaction with the cationic Rose FRN dyes. Besides, the $-OH$ group on the chitosan composite could interact with the cationic dyes through hydrogen bonding. However, the biosorption capacity reduced after pH 10 might be attributed to the excessive OH^- reacted with cationic dyes through precipitation.



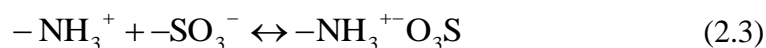
Besides, there are many types of cationic dyes, including methylene blue, malachite green, methyl violet, crystal violet and so on. The similar finding was reported for the biosorption of methylene blue using chitosan/zeolite, chitosan/bentonite, chitosan/activated carbon, chitosan/silica/ZnO and chitosan/clay composites (Metin, Çiftçi and Alver, 2013; Dotto, et al., 2016; Li, et al., 2017; Hassan, et al., 2019; Kausar, et al., 2019). The respective chitosan composite achieved a maximum biosorption capacity at high pH.

In addition, the biosorbents such as chitosan/ Fe_3O_4 /graphene oxide, chitosan/ Fe_3O_4 /glutaraldehyde and chitosan/ZnO composites were employed to remove crystal violet, malachite green and methyl violet, respectively (Tran, et al., 2017; Azari, et al., 2019; Muinde, et al., 2020). It was observed that their removal efficiency of cationic dyes also increased at high pH. However, the biosorption efficiency of cationic dyes was reduced at low pH, as reported in the literature. The low biosorption efficiency might be due to the competition of

H⁺ with cationic dyes for the binding sites on the chitosan composite surface under acidic condition.

Next, Travlou, et al. (2013) studied the effect of pH for the biosorption of anionic reactive black dyes using chitosan/graphene oxide as the biosorbent. It was reported that the chitosan/graphene oxide exhibited a neutral charge surface when pH was at 6.8. The biosorption efficiency of reactive black increased significantly when solution pH was reduced from 12 to 2. Hence, chitosan/graphene oxide composite had a positively charged surface as the optimal solution pH below 6.8. At high pH, the high amount of OH⁻ in the aqueous solution increased the repulsive force between -COO⁻ groups and anionic dyes, resulting in low biosorption efficiency of anionic dyes (Coura, Profeti and Profeti, 2020).

The similar findings also reported in the literature for chitosan/MWCNTs, chitosan/PVA, chitosan/cellulose and chitosan/quartzite composites (Abbasi and Habibi, 2016; Anitha, Kumar and Kumar, 2016; Wang, et al., 2018; Coura, Profeti and Profeti, 2020). The respective chitosan composite was used to remove reactive orange, reactive black, direct blue, eosin yellow and congo red. These anionic dyes consist of -SO₃⁻ groups with negatively charged. When pH below p*H*_{pzc}, -NH₂ groups on the chitosan composite surface were protonated to form positively charged amine groups (-NH₃⁺) under acidic condition. Consequently, the electrostatic interaction occurred between -NH₃⁺ groups of chitosan composite with -SO₃⁻ groups of anionic dyes as presented in Equation 2.3 (Travlou, et al., 2013).



2.5.2 Effect of Biosorbent Dosage

The biosorbent dosage is an important factor in determining the optimum amount or saturation point. At saturation point, any further increment in the amount of biosorbent will not contribute to any significant improvement in the biosorption process. In general, introducing a high amount of biosorbent will increase the availability of vacant biosorption sites and also provide a large surface area for the biosorption of dye molecules (Al-Manhel, Al-Hilphy and

Niamah, 2018). Consequently, a high amount of organic dyes can be adsorbed on the biosorbent active site, thereby increasing the removal efficiency of organic dyes.

For instance, the removal efficiency of reactive blue was improved by increasing the chitosan/MgO dosage from 2 to 14 g/L (Nga, Thuy Chau and Viet, 2020). Nevertheless, it was reported that the removal efficiency increased slightly from 58.70 to 59.82 % when the biosorbent dosage was further increased to 16 g/L. Hence, it concluded that 14 g/L was considered as the optimum biosorbent dosage. The results indicated if the biosorbent dosage exceeded the optimum biosorbent dosage, it would not provide any improvement in the biosorption process due to the unsaturated biosorbent active sites.

Similarly, the biosorption efficiency of methylene blue also increased from 52.52 to 76.78 % when the chitosan/carbon clay composite was increased from 0.1 to 0.2 g/L (Marrakchi, Hameed and Hummadi, 2020). However, the biosorption efficiency eventually decreased to 77.24 % when the dosage was 0.3 g/L. Therefore, the optimal dosage of chitosan/carbon clay composite was determined to be 0.2 g/L. This might be caused by the overlapping or agglomeration of excessive biosorbent particles that would block the binding sites of other biosorbent. Introducing excessive biosorbent in the biosorption process resulted in an equilibrium imbalance between the vast number of biosorbent binding sites and a constant number of dye molecules (Salam, Makki and Abdelaal, 2011). As a result, the biosorption capacity was reduced due to the decrease in the surface area of chitosan composite and the availability of biosorption sites. A similar finding also reported for chitosan/PVA and chitosan/activated carbon composites (Anitha, Kumar and Kumar, 2016; Fatombi, et al., 2019). The biosorption efficiency of anionic dyes reduced when the biosorbent dosage was added in excess amounts.

2.5.3 Effect of Initial Dye Concentration

The initial concentration of dyes is also a major influencing factor in the biosorption process which can be studied through biosorption isotherm models. Figure 2.7 illustrates the effect of initial dye concentration on biosorption capacity of chitosan/kaolin clay composite at a constant time of 400 min (Jawad,

et al., 2020). The initial dye concentration was studied in the range of 50-400 mg/L. The results revealed that the biosorption capacity increased with an increase in the initial dye concentration. At the initial biosorption process, more binding sites on the chitosan composite surface were available for the biosorption of dye molecules. Besides, the high initial concentration of dyes provided a greater driving force required to overcome the mass transfer resistance between the liquid phase and solid phase (Abdel Maksoud, et al., 2020). It could increase the mass transfer of organic dyes to binding sites across the boundary layer of biosorbent particles against the concentration gradient.

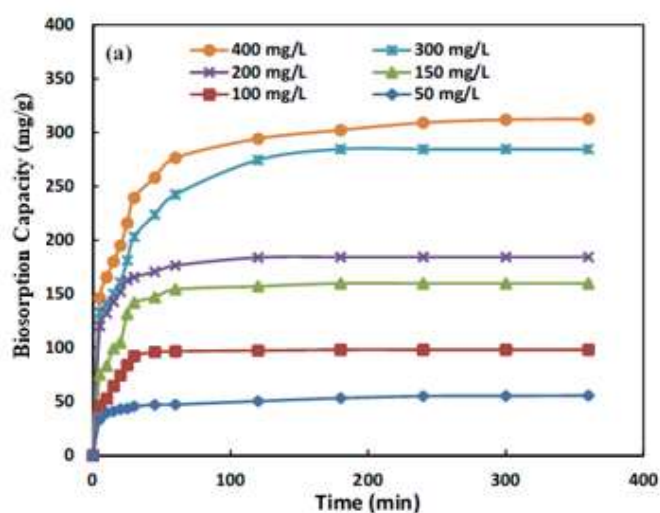


Figure 2.7: Effect of Initial Dye Concentration on Biosorption Capacity of Chitosan/Kaolin-clay Composite at Constant Time (Jawad, et al., 2020).

However, the biosorption capacity of chitosan composite decreased and remained constant after a period of time. This might be due to the saturation of chitosan composite surface, where dye molecules have occupied most binding sites (Li, et al., 2012; Jawad, et al., 2020). As a result, excessive dye molecules were not adsorbed on the binding sites due to saturation of binding sites, thus reducing the biosorption capacity. Similar findings also reported in the literature for chitosan/PVA, chitosan/activated carbon and chitosan/MgO composites (Li, et al., 2012; Rangabhashiyam, Anu and Selvaraju, 2013; Nga, Thuy Chau and Viet, 2020). The respective composite also exhibited high biosorption efficiency as the initial dye concentration increased.

2.5.4 Effect of Contact Time

Contact time is one of the most significant parameters as it can be employed to estimate the biosorption equilibrium and biosorption kinetic models. The contact time can be defined as the time given for the immersion of a given amount of biosorbent in a constant volume and concentration of organic dyes in the solution (Sadeek, et al., 2015). Figure 2.8 demonstrates the effect of contact on the biosorption efficiency of cationic dyes at a constant initial dye concentration of 2.3 mg/L by using chitosan/ZnO composite as the biosorbent. According to Figure 2.8, the biosorption rate was significantly accelerated during the first 15 min with a deeper gradient (Muinde, et al., 2020). This might be due to the abundance of active sites available on the biosorbent surface that could be easily accessed by the organic dyes.

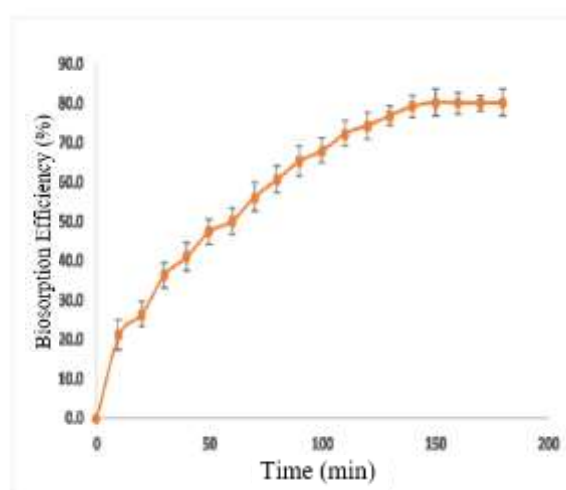


Figure 2.8: Effect of Contact Time on Biosorption Efficiency of Cationic Dyes at Constant Initial Dye Concentration of 2.3 mg/L (Muinde, et al., 2020).

Over a period of time, a large amount of organic dyes was adsorbed on the active sites of the chitosan composite surface through intermolecular interaction. Consequently, the biosorption rate decreased until an equilibrium state was achieved at 180 min with the maximum biosorption efficiency of 80.10 % (Muinde, et al., 2020). The decrease in concentration gradient with contact time could be attributed to a decrease in vacant binding sites for organic dye biosorption. The remaining organic dyes in the solution competed with each other to occupy the remaining active sites on the biosorbent surface. Therefore,

sufficient time should be ensured to establish the solid-liquid equilibrium (Abdel Maksoud, et al., 2020). Besides, Rangabhashiyam, Anu and Selvaraju (2013) and Nga, Thuy Chau and Viet (2020) also discovered similar findings in which the biosorption rate decreased gradually as contact time increased.

2.5.5 Effect of Temperature

Temperature is considered an important parameter that will affect the diffusion rate of sorbates via the external boundary layer surrounding the biosorbent. The information obtained from temperature can determine whether the nature of the biosorption process is endothermic or exothermic (Sargin, Arslan and Kaya, 2019). In general, the biosorption process at high temperatures can increase the collision frequency between the biosorbent and sorbate, thereby enhancing the biosorption rate. In addition, an increase in temperature will decrease the thickness of the boundary layer surrounding the biosorbent. Consequently, the mass transfer resistance of sorbates across the boundary layer is reduced. This will eventually increase the diffusion rate of dye molecules moving from the aqueous phase to the biosorbent surface.

In the research work of Travlou, et al. (2013), the chitosan/graphene oxide composite was used as the biosorbent to remove organic dyes. The effect of temperature was investigated in the range of 30 to 60 °C. It was reported that the removal efficiency of organic dyes increased when the temperature was raised from 30 to 45 °C. The result indicated the dye biosorption was an endothermic process that required a high amount of heat supplied to the process. However, the removal efficiency reduced as the temperature was further increased to 60 °C. The excessive heat supplied to the biosorption might lead to the deactivation or the destruction of binding sites on the biosorbent surface (Wang and Chen, 2014). Therefore, the removal efficiency decreased at high temperature.

Nevertheless, Kausar, et al. (2019) discovered a different finding where the biosorption capacity of chitosan/clay decreased with increasing temperature from 30 to 60 °C. The result suggested that the biosorption of direct Rose FRN dye was an exothermic process that released heat to the surrounding. Hence, an increase in temperature would supply a high amount of heat to the biosorption process, which could deactivate the binding site on the chitosan composite

surface. Furthermore, Bahrudin, Nawi and Sabar (2019) also observed a similar decreasing trend in the biosorption capacity of chitosan/ montmorillonite when the temperature was increased.

2.5.6 Comparison Performance for Various Types of Chitosan Composites

Table 2.3 and Table 2.4 compare the performance for various types of chitosan composites used to remove cationic dyes and anionic dyes under different optimum operating conditions. The results revealed that the optimal pH range for the removal of cationic dyes was between 8 and 11. As for the removal of anionic dyes, the optimal pH range was found to be between 2 and 6.8 under acidic condition. In addition, all the biosorption process were operated in the temperature range of 25–45 °C.

Among the chitosan composites listed in Table 2.3, chitosan/ZnO exhibited the highest removal efficiency of cationic dyes. It could remove 98.50 % of malachite green dyes at pH 8 with a biosorbent dosage of 2.4 g/L, an initial dye concentration of 50 mg/L and a contact time of 180 min. This might be due to a high amount of biosorbent being added to the sample solution, which increased the number of vacant binding sites and surface area for the biosorption of dyes (Muinde, et al., 2020). Besides, it was observed that chitosan/bentonite composite took the longest contact time to remove 88.00 % of methylene blue dyes with a low biosorbent dosage of 0.2g/L. When low biosorbent dosage was added to a constant initial dye concentration of 100 mg/L, a longer time was needed to achieve the solid-liquid equilibrium (Dotto, et al., 2016).

According to Table 2.4, chitosan/kaolin clay composite could remove the highest amount of anionic dyes with 99.50 %. The biosorption process was carried out for 30 min at a temperature of 30 °C using the biosorbent dosage of 0.6 g/L and initial dye concentration of 140 mg/L. Meanwhile, the solution pH was adjusted to pH 4 in order to create an acidic condition for the biosorption of remazol brilliant blue. The high removal efficiency could be attributed to the low pH, which increased the number of positively charged binding sites. This eventually improved the electrostatic attraction between positively charged chitosan/kaolin clay composite and negatively charged dyes (Xie, et al, 2013).

Table 2.3: Removal Efficiency of Cationic Dyes Using Various Types of Chitosan Composites under Different Operating Conditions.

| Chitosan Composites | Cationic Dyes | pH | Biosorbent Dosage (g/L) | Initial Dyes Concentration (mg/L) | Contact time (min) | Temperature (°C) | Dye Removal Efficiency (%) | References |
|--|----------------------|-----------|--------------------------------|--|---------------------------|-------------------------|-----------------------------------|--------------------------------|
| Chitosan/clay | Direct Rose FRN | 10 | 0.2 | 100 | 40 | 30 | 80.10 | Kausar, et al., (2019) |
| Chitosan/zeolite | Methylene blue | 9 | 2.0 | 100 | 138.65 | 30 | 84.85 | Metin, Çiftçi and Alver (2013) |
| Chitosan/ZnO | Malachite green | 8 | 2.4 | 50 | 180 | 30 | 98.50 | Muinde, et al. (2020) |
| Chitosan/activated carbon | Methylene blue | 11 | 1.0 | 400 | 60 | 30 | 91.02 | Fatombi, et al. (2019) |
| Chitosan/bentonite | Methylene blue | 10 | 0.2 | 100 | 360 | 25 | 88.00 | Dotto, et al. (2016) |
| Chitosan/Fe₃O₄/graphene oxide | Methyl violet | 11 | 1.0 | 100 | 70 | 27 | 87.6 | Tran, et al. (2017) |

Table 2.4: Removal Efficiency of Anionic Dyes Using Various Types of Chitosan Composites under Different Operating Conditions.

| Chitosan Composites | Anionic Dyes | pH | Biosorbent Dosage (g/L) | Initial Dyes Concentration (mg/L) | Contact time (min) | Temperature (°C) | Dye Removal Efficiency (%) | References |
|--------------------------------|------------------------|-----------|--------------------------------|--|---------------------------|-------------------------|-----------------------------------|--------------------------------|
| Chitosan/fly ash | Reactive orange | 4 | 7.0 | 300 | 60 | 45 | 88.00 | Xie, et al. (2013) |
| Chitosan/MgO | Reactive blue | 6.8 | 9.3 | 100 | 120 | 30 | 79.50 | Nga, Thuy Chau and Viet (2020) |
| Chitosan/PVA | Eosin yellow | 6 | 2.0 | 50 | 40 | 30 | 86.70 | Anitha, Kumar and Kumar (2016) |
| Chitosan/cellulose | Congo red | 6.6 | 2.5 | 500 | 625 | 30 | 95.00 | Wang, et al. (2018) |
| Chitosan/kaolin clay | Remazol brilliant blue | 4 | 0.6 | 140 | 30 | 30 | 99.50 | Xie, et al. (2013) |
| Chitosan/graphene oxide | Reactive blue | 2 | 1.0 | 250 | 1440 | 25 | 86.00 | Kamal et al. (2017) |

Next, chitosan/cellulose composite demonstrated the second highest dye removal efficiency among the biosorbents listed in Table 2.4. It could remove 95.00 % of congo red dyes with a biosorbent dosage of 2.5 mg/L and an initial dye concentration of 500 mg/L. The high initial concentration could increase the driving force and reduce the mass transfer resistance of dye molecules moving from the liquid phase to the chitosan composite surface (Wang, et al, 2018). However, a longer contact time was required to ensure most of the dye molecules were adsorbed on the binding sites of chitosan/cellulose composite and achieved the solid-liquid equilibrium.

Therefore, the biosorption efficiency was mainly affected by solution pH, biosorbent dosage, initial pollutant concentration, contact time and temperature. Among the parameters studied, solution pH contributed the significant effects on the dye removal efficiency. This is because the solution pH could affect the surface charge of chitosan composite and the type of dyes, eventually affecting dye removal efficiency. The results suggested that the dye removal process was chemisorption, which involved electrostatic interaction and ions exchange between chitosan composite and dye molecules. However, the physisorption process depended on the binding sites provided by chitosan composite and the amount of dyes adsorbed on the binding sites. The physisorption process was mainly affected by biosorbent dosage, initial dye concentration, contact time and temperature.

CHAPTER 3

METHODOLOGY AND WORK PLAN

3.1 Literature Review Methodology

A literature review study was conducted to evaluate the performance of various chitosan composites on the biosorption of dyes. Therefore, a systematic approach was developed and employed to manage a large amount of information to create a review that meets the publication requirements (Rekik, et al., 2018). This approach allows narrowing down the literature to the specific research objectives in order to determine the factors that affect the dye biosorption process. According to the method proposed by Snyder (2019), the literature review methodology mainly involved five steps: i) review planning; ii) literature searching process; iii) publication screening and selection; iv) data extraction; v) data analysis and report writing. The overall literature review methodology was presented in the form of a flowchart, as shown in Figure 3.1. For an in-depth understanding of each step, a detailed explanation for each step was conducted in the following subsections.

3.2 Review Planning

The problem statement, objectives and scope for this research were established in Chapter 1 during the initial review planning. The problem statement was identified to determine the existing problems that currently need to be addressed. It provides the context for the research study and generates the questions which the research aims to answer. For instance, the problem statements would be the current status of dyes in wastewater, how to remove dyes from wastewater and the limitation of conventional adsorbents. Once the problem statement was identified, the objective of this study was established to overcome the problems described in the problem statement. This was followed by a review of the existing literature to help formulate and clearly define the scope of the study while meeting the objectives of the study (Stone and Rahimifard, 2018).

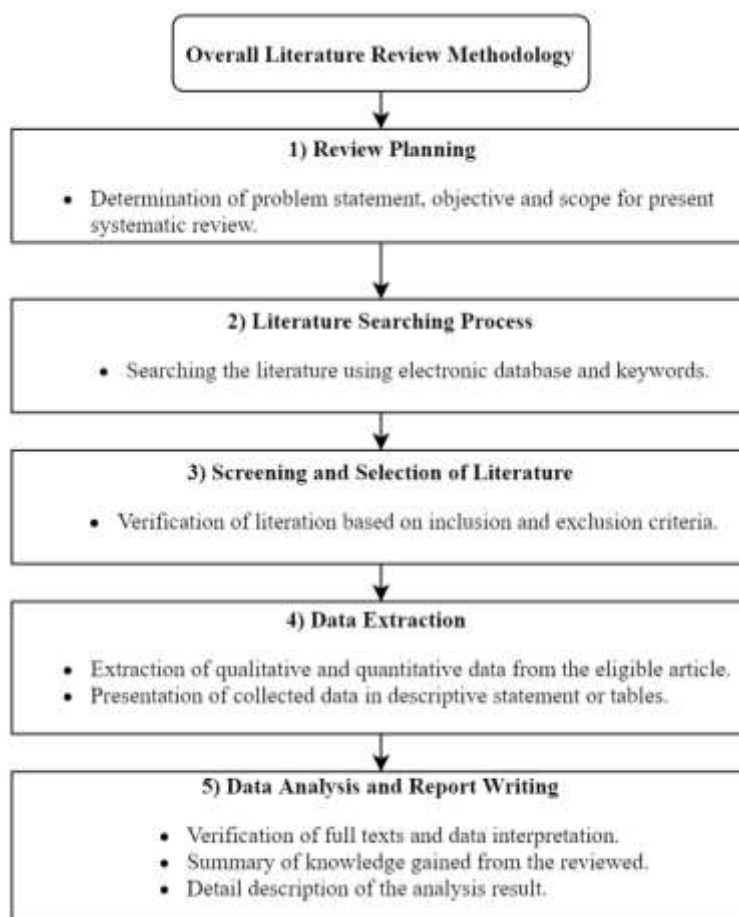


Figure 3.1: Overall Literature Review Methodology Flow Chart.

3.3 Overall Research Flow

The literature search was conducted for articles published between 2010 and 2021. The scientific publications of relevant journals were extracted from several electronic databases such as Elsevier's Science Direct, Research Gate, Google Scholar, SpringerLink and Scopus. Several keywords or search terms were selected to identify the related literature, avoid bias in the study, and broaden the search for better results (Ortiz-Martínez, et al., 2019). Since the title of this study is “Application of chitosan composite for the removal of organic dyes”, therefore the keywords selected for the search in electronic databases should pertain to these aspects, including chitosan composites, dye removal and biosorption processes. The Boolean strings employed for the current systematic review were as follows: chitosan or chitosan composite; and dye biosorption, dye adsorption or dye removal. Besides, the references in the retrieved article were also explored for more relevant articles. After conducting the search process, 323 journals were considered as potentially relevant articles.

3.4 Screening and Selection of Literatures

In order to ensure the identified journal articles were well matched to the review question, the titles and abstracts from 323 journals were screened and evaluated based on the eligibility criteria. The eligibility criteria were divided into inclusion and exclusion criteria which provided the boundaries for the current systematic review and also applied in the database search step (Snyder, 2019). It helps to determine whether the articles are relevant to be used as the reference in this research study (Azari, et al., 2020). Firstly, the inclusion criteria included the original articles published in the English language in peer-reviewed journals that were related to the use of chitosan composite as a biosorbent in the dye biosorption process.

However, research papers and non-English written studies published before 2011 were excluded. In addition, non-systematic narrative reviews, presentations, review papers, conference proceedings, and editorial material (Wikipedia) were excluded because they were considered opinion articles or guest reviews (Onwuegbuzie and Frels, 2016). With respect to the subject, the selected article mainly focused on the performance of chitosan composite material to remove the dye in the biosorption process. Therefore, research papers with repetitive content or irrelevant topics such as the use of adsorbent other than chitosan composites for dye removal and chitosan composite used for other application process were also excluded. After conducting the screening process, 161 articles that met the eligibility criteria were downloaded in full text and documented carefully for further deep reading and data analysis.

3.5 Data Extraction

After screening and selecting the eligible articles, qualitative and quantitative data were gathered and extracted from the relevant literature for the study of chitosan composites, characterisation techniques, factors affecting biosorption, biosorption kinetics, isotherms and thermodynamics. This step was performed prior to the data analysis to ensure that adequate data were available for the analysis in Chapter 4. The qualitative data such as literature theories and observation described in words were gathered from the discussion among the researchers about a topic (Galadima and Muraza, 2020). It was then presented in descriptive statements that conceptualised an idea or theoretical viewpoint.

In contrast, the collected quantitative data were extracted from the experiment results and expressed in number form (Galadima and Muraza, 2020). The collected data were then organised in tabular form according to the type of chitosan composites, the type of dyes, the parameter studies, the name of authors and the year of publications using Microsoft Excel. In this way, the collected data from different works of literature could be compared and analysed easily.

3.6 Data Analysis and Report Writing

At the last step, the data analysis was carried out to summarise the collected data and discover useful information for data interpretation. The data collected was interpreted by using analytical and logical reasoning to determine the correlations, patterns and trends in the results. In general, the qualitative and quantitative analysis were used in combination to analyse the data expressed in words and numbers, respectively (Rekik, et al., 2018).

In qualitative analysis, the data collected were analysed and categorised according to similar factors under a keyword definition to identify their similar themes, connections and patterns that could be used for answering the review questions. Afterwards, the analysed data were interpreted and summarised to propose new findings and conclusions to provide the reader with a deep understanding of the concepts and theories (Monteiro, et al., 2018). In contrast, the data collected for quantitative analysis were conducted using statistical methods and reported in tabular form. The data were analysed to investigate the relationship between the variables and to generate new insights into the relationships between concepts that were studied separately in the literature (Snyder, 2019). This analysis was also used to verify that the results fit well with the theory and hypotheses. After analysing the data, the interpreted data, conclusions and new findings were described in detail in the report writing in response to the research questions. In the context of the present review, Chapter 4 reports the findings extracted from other literature that is relevant to the review objective.

CHAPTER 4

RESULTS AND DISCUSSION

4.1 Characterisation Studies of Chitosan Composites

As with all innovative products, a major issue hindering the application of chitosan composites was reproducibility. Even with a proper methodological process was adhered to, this problem was unavoidable because the synthesised chitosan composites had a high tendency to be polydispersed in their morphology and changing their desired functions (Jacob, et al., 2018). This was why characterisation techniques were important for the study of chitosan composites since they could provide the information to determine the physical and chemical properties of the chitosan composites that could affect the removal efficiency of dyes. Therefore, various techniques such as SEM, EDX, surface area analysis, FTIR, XRD and TGA used to characterise chitosan composites were extensively discussed in the subsequent subsections along with descriptions of their use in recent literature.

4.1.1 Scanning Electron Microscopy (SEM)

SEM is the most commonly used characterisation technique for chitosan composites. SEM micrographs are generated to determine the morphological properties such as surface roughness, diameter and the structure of the cell wall that would affect the porosity of chitosan composites available for the adsorption of dyes (Chen, et al., 2014). The immobilisation of reinforcing material on the chitosan matrix can be examined from the SEM micrograph to analyse whether the reinforcing material is distributed homogeneously or heterogeneously on the chitosan surface (Yaashikaa, et al., 2020). The formation of chitosan composite was considered successful when the chitosan composite exhibited the similar surface structure of pristine chitosan and the reinforcing materials by comparing their SEM micrographs.

After conducting several review studies on the SEM micrographs of chitosan composite, the SEM micrographs indicated that the chitosan composites in Figure 4.1(b) had a larger surface area with a heterogeneous, irregular and rough surface as compared to pristine chitosan in Figure 4.1(a)

(Wan Ngah, et al., 2012; Azari, et al., 2019; Kausar, et al., 2019). It was also observed that the raw chitosan had a homogenous surface with banding and shrinkage but with less porous (Salam, Makki and Abdelaal, 2011; Azari, et al., 2019). Furthermore, SEM images can be used to verify whether the dyes molecules have successfully adsorbed on the surface of chitosan composite by observing the surface roughness (Chen, et al., 2014). Figure 4.1(c) demonstrates the surface structure of the activated carbon/chitosan/papaya seed (ACCHPS) composites changed significantly after the dye biosorption process. The rough surface of composite was transformed to a smooth surface with less porous.

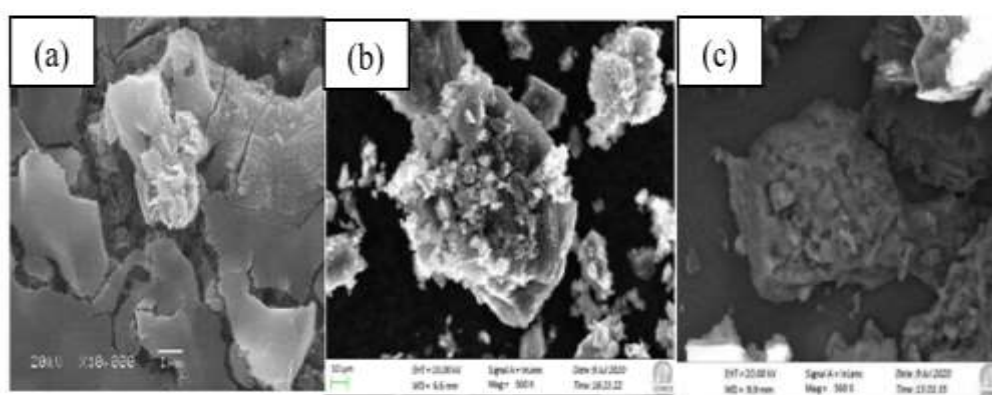


Figure 4.1: SEM Micrographs of (a) Pure Chitosan (Jawad and Abdulhameed, 2020a), (b) ACCHPS Composite with Unloaded Dyes and (c) ACCHPS Composite with Loaded Dyes (Idohou, et al., 2020).

This finding indicated that the dye molecules were effectively diffused into the pores and adsorbed on the adsorption site of chitosan, thereby reducing the porosity of chitosan composite. The dye molecules also interacted with the surface functional groups and resulted in the formation of layers on the surface of the composite (Idohou, et al., 2020). Similar observations also found in the dye biosorption process using the chitosan composite containing graphene oxide, zeolite, activated carbon, ZnO, Fe₃O₄ coupled with graphene oxide, kaolin clay and MgO (Han, et al., 2011; Metin, Çiftçi and Alver, 2013; Rangabhashiyam, Anu and Selvaraju, 2013; Arafat, et al., 2015; Tran, et al., 2017; Jawad, et al., 2020; Nga, Thuy Chau and Viet, 2020).

Besides, Figure 4.2(a) to Figure 4.2(c) reveal that the surface structure of chitosan composites incorporated with cellulose, PVA and MWCNTs, respectively. They exhibited a similar characteristic structure where the chitosan composites were arranged in randomly entangled network structures with multiple membrane layers. The internal structure of the respective composites had a good homogeneity, indicating that the reinforcing materials had good miscibility with chitosan. This was attributed to the dissolution of reinforcing materials and chitosan in sodium hydroxide solution by hydrogen bonding (Wang, et al., 2018). The findings also demonstrated that the cellulose, PVA and MWCNTs were successfully embedded on the chitosan matrix.

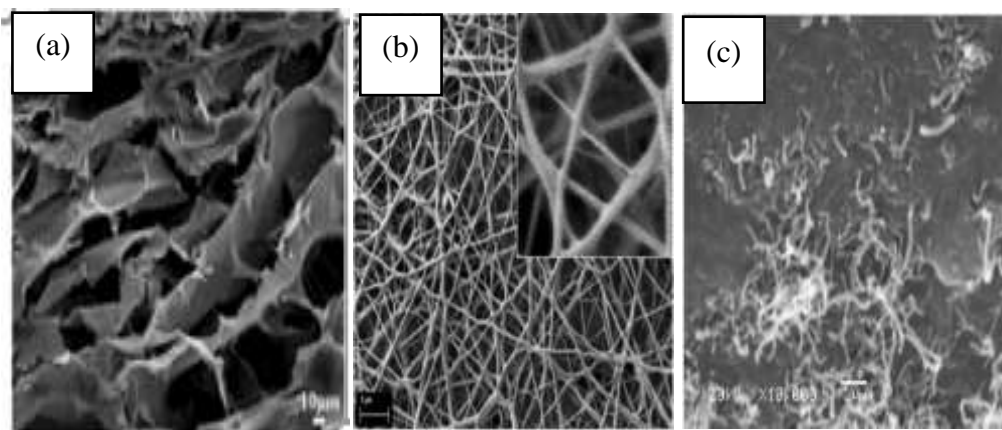


Figure 4.2: SEM Micrographs of (a) Chitosan/Cellulose (Wang, et al., 2018), (b) Chitosan/PVA (Anitha, Kumar and Kumar, 2016) and (c) Chitosan/MWCNTs Composites (Salam, Makki and Abdelaal, 2011).

4.1.2 Energy Dispersive X-ray (EDX)

Furthermore, EDX is commonly used in combination with SEM to determine the elemental composition of a sample before and after the modification process in order to confirm the formation of chitosan composite. Besides, EDX also has been employed in most of the characterisation studies to examine the elemental composition of chitosan composites after the dye biosorption process. The EDX analysis can verify whether the dye molecules have successfully adsorbed on the chitosan composite. Table 4.1 summarises the elemental composition of pure chitosan and chitosan composites loaded with and without dyes.

Table 4.1: Elemental Composition of Chitosan Composites Before and After Biosorption of Dyes.

| Chitosan Composites | Before/After Biosorption | Elemental Compositions | References |
|--|---------------------------------|--|--|
| Pure Chitosan | Before | 51.04 wt% Carbon (C), 30.48 wt% oxygen (O) and 18.48 wt% nitrate (N) | Marrakchi, Hameed and Hummadi (2020) |
| Chitosan/kaolin clay | Before | 23.04 wt% C, 33.46 wt % O, 7.01 wt% N, 30.97 wt% silicon (Si) and 4.06 wt% alumina (Al) and 1.46 wt% phosphate (P) | Jawad, et al. (2020) |
| | After | 31.84wt% C, 21.28 wt% O, 7.93 wt% N, 28.56 wt % Si, 3.25 wt% Al, 1.27 wt% P and 5.87 wt % sulphur (S) | |
| Chitosan/quartzite | Before | 23.01 wt% C, 39.08 wt% O, 36.34 wt% Si, 1.39 wt% calcium (Ca), 0.18 wt% magnesium (Mg) | Coura, Profeti and Profeti (2020) |
| | After | 23.14 wt% C, 39.57 wt% O, 36.78 wt% Si, 0.40 wt% Ca, 0.11 wt% Mg | |
| Chitosan-glyoxal/titanium oxide | Before | 1.52 wt% C, 0.45 wt% O, 0.91 wt% titanium (Ti), 97.12 wt% aura (Au) | Mohammad, Abdulhameed and Jawad (2019) |
| | After | 2.56 wt% C, 0.81 wt% O, 0.92 wt% S, 0.96 wt% Ti, 94.76 wt% Au | |

Table 4.1: Elemental Composition of Chitosan Composites Before and After Biosorption of Dyes (Continued).

| Chitosan Composites | Before/After Biosorption | Elemental Compositions | References |
|----------------------------------|-------------------------------------|--|--------------------------|
| Chitosan/zeolite | Before | 2.54 wt% C, 6.07 wt% N, 58.18 wt% O, 1.13 wt% sodium (Na), 0.59 wt% Mg, 4.95 wt% Al, 24.63 wt % Si, 1.91 wt% Ca | Dehghani et al. (2017) |
| | After | 2.63 wt% C, 4.62 wt% N, 58.70 wt% O, 1.63 wt% Na, 1.10 wt% Mg, 5.26 wt% Al, 23.14 wt % Si, 1.89 wt% Ca, 0.62 wt% S, 1.89 wt% chlorine | |
| Chitosan/ignosulfonate | Before | 47.86 wt% C, 43.49 wt% O, 7.05 wt% N, 1.55 wt% Na, 0.05 wt% S | Gu, et al. (2019) |
| | After | 53.14 wt% C, 34.23 wt% O, 9.47 wt% N, 2.85 wt% S, 0.32 wt% Na | |
| Chitosan/activated lignin | After | 34.63 wt% O, 8.59 wt% N, 52.31 wt% C, 3.85 wt% S, 0.62 wt% Na | Albadarin, et al. (2017) |
| Chitosan/silica oxide | Before | 29.75 wt% O, 8.14 wt% N, 33.04 wt% C, 24.68 wt% Si, 4.39 wt% Na | Riyanti, et al. (2020) |

It was observed that pure chitosan mainly comprised C, O and N elements. After the modification, additional elements were presented in the chitosan composite. For instance, Si and Al elements were widely found in chitosan/carbon-based composites, indicating the chitosan composites were successfully synthesised (Dehghani, et al, 2017; Jawad, et al., 2020). The presence of P was caused by the use of crosslinkers such as tripolyphosphate and epichlorohydrin, whereas Na was derived from sodium hydroxide to neutralise the composite during the crosslinking reaction (Wan Ngah, et al., 2012). After the biosorption process, there was an increase in the C and O composition percentage as well as the existence of S in the chitosan composite, which further proved that the dye molecules were successfully adsorbed on the composite surface (Mohammad, Abdulhameed and Jawad, 2019).

4.1.3 Surface Area Analysis

Surface properties such as Brunauer–Emmett–Teller (BET) specific surface area, total pore volume and average pore diameter of chitosan composite are among the significant contributors that will affect the performance and biosorption capacity of chitosan composite in the dye biosorption process. The agglomeration of nanoparticles on the chitosan surface may reduce the BET specific surface area of the composite and eventually decrease the dye adsorption. However, the uptake of dyes is not limited to physical adsorption in which ion exchange, surface functional groups and electrostatic interaction of chitosan composites also made a significant contribution to the dye remediation (Luo, Bai and Zhu, 2018).

The surface properties can be determined using a nitrogen physisorption isotherm (Chen, et al., 2014). The BET specific surface area can be expressed as the total surface area per unit mass of the chitosan composite, which strongly correlates with its pore size distribution and porosity. Next, the total pore volume can be defined as the void volume per unit mass of chitosan composite. The high BET specific surface area can provide more adsorption sites on the surface of chitosan composites, thus increasing the dye removal efficiency (Rocha, et al., 2020). Table 4.2 summarises the surface properties of various reinforcing materials, pure chitosan and synthesised chitosan composite for the removal of dyes.

Table 4.2: Surface Properties of Various Chitosan Composites.

| Chitosan Composites | BET specific surface area, S_{BET} (m ² /g) | | | Total Pore Volume, V_p (cm ³ /g) | Average Pore Diameter, d_p (nm) | References |
|---|---|----------|-----------|---|--|--|
| | Blending | Pure | Composite | | | |
| | Material | Chitosan | | | | |
| Chitosan/clay | - | 8.14 | 10.41 | 0.0067 | 2.59 | Kausar, et al. (2019) |
| Chitosan/carbon clay | 168.45 | - | 18.41 | 0.0238 | 4.41 | Marrakchi, Hameedb and Hummadi, (2020) |
| Chitosan/activated carbon | 458.23 | 0.141 | 256.82 | 0.1400 | 2.21 | Fatombi, et al. (2019) |
| Chitosan/ZnO | 9.79 | 1.75 | 2.24 | 0.0078 | 12.20 | Nguyen, Nguyen and Nguyen (2020) |
| Chitosan/Fe ₃ O ₄ /glutaraldehyde | 134.00 | - | 101.20 | 0.5880 | 11.00 | Azari, et al. (2019) |
| Chitosan/quartzite | - | 3.29 | 55.50 | 0.0550 | 3.95 | Coura, Profeti and Profeti (2020) |
| Chitosan/graphene oxide | - | 0.28 | 1.81 | 0.4980 | 7.14 | Kamal, et al. (2017) |
| Chitosan/silica | 739.00 | 150.0 | 247.00 | 1.013 | 16.40 | Wang, et al. (2015) |
| Chitosan/kaolin clay | - | 0.70 | 43.70 | 0.0800 | 7.08 | Jawad, et al. (2020) |
| Chitosan/ montmorillonite | 205.00 | 3.80 | 4.40 | 0.0760 | 6.96 | Bahrudin, Nawi and Sabar (2019) |

Generally, raw chitosan before the modification process had a lower BET specific surface area with a flak-like, less porous and homogeneous surface structure as confirmed by the SEM images discussed in the previous subsection (Salam, Makki and Abdelaal, 2011). After the chitosan modification process, the same trend was observed in Table 4.2, where all the chitosan composites had a larger BET specific surface area and total pore volume than raw chitosan. However, the chitosan/silica composite exhibited the largest BET specific surface area and total pore volume. This might be resulted from the attachment of the nanosized particles with a larger surface area on the chitosan surface and gave rise to a rough surface (Marrakchi, Hameedb and Hummadi, 2020). However, the BET specific surface area and total pore volume of composites were lower than the incorporated material. This might be attributed to the small part of silica pores being partly blocked by chitosan through the association of $-OH$ and $-NH_2$ functional groups in chitosan with the incorporated material (Kamal, et al., 2017; Azari, et al., 2019).

Based on the International Union of Pure and Applied Chemistry (IUPAC) classification, the pore size distribution of chitosan composite can be classified into three categories: i) micropores when the average pore diameter is less than 2 nm, ii) mesopores when the average pore diameter is between 2 and 50 nm and iii) macropores when it is more than 50 nm (Danish and Ahmad, 2018). Most of the chitosan composites listed in Table 4.2 were classified as mesoporous materials since their average pore diameter were within the range of 2-50 nm. The larger average pore diameter of composite could increase the accessibility of dye molecules diffused into the internal surface of composite and adsorbed on the adsorption site of chitosan composites. For instance, the average pore diameter of chitosan/kaolin clay composite (7.06 nm) was found to be larger than Reactive Blue 19 dye molecules (1.6 nm). As a result, dye molecules could easily penetrate into the inner pore of the composite and achieved 70.5 % removal of Reactive Blue 19 with an adsorption capacity of 560.9 mg/g (Jawad, et al., 2020).

The finding was comparable to other literature where the same trend was observed after chitosan was coated with zeolite, calcium alginate, cellulose and quartzite (Metin, Çiftçi and Alver, 2013; Vijayaraghavan, et, al., 2017; Wang, et al., 2018; Coura, Profeti and Profeti, 2020). The findings clearly proved that

incorporating reinforcing materials in the chitosan matrix greatly improved the surface properties of chitosan composite. The pristine chitosan with flak-like structure had been transformed to the rough surface with irregular shapes and sizes as supported by SEM micrographs (Bahrudin, Nawi and Sabar, 2019).

4.1.4 Fourier Transform Infrared (FTIR)

FTIR spectroscopy is a complementary technique for identifying chemical structure and surface functional groups present in the chitosan composites (Vinod, et al., 2020). As mentioned earlier, the dye biosorption process mainly depended on the functional groups present in the chitosan composites. They would interact with the dye molecules through weak electrostatic interactions, intermolecular hydrogen bonding and van der Waals interactions. In general, the specific functional groups present in the material could be determined based on the absorption bands and specific peaks observed in the FTIR spectrogram (Samrot, et al., 2020). It was observed that the FTIR spectrogram was constructed from the graph of transmittance against the wavelength.

Besides, different types of chitosan composites will produce unique spectra which are attributed to the stretching and bending vibration of the functional groups present in the respective chitosan composites (Li, et al., 2016; Quesada, et al., 2020). Therefore, FTIR spectroscopy is also used to ensure that the reinforcement materials are well immobilised in the chitosan matrix by identifying the new formation bonds. Hence, the pure chitosan and reinforcement material will be characterised separately as well. If the functional groups of the pure chitosan and the reinforcement materials are detectable in the FTIR spectrogram of chitosan composite, the result suggests that the chitosan composite is synthesised successfully. Moreover, the FTIR spectrum should be as similar as possible to the existing literature to ensure that the synthesised chitosan composite was composed of chitosan and reinforcement materials.

For example, Figure 4.3(a), (b) and (c) demonstrate the FTIR spectra of pure silica (reinforcement material), pure chitosan and chitosan/silica composite, respectively. The symmetrical and asymmetrical stretching vibrations of Si–O–Si bonds from the silica compound were observed at the peaks of 1083 and 803 cm^{-1} in the FTIR spectrum of chitosan/silica composite (Bahalkeh, et al., 2020). On the other hand, the absorption bands that appeared at 1561, 1641, 1090 and

656 cm^{-1} were denoted to the stretching vibration of CONH_2 , NH_2 , C-O-C and aromatic rings from the chitosan compound, respectively. As illustrated in Figure 4.3(c), the stretching vibration of O-H and N-H bonds at approximately 3347 cm^{-1} became wider because of the development of hydrogen bonding between $-\text{OH}$ and $-\text{NH}_2$ groups in chitosan and Si-O-Si bonds in silica compounds. The detection of these functional groups in the related spectrum confirmed the successful synthesis of chitosan/silica composite.

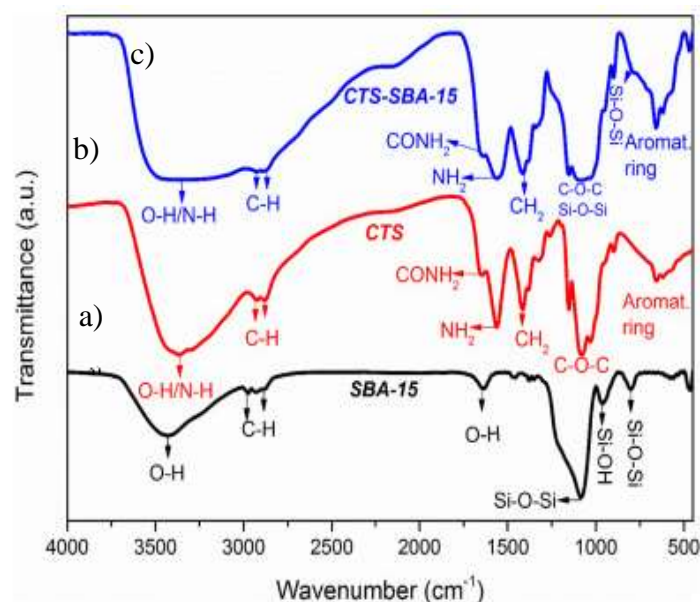


Figure 4.3: FTIR Spectra of (a) Silica, (b) Chitosan and (c) Chitosan/Silica Composite (Bahalkeh, et al., 2020).

Besides, several characterisation studies had been conducted to compare the FTIR spectra of various chitosan composites with the materials separately, concluding that the chitosan composite was a combination of both materials. A similar finding was reported in the literature where pure chitosan had similar functional groups. The major functional groups of chitosan with the respective wavelength are summarized in Table 4.3. For instance, the FTIR spectrum of pure chitosan had a typical wide absorption band of 3550-3200 cm^{-1} belonging to the O-H stretching that overlapped with the N-H stretching (Kumari, et al., 2015). The absorption bands located at 1385-1364, 1480-1440, 1580-1530, 1650-1620 and 2950-2860 cm^{-1} were referred to the C-N stretching in amide III, C-H bending, N-H bending of amide II, C=O stretching of amide I and C-H

stretching, respectively. The respective absorption bands can be found naturally in the pristine chitosan. Finally, the existence of ether group and glycosidic bonds could be confirmed by observing the absorption band at 1157-1031 and 990-890 cm^{-1} (Li, et al., 2016; Quesada, et al., 2020).

Table 4.3: Functional Groups of Chitosan with The Respective Wavelength (Kumari, et al., 2015; Li, et al., 2016; Quesada, et al., 2020).

| Wavelength (cm^{-1}) | Functional Groups |
|---------------------------------|---|
| 3550-3200 | O–H stretching overlapped with N–H stretching |
| 2950-2860 | C–H stretching |
| 1711-1700 | C=O stretching |
| 1650-1620 | C=O stretching of amide I |
| 1580-1530 | N–H bending of amide II |
| 1480-1440 | C–H bending |
| 1385-1364 | C–N stretching in amide III |
| 1157-1031 | Asymmetric C–O stretching in ether group |
| 990-890 | Stretching in glycosidic bonds |

Next, Table 4.4 summarises and tabulates the FTIR spectra of chitosan composites with their respective functional groups. The chitosan composites listed in Table 4.4 had a similarity where the characteristic bonds of pure chitosan such as O–H, C–H, C=O, N-H and C–O bonds were preserved in the chitosan composites. After the modification of chitosan, new formation bonds existed in the chitosan composites. Similar findings were obtained for the chitosan/clay, chitosan/kaolin clay, chitosan/quartzite and chitosan/bentonite composites, where they exhibited Si-O and Si-O-Si bonds at the absorption bands ranging between 1 165 and 1 050 cm^{-1} . In addition, the absorption bands at 676 and 500-795 cm^{-1} in the FTIR spectra of chitosan composite were assigned to the Al-O-Mg bond vibration of clay and Si-O-Al bond vibration of kaolin clay, respectively. These additional bonds could not be identified in the pure chitosan. Therefore, the results verified that clay, kaolin clay, quartzite and bentonite were successfully immobilised in the chitosan matrix.

Table 4.4: Summarisation of FTIR Spectra of Various Types of Chitosan Composites.

| Chitosan Composites | Wavelength (cm⁻¹) | Functional Groups | References |
|----------------------------------|-------------------------------------|--|-------------------------|
| Chitosan/clay | 1410 | CH–OH of raw chitosan | Kausar, et al. (2019) |
| | 1532 | N–H vibration of –CH ₂ and –NHCOCH ₃ group | |
| | 1538 | C=O group of chitosan | |
| | 1603 | C–H stretching of alkanes | |
| | 2918 | O–H stretching vibration | |
| | 2850 and 2853 | –CH ₂ stretching vibration | |
| | 676 | Al–O–Mg bond of clay | |
| | 1031 | Si–O bond vibration of clay | |
| Chitosan/activated carbon | 3410 | O–H stretching | Fatombi, et al. (2019). |
| | 1364 | C–N stretching from amide III in chitosan | |
| | 891 | N–H stretching vibration in primary and secondary amines | |
| | 1573 | N–H stretching vibration of amide II of chitosan | |
| | 1068 | C–O stretching or O–H deformation in carboxylic acid of activated carbon | |

Table 4.4: Summarisation of FTIR Spectra of Various Types of Chitosan Composites (Continued).

| Chitosan Composites | Wavelength (cm⁻¹) | Functional Groups | References |
|-----------------------------|-------------------------------------|---|-----------------------------------|
| Chitosan/kaolin clay | 3500 | O–H and N–H stretching | Jawad and Abdulhameed (2020a) |
| | 1645 | N–H bending vibration | |
| | 2900-2860 | C–H stretching vibration | |
| | 1375 | C–N stretching vibration | |
| | 940 | O–H in Al–OH bending vibration | |
| | 500-795 | Si–O–Al vibration | |
| | 1049 | Si–O–Si stretching vibration | |
| Chitosan/quartzite | 3600 to 3300 | O–H and N–H stretching vibration | Coura, Profeti and Profeti (2020) |
| | 2900 | C–H stretching vibration in –CH and –CH ₂ | |
| | 1650 | C=O stretching vibration | |
| | 1580 | N–H bonds of –NHCOCH ₃ | |
| | 1300 | C–H stretching deformation | |
| | 694 | Si–O symmetrical bending vibrations | |
| | 778; 1054 and 1165 | Si–O symmetrical and asymmetrical stretching vibrations | |

Table 4.4: Summarisation of FTIR Spectra of Various Types of Chitosan Composites (Continued).

| Chitosan Composites | Wavelength (cm⁻¹) | Functional Groups | References |
|----------------------------|-------------------------------------|--|--------------------------------|
| Chitosan/ZnO | 3718.76 | O–H and N–H stretching | Arafat, et al. (2015) |
| | 2924 and 2870 | –CH ₂ and –CH ₃ stretching of chitosan | |
| | 1647.21 | C=O stretching of amide I | |
| | 1577.77 | C=C functional group | |
| | 659.66 and 543.93 | O–Zn–O band | |
| Chitosan/MgO | 3697 and 1649 | O–H stretching vibration | Nga, Thuy Chau and Viet (2020) |
| | 3359 | N–H stretching vibration of –NH ₂ of chitosan | |
| | 1557 | N–H bending vibration | |
| | 2878 | C–H stretching | |
| | 1418 and 1377 | CH ₂ or CH ₃ bending vibration | |
| | 1148,1062 and 1029 | Stretching vibration of symmetric and asymmetric C–O from the C–O–C bond linkage | |
| | 894 | Saccharide structure vibration of chitosan | |
| | 667, 591 and 553 | Mg–O vibrations | |

Table 4.4: Summarisation of FTIR Spectra of Various Types of Chitosan Composites (Continued).

| Chitosan Composites | Wavelength (cm⁻¹) | Functional Groups | References |
|----------------------------|-------------------------------------|--|----------------------|
| Chitosan/bentonite | 3450 | O–H and N–H stretching of chitosan | Dotto, et al. (2016) |
| | 1711 | C=O stretching from acetic acid | |
| | 1630 | Amide band I from chitosan | |
| | 1550 | C–N stretching of chitosan | |
| | 1300 | H–C–H links | |
| | 1050 | Si–O bond of bentonite | |
| | 819 | O–Si–O asymmetric stretching | |
| | 701 | Si–O bond deformation and bending stretching | |
| | 505 | O–Si–O asymmetric bending | |
| Chitosan/cellulose | 1200-1400 | C–H and O–H bending | Wang, et al. (2018) |
| | 3420 | –OH and C–OH stretching | |
| | 2930 | CH ₂ stretching vibration | |
| | 1163 | C–O–C stretching absorption band | |
| | 3300-3450 | –OH and –NH ₂ stretching | |
| | 2900 | C–H bond stretching | |
| | 1549 | Secondary amine N–H bending | |

Table 4.4: Summarisation of FTIR Spectra of Various Types of Chitosan Composites (Continued).

| Chitosan Composites | Wavelength (cm⁻¹) | Functional groups | References |
|--------------------------------|-------------------------------------|--|-------------------------------------|
| Chitosan/MWCNTs | 1380 | C–H bonding | Salam, Makki and Abdelaal (2011) |
| | 1155 | O–H and N–H stretching vibration | |
| | 898 | C–H symmetric bending vibration | |
| | 1559 and 1658 | Free –NH ₂ groups | |
| | 1745 | C=O stretch in –NHCOCH ₃ group | |
| | 1532 | N–H bending of amide I | |
| | 3428 | N–H stretching vibration | |
| | 1049 | C=O stretching vibration in CONH | |
| | 1089 | C–O–C bonds | |
| Chitosan/graphene oxide | 3600-3120 | O–H and N–H stretching | Debnath, Parashar and Pillay (2017) |
| | 2906 | C–H stretching | |
| | 1650 | C=O stretching of –NHCOCH ₃ group | |
| | 1576 | N–H bending of –NH ₂ | |
| | 1706 and 1616 | –COOH and C=C stretching | |
| | 1385 | C–OH stretching | |
| | 1065 | C–O–C stretching | |

Table 4.4: Summarisation of FTIR Spectra of Various Types of Chitosan Composites (Continued).

| Chitosan Composites | Wavelength (cm⁻¹) | Functional groups | References |
|--|-------------------------------------|---|----------------------|
| Chitosan/ Fe₃O₄/ glutaraldehyde | 576 | Fe–O bending vibration | Azari, et al. (2019) |
| | 3430 | O–H vibration | |
| | 2861 | C–H group | |
| | 3410 | Primary amine and amide II overlapped with O–H band | |
| | 1558 | N–H bending vibration | |
| | 2350 | C=N bonding between chitosan and lutaraldehyde | |
| ACCHPS | 3443 | O–H functional group antisymmetric stretching vibration | Idohou, et al (2020) |
| | 2915 and 2848 | asymmetric stretching vibration of C-H | |
| | 1625 | C=O stretching vibration in amide I, amide II and amide III | |
| | 1540 | C=O stretching vibration in amide II | |
| | 1242 | C=O stretching vibration in amide III | |
| | 1455 | C–H bending vibration | |
| | 1152 | C–O–H stretching vibration in cellulose | |
| | 1077 | C–O–C stretching vibration in cellulose | |
| | 1029 | C=O functional groups stretching vibration in cellulose | |

Moreover, the peaks corresponding to C-O-H and C=O stretching of graphene oxide appeared at 1400 and 1725 cm^{-1} also found in the chitosan/graphene oxide composites (Debnath, Parashar and Pillay, 2017). The presence of these groups in graphene oxide and their interactions with chitosan also had been reported by Travlou, et al. (2013) and Kamal, et al. (2017).

Furthermore, it was reported that MgO had the major bands at 409 and 666 cm^{-1} due to Mg-O vibrations. The respective bands were shifted to high wavelengths at 553 and 667 cm^{-1} after the immobilisation of MgO on the chitosan surface (Nga, Thuy Chau and Viet, 2020). These results confirmed that chitosan was a matrix for the assembly of MgO nanoparticles and suggested that the formation of intermolecular interactions between chitosan and MgO might occur in the composites. In addition, the oxygen-containing groups in the cellulose structure such as C-O-H, C-O-C and C=O groups were detected in the ACCHPS composite FTIR spectra at 1152, 1077 and 1029 cm^{-1} , respectively. Besides, the peaks identified at 718 cm^{-1} were attributed to C-H and C-C stretching in the aromatic rings of activated carbon (Marrakchi, Hameed and Hummadi, 2020).

After the incorporation of ZnO onto the chitosan surface, additional new peaks appeared at 543.93 and 659.66 cm^{-1} , representing O-Zn-O stretching vibration of ZnO (Arafat, et al., 2015). A similar characteristic peak at 458.35 and 665 cm^{-1} correspondings to Zn-O stretching vibration also reported in the characterisation study of chitosan/ZnO composite by Salehi, et al. (2010). Similarly, the formation of chitosan/ Fe_3O_4 /glutaraldehyde composite could be verified from the specific peaks at 576 and 2350 cm^{-1} , corresponding to the Fe-O bending vibration and C=N bond stretching, respectively (Azari, et al., 2019).

Next, a similar finding was reported in the literature where the stretching vibration of O-H overlapped with N-H in pure chitosan was shifted to a lower wavelength in the chitosan composite when compared to their FTIR spectra (Fatombi, et al., 2019). This finding might be due to the strong interaction between - NH_2 and oxygen-containing groups of chitosan with the functional groups of reinforcement material. It had been reported that a distinct band at 1573 cm^{-1} was a result of bending vibration of aliphatic secondary amine and generation of C=N bond emanating from the reaction of chitosan with a crosslinking agent (Auta and Hameed, 2013; Azari et al., 2019).

Besides, FTIR spectroscopy also can be employed to analyse whether the dye molecules have been adsorbed on the chitosan composite via the identification of new peaks. After the uptake of dyes, additional peaks were observed at 1605, 1612 and 1615 cm^{-1} in chitosan/carbon-clay composites due to the stretching vibrations of ethylenic C=C and aromatic ring C=C bonds in the Indigo Carmine structure (Fatombi, et al., 2019). The FTIR spectrum of ACCHPS composite loaded with methylene blue also demonstrated additional new peaks emerged at 1420, 2848 and 2915 cm^{-1} were assigned to the stretching vibration of C=S, C=C from aromatic rings and C-H groups in methylene blue structure (Marrakchi, Hameed and Hummadi, 2020).

However, different findings were observed in the chitosan/ZnO composite. It was observed that the peaks at 2870 and 2924 cm^{-1} belonging to the CH₂ and CH₃ stretching vibrations of chitosan disappeared after the adsorption of malachite green dye. This might be due to the interaction between the functional groups on the chitosan composite surface with dye molecules through weak electrostatic interaction, intermolecular hydrogen bonding and van der Waals. Therefore, the availability of surface functional groups on the chitosan composite reduced after the biosorption process. Finally, the results concluded that most of the functional groups in composite shifted to lower wavelength and additional new bonds were formed during the adsorption process.

4.1.5 X-ray Diffraction (XRD)

XRD is a widely used technique to evaluate the amorphous and the degree of crystallinity of chitosan composite. In general, the working principle of XRD is by irradiating the incident X-rays directly onto the chitosan composite and then measuring the scattering angle and intensity of the X-rays that leave the chitosan composite (Yaashikaa, et al., 2020). The diffracted X-rays generate a pattern that can provide researchers with a wealth of information on crystal structure, phase properties, lattice parameters and crystalline morphology (Rocha, et al., 2020).

Besides, XRD analysis has been employed to verify the successful incorporation of reinforcement material in the chitosan matrix. The analysis usually will be carried out separately for the pure chitosan and reinforcement

material to evaluate their diffraction patterns. The diffraction patterns also allow the identification of chemical compositions present in chitosan composites by comparing the diffraction pattern of chitosan composite to the known patterns (Jafri, et al., 2018). For any synthesised chitosan composites, the generated XRD diffraction patterns with characteristic peaks should compare with existing XRD patterns in the literature to validate the identification.

For instance, similar XRD patterns of pure chitosan have been reported in the literature where most of the pure chitosan having two characteristic peaks, usually located at approximately 2θ of 10° and 20° (Nakkeeran, et al., 2018; Kausar, et al., 2019). The θ represents Bragg's angle in unit of radian. The finding suggested that pure chitosan was an amorphous material consisting of a large number of $-OH$ and $-NH_2$ groups in its structure. The presence of these functional groups resulted in the formation of hydrogen bonds and the generation of amorphous structures in the chitosan. The 2θ values of pure chitosan obtained in some research works were slightly different. For example, Wan Ngah, et al. (2012) found that the two characteristic peaks were at 9.8 and 19.8° , whereas Huyen, et al. (2017) reported the peaks located at 9.86 and 20.30° . This might be attributed to the degree of chitosan deacetylation (Teofilović, et al., 2014).

Moreover, a similar observation could be seen in the XRD spectra of chitosan composites where the characteristic peak of chitosan at approximately $2\theta = 20^\circ$ became broader after the reinforcement material was added to the chitosan matrix (Xie, et al., 2013; Idohou, et al, 2020). The peak position was moved to a higher diffraction angle, suggesting the formation of strong intermolecular interaction between chitosan and reinforcement material. However, the characteristic peak of chitosan at 2θ of 10° disappeared in the XRD pattern of chitosan composites. The disappearance of the peak might be due to a reduction in crystallinity, which suggested that the chitosan had lost its crystalline structure, resulting from the successful modification of chitosan with reinforcement material (Arafat, et al., 2015; Azari, et al., 2019).

On the other side, the diffraction peaks of activated carbon also showed an amorphous phase at $2\theta = 24.29, 26, 28.1, 30.81$ and 32.05° . The peak at $2\theta = 22.75^\circ$ and the peaks at $2\theta = 24.69$ and 28.52° observed in the XRD patterns of chitosan/activated-carbon composite were attributed to chitosan and

activated carbon, respectively (Fatombi, et al., 2019). Due to the formation of a hydrogen bond between chitosan functional groups and crosslinking with epichlorohydrin, the crosslinked composites resulted in a decrease in the peak intensity and crystallinity, concluding that the composite became more amorphous than pristine chitosan. Similarly, Auta and Hameed (2013) and Quesada, et al. (2020) also reported the characteristic peaks of chitosan and activated carbon were presented in chitosan/activated carbon composite.

Due to the amorphous nature of chitosan, two broad peaks at $2\theta = 14.9$ and 20.3° were exhibited in the chitosan/graphene-oxide composite loaded with different graphene oxide content (Han, et al., 2011). The diffraction patterns of all the composite films were similar to the raw chitosan. However, the crystallinity of chitosan reduced after the introduction of graphene oxide. The diffraction peaks corresponding to graphite oxide were not visible in the composite films, indicating their exfoliation. However, with the increase of graphene oxide content, the chemical structure of chitosan in the composite membrane hardly changed. This indicated the interaction between chitosan and graphene oxide was mainly a physical reaction rather than a chemical reaction (Travlou et al., 2013; Kamal, et al., 2017).

In addition, raw clay was successfully immobilised in the chitosan matrix, as evident from the diffraction peaks in the XRD patterns of chitosan/clay composite at $2\theta = 23.40, 43.07$ and 53.80° (Hassan, et al., 2019). The respective diffraction peaks were assigned to the presence of quartz, calcite and dolomite. For the synthesis of chitosan/bentonite composite, the characteristic diffraction peaks determined at $2\theta = 6.0$ and 25.0° corresponded to bentonite and chitosan, respectively (Dotto, et al., 2016).

In the XRD diffractogram of chitosan/ Fe_3O_4 /glutaraldehyde composite, six characteristic peaks of Fe_3O_4 at $2\theta = 35.4, 43.1, 52.4, 59.8, 63.1$ and 73.4° were also observed along with $2\theta = 20.4^\circ$ corresponding to chitosan. This indicated the maintenance of Fe_3O_4 polygon phase after chitosan loading (Azari, et al., 2019). In addition, Fan, et al. (2013) also reported a similar finding where six characteristic peaks of Fe_3O_4 at $2\theta = 30.15, 36.27, 43.32, 53.89, 57.13,$ and 62.29° also appeared in the magnetic β -cyclodextrin-chitosan/graphene oxide composite. This indicated the composite was successfully loaded with Fe_3O_4 . Furthermore, the diffraction peaks corresponding to kaolin clay in the XRD

spectra of chitosan/kaolin clay composite were at $2\theta = 12.4, 19.9, 24.8, 35.9, 38.4, 45.5, 55.2$ and 62.3° (Jawad and Abdulhameed, 2020a). The peak at around $2\theta = 20.5^\circ$ confirmed the presence of chitosan in the composite. Similar XRD patterns of kaolin clay and chitosan were also reported by Jawad, et al. (2020) for the synthesis of epichlorohydrin crosslinked chitosan/kaolin-clay composite.

Moreover, the chemical composition of chitosan composites also can be determined by superimposing the lattice plane to a database called Joint Committee on Powder Diffraction Specifications (JCPDS). For instance, the diffraction peaks of $2\theta = 39.97, 58.91$ and 62.15° in the XRD patterns of chitosan/MgO composite were well-matched with the cubic lattice of MgO according to JCPDS No. 4-829. The XRD spectra could be indexed to the (111), (110) and (220) planes of the MgO, respectively (Nga, Thuy Chau and Viet, 2020).

As for chitosan/ZnO composite, the peaks at 2θ values of 31.8, 34.4, 36.2, 47.5, 56.6, 62.8, 66.3, 68.1, and 69.3° were assigned to the crystal planes of ZnO at (100), (002), (101), (102), (110), (103), (200), (112) and (201), respectively (Arafat, et al., 2015). Furthermore, Salehi, et al. (2010) and Muinde, et al. (2020) also obtained similar results after introducing ZnO in the chitosan matrix. The respective lattice planes were consistent with the crystallographic data of ZnO with the JCPDS No. 36-1451. A broad peak at $2\theta = 20^\circ$ attributed to the amorphous chitosan also found in the modification of chitosan with MgO and ZnO. The results indicated that the chitosan composites were successfully synthesised.

Besides, XRD can also be employed to determine the crystalline particle size based on the Debye-Scherrer equation. According to the Debye-Scherrer equation, the crystallite sizes of Fe_3O_4 , chitosan and chitosan/ Fe_3O_4 composite were 28, 145 and 73 nm, respectively (Azari, et al., 2019). Furthermore, Salehi, et al. (2010) reported the chitosan/ZnO composite had a particle size of 28 nm. After the adsorption of dyes, the crystallinity of chitosan decreased. The characteristic peak of chitosan in the composite was shifted from 21.7 to 21.0° . The shifting at different angles might be due to the compression and expansion of the layers after the adsorption of dyes. The characteristic peak in the composite at $2\theta = 32.04, 43.1$ and 53.8° were attributed to the presence of quartz, calcite and dolomite, respectively (Kausar, et al., 2019).

4.1.6 Thermogravimetric (TGA)

TGA is a widely used thermal analysis technique to study the differences between chitosan and chitosan composite based on their thermal stability and thermal degradation. After conducting several literature studies, TGA was primarily carried out under controlled temperature conditions in the constant flow rate of the nitrogen atmosphere. The thermal stability and thermal degradation of a sample could be investigated by determining the weight loss of a sample as a function of temperature. Table 4.5 summarises the weight loss of samples and the thermal degradation temperature at different thermal degradation stages. Generally, all the investigated chitosan and chitosan composite experienced three thermal degradation stages except chitosan/silica/ZnO and chitosan/quartzite composites, where only two stages were observed.

The first stage that occurred below 200 °C was attributed to the desorption of water molecules physically adsorbed on the composite surface during the dehydration process (Salehi, et al., 2010). The second stage from 200 to 400 °C was probably due to the thermal degradation of chitosan and decomposition of volatile organic compounds since the reinforcement material was thermally stable in the temperature range. They were attributed to further deacetylation, depolymerisation through cleavage of glycosidic linkage, and the subsequent oxidation of the residues (Travlou, et al., 2013). As for the last stage, it corresponded to the carbonisation process. The decomposition of residues occurred in accordance with the degradation of the pyranose ring under extremely high temperatures at above 400 °C (Alizadeh, et al., 2018)

It was found that the thermal stability of pristine chitosan was lower than that of chitosan composite when subjected to high temperature conditions and its weight loss was higher. The TGA results indicated that the incorporation of reinforcement material in the chitosan matrix as a thermal barrier had significantly improved the thermal stability of the composite. This was mainly due to the high thermal stability and the degree of dispersion of reinforcement material which provided lower weight loss as could be seen in the final residue of the thermal process. The increase in thermal stability was also an outcome of strong chemical interaction between chitosan and reinforcement material.

Table 4.5: TGA Data for Chitosan Composite at Different Thermal Degradation Stages.

| Chitosan Composites | First Stage | | Second Stage | | Third Stage | | References |
|---|-------------|----------|--------------|----------|-------------|----------|-----------------------------------|
| | Temperature | Weight | Temperature | Weight | Temperature | Weight | |
| | (°C) | loss (%) | (°C) | loss (%) | (°C) | loss (%) | |
| Chitosan | 25-125 | 12 | 170-265 | 41.00 | 265-530 | 45.00 | Kausar, et al. (2019) |
| Chitosan/ZnO | 50-150 | 13.49 | 220-350 | 16.21 | 350-600 | 8.67 | Arafat, et al. (2015) |
| Chitosan/quartzite | 45-110 | 1.00 | 225-500 | 12.00 | - | - | Coura, Profeti and Profeti (2020) |
| Chitosan/bentonite | 30-140 | 10.00 | 227-377 | 34.87 | >377 | 15.00 | Teofilović, et al. (2014) |
| Chitosan/MWCNTs | 50-155 | 10.00 | 225-325 | 21.00 | 325-1125 | 38.00 | Abbasi and Habibi (2016) |
| Chitosan/silica/ZnO | 50-250 | 12.00 | 290-630 | 23.00 | - | - | Hassan, et al. (2019) |
| Chitosan/γ-Fe₂O₃ | 27-150 | 17.00 | 150-480 | 40.00 | 480-780 | 11.00 | Zhu, et al. (2010) |
| Chitosan/activated carbon | 45-110 | 7.00 | 110-315 | 38.33 | 315-510 | 42.17 | Fatombi, et al. (2019) |
| Chitosan/MgO | 25-100 | 12.00 | 250-350 | 36.00 | 350-600 | 24.00 | Nga, Thuy Chau and Viet (2020) |

Moreover, these findings were consistent with the results obtained by other researchers. They also reported the thermal stability of chitosan had greatly improved after the incorporation of graphene oxide, bentonite, activated carbon, clay, quartzite and MgO (Travlou, et al., 2013; Teofilović, et al., 2014; Fatombi, et al., 2019; Kausar, et al., 2019; Coura, Profeti and Profeti, 2020; Nga, Thuy Chau and Viet, 2020).

Among the composites shown in Table 4.5, the chitosan/ZnO composite was the most thermal stable where it contributed the least weight loss during the heating process. The discussion above could be supported by the TGA graph of chitosan, ZnO, and chitosan/ZnO composite in Figure 4.4. In the TGA curve of chitosan, the first stage occurred below 120 °C with weight loss of 13.49 %, whereas the second and third stages occurred in the temperature range of 220-350 °C and above 350 °C with weight loss of 26.50 % and 13.49 %, respectively (Nguyen, Nguyen and Nguyen, 2020). ZnO nanoparticle is a metal oxide that could withstand extremely high temperature up to 800 °C with 2.08 % weight loss were introduced in the chitosan matrix for the synthesis of chitosan/ZnO composite. As compared to the composite, the maximum degradation rate of pure chitosan at the second stage was shifted from 251.8 to 261.2 °C with a lower weight loss of 16.21 %. The degradation rate of residual chitosan in the third stage was transferred from 440.8 °C in chitosan to 459.5 °C accounted for 8.67 % weight loss. Other researchers also reported similar results (Salehi, et al., 2010; Arafat, et al., 2015).

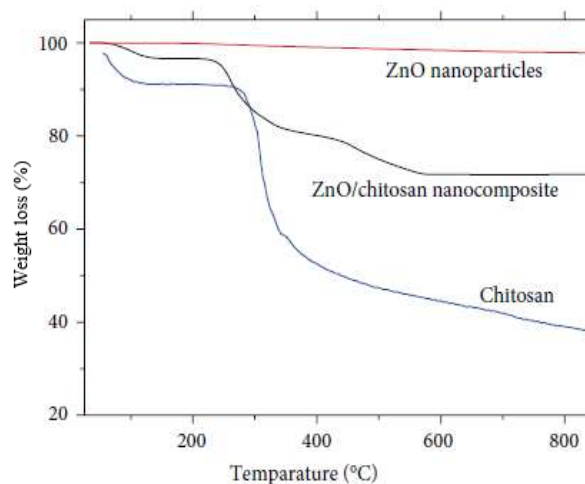


Figure 4.4: TGA Graph of Chitosan, ZnO Nanoparticle and Chitosan/ZnO Composite (Nguyen, Nguyen and Nguyen, 2020).

On the contrary, the chitosan/activated carbon composite experienced the highest weight loss during the heating process, as shown in Table 4.5. This might be attributed to the incorporation of cellulose which consisted a high amount of lignin, hemicellulose, cellulose and volatile matter on the chitosan matrix (Bazan, et al., 2016; Wyasu, et al., 2016). In the first stage, a minor weight loss of approximately 7.00 % occurred in the temperature range of 45-110 °C was attributed to the evaporation of water absorbed on the composite surface. In the second stage, hemicellulose, cellulose and volatile matter were decomposed when temperature increased from 110 to 315 °C and resulted in 38.33 % weight loss. Finally, the thermal process continued up to 510 °C and experienced a weight loss of 42.17 % due to the decomposition of lignin and surface functional groups. Although chitosan/activated carbon exhibited the highest weight loss compared to other composites, its thermal stability was higher than pure chitosan and pure activated carbon. A similar observation was also reported in the TGA study of chitosan/activated carbon conducted by Quesada, et al. (2020).

4.2 Biosorption Kinetics

The biosorption kinetic studies are very useful in determining the biosorption rate of dye molecules on the surface of the chitosan composite and the time required to achieve biosorption equilibrium (Nešić, Veličković and Antonović, 2013). The kinetic studies are conducted to identify the rate-limiting step and biosorption mechanism such as mass transfer, diffusion and chemical reaction. Several mathematical models have been employed in the literature to investigate kinetic studies.

In a recent analysis, the fitness of experimental data of dyes removal by chitosan composite was examined using two common kinetic models namely, pseudo-first-order (PFO) and pseudo-second-order (PSO) kinetic model equations. These kinetic models can evaluate whether the biosorption process involves physisorption or chemisorption as well as investigate the reaction order. The corresponding kinetic models are expressed in Equation 4.1 and Equation 4.2 (Zhang, Zhou and Ou, 2012; Abbasi and Habibi, 2016). The PFO kinetic model reveals that the rate of dye biosorption is proportional to the amount of dye adsorbed on the chitosan composite. The PSO kinetic model shows that the

biosorption rate is proportional to the square of the amount of dyes adsorbed on the biosorbent (Jabar, et al., 2020).

PFO model linear equation,

$$\log(q_e - q_t) = \log q_e - \left(\frac{k_1}{2.303}\right)t \quad (4.1)$$

PSO model linear equation,

$$\frac{t}{q_t} = \frac{1}{k_2 q_e^2} + \left(\frac{1}{q_e}\right)t \quad (4.2)$$

where

q_e = mass of dyes adsorbed per unit mass of chitosan composite at equilibrium condition, mg/g

q_t = mass of dyes adsorbed per unit mass of chitosan composite at any time t , mg/g

t = contact time, min

k_1 = rate constant of PFO model, min^{-1}

k_2 = rate constant of PSO model, $\text{g}/(\text{mg}\cdot\text{min})$

The selection of the kinetic models mainly depends on the fitness of the experimental data based on the coefficient of determination (R^2) value. Besides, the calculated biosorption at equilibrium value should be close to the experimental biosorption at equilibrium value (Simonin, 2016). If the experiment data is well fitted to the PFO model with a R^2 value close to 1, it suggests that physical sorption will be the rate-limiting step of the biosorption. Vice versa in the case of the PSO model, the rate-limiting step is the chemisorption. In general, the biosorption rate constants and biosorption at equilibrium value of both kinetic models are computed based on the slope and intercept of the graph, respectively. The slope and the intercept of the linear plot of $\log(q_e - q_t)$ against t are used to predict the rate constant and biosorption at equilibrium values for the PFO model. As for the PSO model, the rate constant

and biosorption at equilibrium values are determined based on the slope and intercept of the linear graph of t/q_t against t (Rangabhashiyam and Balasubramanian, 2019).

The kinetic data for the removal of various dyes using different types of chitosan composites obtained from the literature are summarised in Table 4.6. It could be observed that all the biosorption processes studied in the literature were well fitted to the PSO kinetic model with a higher R^2 value than the PFO model. Furthermore, the value of biosorption at equilibrium calculated from the PSO model demonstrated a smaller difference with the experimental biosorption at equilibrium value than those calculated from the PFO model. Therefore, these findings suggested that the biosorption of dyes was better defined by the PSO model instead of the PFO model. The findings indicated that the biosorption of dye molecules was dominated by chemical sorption, which involved the sharing of valence forces or electron exchange between the dyes and the active sites on the surface of chitosan composite (Abbasi and Habibi, 2016).

Among the chitosan composites listed in Table 4.6, chitosan/cellulose composite demonstrated the highest experimental biosorption at equilibrium value of 381.70 mg/g. This might be attributed to the high availability of surface functional groups on chitosan/cellulose such as $-OH$ and $-COOH$ groups provided by the cellulose that facilitated the chemical interaction with dye molecules. According to the SEM analysis conducted by Wang, et al. (2018), the result indicated that chitosan/cellulose composite showed an internal structure with highly porous and multiple membrane layers. Therefore, the high porosity of chitosan/cellulose composite contributed to a large adsorption site for the biosorption of dyes, resulting in high biosorption capacity.

Since PFO and PSO models could only be employed to evaluate the type of biosorption, therefore the diffusion mechanism of the dye biosorption was studied by applying the intraparticle diffusion model. The respective model was developed by Weber and Morris and expressed in Equation 4.3 (Dehghani, et al., 2017; Fatombi, et al., 2019). The intraparticle diffusion model can determine the type of biosorption mechanisms that limits the biosorption rate.

Table 4.6: Kinetic Constants of PFO and PSO Kinetic Models for Biosorption of Various Dyes onto Chitosan Composites.

| Chitosan Composites | Type of Dyes | $q_{e,exp}$ (mg/g) | PFO Model | | | PSO Model | | | References |
|---------------------------|----------------|-----------------------|-----------------------|-------------------------------|--------|-----------------------|-----------------------|--------|-----------------------------------|
| | | | $q_{e,cal}$ (mg/g) | k_1 (min ⁻¹) | R^2 | $q_{e,cal}$ (mg/g) | k_2 (g/(mg·min)) | R^2 | |
| Chitosan/quartzite | Reactive black | 20.15 | 18.91 | 6.100 | 0.9682 | 21.55 | 0.0003 | 0.9918 | Coura, Profeti and Profeti (2020) |
| Chitosan/zeolite | Methylene blue | 23.04 | 7.40 | 0.0820 | 0.8000 | 23.75 | 0.0210 | 0.9970 | Dehghani, et al. (2017) |
| Chitosan/activated carbon | Indigo carmine | 23.98 | 7.80 | 0.7930 | 0.7790 | 2.04 | 0.8650 | 0.9980 | Fatombi, et al. (2019) |
| Chitosan/cellulose | Congo red | 381.70 | 376.70 | 0.0106 | 0.8552 | 419.20 | 5.04×10^{-6} | 0.9529 | Wang, et al. (2018) |
| Chitosan/graphene oxide | Congo red | 2.53 | 2.53 | 0.2440 | 0.8680 | 2.35 | 0.8650 | 0.9990 | Kamal, et al. (2017) |
| Chitosan/MgO | Reactive blue | 10.47 | 6.07 | 0.0051 | 0.7287 | 8.55 | 0.0045 | 0.9775 | Nga, Thuy Chau and Viet (2020) |

Table 4.6: Kinetic Constants of PFO and PSO Kinetic Models for Biosorption of Various Dyes onto Chitosan Composites (Continued).

| Chitosan Composite | Type of Dyes | $q_{e,exp}$ (mg/g) | PFO Model | | | PSO Model | | | Reference |
|--|-----------------|-----------------------|-------------|----------------------|--------|-------------|--------------|--------|---------------------------|
| | | | $q_{e,cal}$ | k_1 | R^2 | $q_{e,cal}$ | k_2 | R^2 | |
| | | | (mg/g) | (min ⁻¹) | | (mg/g) | (g/(mg·min)) | | |
| Chitosan/ZnO | Acid Black 26 | 92.00 | 53.46 | 0.4190 | 0.9360 | 100.00 | 0.0330 | 1.0000 | Salehi, et al. (2010) |
| Chitosan/clay | Rose FRN | 12.12 | 12.01 | 0.1770 | 0.9140 | 12.26 | 0.0358 | 0.9560 | Kausar, et al. (2019) |
| Chitosan/kaolin-clay | Reactive blue | 312.40 | 296.10 | 0.0640 | 0.9200 | 316.60 | 0.0320 | 0.9800 | Jawad, et al. (2020) |
| Chitosan/MWCNT | Direct blue | 30.12 | 3.90 | 0.0083 | 0.9670 | 30.12 | 0.0007 | 0.9730 | Abbasi and Habibi (2016) |
| Chitosan/alumina | Methyl orange | 41.76 | 10.14 | 0.0490 | 0.8430 | 43.59 | 0.0070 | 0.9990 | Zhang, Zhou and Ou (2012) |
| Chitosan/bentonite | Amido Black 10B | 239.90 | 121.10 | 0.0093 | 0.9840 | 246.90 | 0.0002 | 0.9965 | Liu, et al. (2015) |
| Chitosan/ γ-Fe₂O₃ | Methyl orange | 31.58 | 25.14 | 0.0059 | 0.9800 | 36.26 | 0.0003 | 0.9950 | Zhu, et al. (2010) |

Intraparticle diffusion model linear equation,

$$q_t = k_p t^{0.5} + C \quad (4.3)$$

where

k_p = rate constant of intraparticle diffusion, mg/(g·min^{0.5})

C = y-intercept of the graph that related to the boundary layer thickness, mg/g

Generally, the biosorption process was assumed to take place in these three consecutive steps: film diffusion, intraparticle diffusion and biosorption (Michalak, Chojnacka and Witek-Krowiak, 2013). Firstly, it involved the external mass transfer of dye molecules from the bulk solution across the boundary layer to the external surface of the chitosan composite. Secondly, it involved intraparticle diffusion, where the dye molecules diffused from the external surface to the internal surface of chitosan composite by passing through the pores. Lastly, it was followed by the biosorption of dye molecules on the binding sites of chitosan composite until achieving equilibrium (Vidal and Moraes, 2019).

By plotting the linear graph of q_t against $t^{0.5}$, the values of the rate constant of intraparticle diffusion and y-intercept can be obtained from the slope and intercept of the graph. For example, Figure 4.5 demonstrates the linear plot of q_t against $t^{0.5}$ of intraparticle diffusion model for the biosorption of Reactive Blue 5 dyes using chitosan/quartzite composite (Wang, et al., 2018). According to Figure 4.5, the biosorption process comprised three sections of the linear line. The first section with a deeper gradient was attributed to the effect of the boundary layer. The dye molecules were transported through film diffusion at a high diffusion rate to the external surface of chitosan/cellulose composite. Once the external surface was saturated, the dye molecules further diffused through the pore and reached the internal surface of chitosan/cellulose. This phenomenon was resulted from the intraparticle diffusion effect and was represented by the second section with a smaller gradient. Lastly, the equilibrium adsorption of dye molecules on the binding site of chitosan composite occurred in the third section of the linear line.

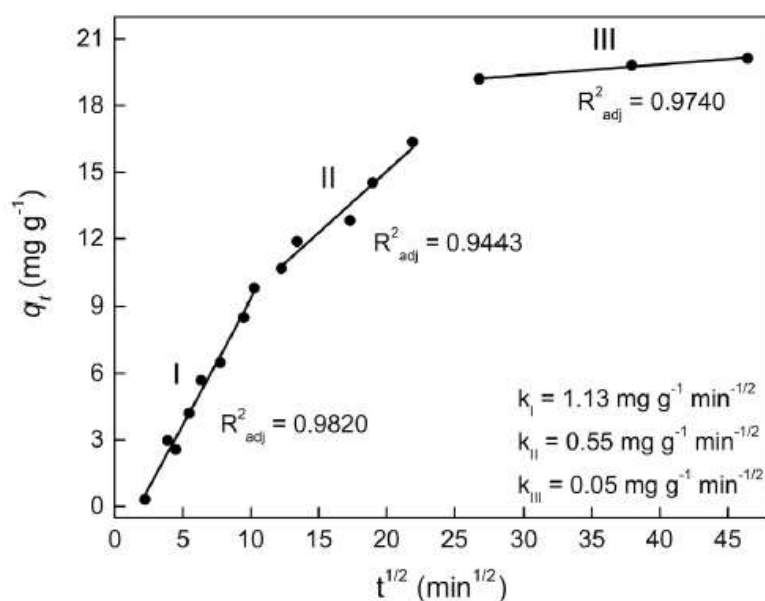


Figure 4.5: Linear Graph of Intraparticle Diffusion Model for Biosorption of Reactive Blue 5 by Chitosan/Quartzite Composite (Wang, et al., 2018).

Similar findings also reported in the literature on the synthesis of chitosan composite with the incorporation of ZnO, γ -Fe₂O₃, zeolite, PVA and activated carbon (Salehi, et al., 2010; Zhu, et al., 2010; Dehghani, et al., 2017; Habiba, et al., 2017; Fatombi, et al., 2019). After conducting the literature studies, the values of the rate constant of intraparticle diffusion and y-intercept for various chitosan composites are tabulated in Table 4.7. According to the model, if the intraparticle diffusion is the rate-limiting step in the dye biosorption process, the linear line should intercept the origin. However, none of the model lines for the investigated chitosan composites passed through the origin. The greater y-intercept value implied that the biosorption process was influenced not only by the intraparticle diffusion but also by a certain degree of boundary layer (Jabar, et al., 2020). The greater the value of y-intercept, the more significant the boundary layer effect.

Table 4.7: Intraparticle Diffusion Model Parameters for Biosorption of Dyes by Chitosan Composites.

| Chitosan Composites | Types of Dyes | Intraparticle Diffusion Model | | References |
|--|----------------|---------------------------------------|---------------|-------------------------|
| | | k_p (mg/(g·min ^{0.5})) | C (mg/g) | |
| Chitosan/zeolite | Methylene blue | 0.501 | 19.23 | Dehghani, et al. (2017) |
| Chitosan/activated carbon | Indigo carmine | 1.648 | 20.865 | Fatombi, et al. (2019) |
| Chitosan/cellulose | Congo red | 0.1553 | 389.9 | Wang, et al. (2018) |
| Chitosan/ZnO | Acid black | 12.84 | 38.9 | Salehi, et al. (2010) |
| Chitosan/PVA | Methyl orange | 1.517 | 9.343 | Habiba, et al. (2017) |
| Chitosan/ γ-Fe₂O₃ | Methyl orange | 0.63362 | 14.61 | Zhu, et al. (2010) |

4.3 Biosorption Isotherms

The biosorption isotherms are widely used to investigate the interaction type between dye molecules and chitosan composites as well as to estimate the maximum biosorption capacity. There are two common biosorption isotherm models such as Langmuir and Freundlich isotherm models, have been employed in the literature to determine the mass of dye molecules adsorbed onto the chitosan composite surface and the equilibrium concentration of dyes (Michalak, Chojnacka and Witek-Krowiak, 2013; Huyen, et al., 2017).

The Langmuir isotherm model assumes that the biosorption occurred on the homogenous surface of chitosan composite where the dye molecules adsorbed on a constant number of chitosan composite binding sites (Kamal, et al., 2017). Once the binding sites of chitosan composite were saturated, no further biosorption will occur as the maximum biosorption capacity was achieved. A monolayer of molecular thickness was formed on the chitosan

composite surface with no interaction between the dye molecules. Besides, the adsorption energy and enthalpy were assumed to be distributed equivalent to chitosan composite binding sites (Coura, Profeti and Profeti, 2020). The Langmuir isotherm model can be expressed in non-linear and linear as presented in Equation 4.4 and Equation 4.5, respectively (Zhang, Zhou and Ou, 2012; Abbasi and Habibi, 2016).

Langmuir isotherm model in non-linear form,

$$q_e = \frac{q_{\max} K_L C_e}{1 + K_L C_e} \quad (4.4)$$

Langmuir isotherm model in linear form,

$$\frac{C_e}{q_e} = \frac{1}{q_{\max} K_L} + \left(\frac{1}{q_{\max}}\right) C_e \quad (4.5)$$

where

C_e = equilibrium concentration of dyes, mg/L

q_{\max} = maximum biosorption capacity, mg/g

K_L = Langmuir constant, L/mg

Besides, another important Langmuir constant in the Langmuir isotherm model namely, separation factor can be employed to determine whether the dye biosorption is favourable, non-favourable, linear or irreversible. If the value of separation factor falls within the range between zero and one, it is considered a favourable biosorption process. Otherwise, the biosorption process is considered non-favourable when the separation factor value obtained is more than one. Meanwhile, the biosorption is considered linear when the separation factor value is equal to one and irreversible when the separation factor value is equal to zero (Liu, Zheng and Wang, 2010). The mathematical representation of separation factor is presented in Equation 4.6.

Separation factor of Langmuir isotherm model,

$$R_L = \frac{1}{1 + K_L C_o} \quad (4.6)$$

where

R_L = separation factor

C_o = concentration of dyes at initial process, mg/L

In contrast, the Freundlich isotherm model assumed that the biosorption took place on the heterogeneous surface of chitosan composite with the interaction between multilayer adsorption of dye molecules (Sadeghi-Kiakhani, Arami and Gharanjig, 2013). It also assumed the adsorption energy was non-uniformly distributed on the chitosan composite surface (Coura, Profeti and Profeti, 2020). The non-linear and linear form of Freundlich isotherm model equations are expressed in Equation 4.7 and Equation 4.8, respectively (Zhang, Zhou and Ou, 2012; Abbasi and Habibi, 2016). The heterogeneity factor (n) is significant in analysing the type of biosorption involved in the biosorption process. The biosorption process is linear when the value of heterogeneity factor is equal to one. Conversely, when heterogeneity factor is less than one or greater than one, the removal of dyes involves chemisorption or physisorption.

Freundlich isotherm model in non-linear form,

$$q_e = K_F C_e^{1/2} \quad (4.7)$$

Freundlich isotherm model in linear form,

$$\log q_e = \log K_F + \frac{1}{n} \log C_e \quad (4.8)$$

where

K_F = Freundlich constant related to the adsorption capacity, $(\text{mg/g})(\text{L/g})^{1/n}$

The linear plots for both isotherm models are established using the linear equation instead of the non-linear equation so that the adsorption isotherm parameters can be determined easily from the slope and intercept of the graph. For instance, the isotherm parameter values such as Langmuir constant and maximum biosorption capacity for the Langmuir isotherm model are obtained by plotting C_e/q_e against C_e . The slope and intercept of the respective graph represent Langmuir constant and maximum biosorption capacity, respectively. For the Langmuir isotherm model, the heterogeneity factor and Freundlich constant values can be computed from the slope and intercept of the linear plot, respectively by plotting $\log q_e$ against $\log C_e$. Table 4.8 tabulates and summarises the adsorption isotherm parameters of Langmuir and Freundlich isotherm models for the biosorption of dyes using different types of chitosan composites as biosorbents.

According to Table 4.8, the results revealed that most of the biosorption process fitted into the Langmuir isotherm model with a higher R^2 value than the Freundlich isotherm model. Langmuir isotherm model suggested that a monolayer of dye molecules was formed on the homogeneous surface of chitosan composite and no interaction between the dye molecules. The interaction between dye molecules and chitosan composite was stronger, reflecting that it was chemisorption. Since all of the Langmuir constant values were in the range between zero and one, this indicated that it was a favourable biosorption process.

However, some researchers found that the biosorption processes using chitosan/quartzite, chitosan/zeolite and chitosan/MgO as biosorbents were followed the Freundlich isotherm model with a higher R^2 value than the Langmuir isotherm model. The findings implied that the biosorption of dyes occurred on the heterogeneous surface. The interaction occurred between the dye molecules with chitosan composite and between the adsorbed dye molecules, resulting in the formation of multilayer molecular thickness. This was due to the presence of impurities adsorbed on the chitosan composites during the modification of pure chitosan (Huyen, et al., 2017). The impurities on the chitosan composite surface would cause different level of binding energy for the biosorption of organic dyes. The calculated heterogeneity factor values were more than one which indicated the removal of dyes involved physisorption.

Table 4.8: Adsorption Isotherm Parameters of Langmuir and Freundlich Isotherm Model for Biosorption of Various Dyes by Different Types of Chitosan Composites.

| Chitosan Composites | Type of Dyes | q_{max} (mg/g) | Langmuir Isotherm Model | | | Freundlich Isotherm Model | | | References |
|----------------------------------|----------------|---------------------|-------------------------|--------|--------|-------------------------------------|-------|--------|-----------------------------------|
| | | | K_L (L/mg) | R_L | R^2 | K_F (mg/g)(L/g) ^{1/n} | n | R^2 | |
| Chitosan/quartzite | Reactive black | 41.67 | 0.0300 | 0.4762 | 0.9580 | 9.17 | 3.900 | 0.9632 | Dehghani, et al. (2017) |
| Chitosan/zeolite | Methylene blue | 24.51 | 0.3030 | 0.1160 | 0.9560 | 8.82 | 3.788 | 0.9990 | Fatombi, et al. (2019) |
| Chitosan/activated carbon | Indigo carmine | 208.33 | 0.0230 | 0.4600 | 0.9954 | 14.18 | 1.190 | 0.9878 | Wang, et al. (2018) |
| Chitosan/cellulose | Congo red | 381.70 | 0.2633 | 0.0047 | 0.9729 | 132.90 | 5.488 | 0.8158 | Kamal, et al. (2017) |
| Chitosan/graphene oxide | Congo red | 370.37 | 0.0366 | 0.0546 | 0.9820 | 10.84 | 1.818 | 0.9160 | Coura, Profeti and Profeti (2020) |
| Chitosan/ZnO | Acid black | 227.30 | 0.0482 | 0.2075 | 0.9960 | 101.13 | 7.905 | 0.9620 | Nguyen, Nguyen and Nguyen (2020) |

Table 4.8: Adsorption Isotherm Parameters of Langmuir and Freundlich Isotherm Model for Biosorption of Various Dyes by Different Types of Chitosan Composites (Continued).

| Chitosan Composites | Type of Dyes | q_{max} (mg/g) | Langmuir Isotherm Model | | | Freundlich Isotherm Model | | | References |
|--|----------------|---------------------|-------------------------|--------|--------|-------------------------------------|-------|--------|--------------------------------|
| | | | K_L (L/mg) | R_L | R^2 | K_F (mg/g)(L/g) ^{1/n} | n | R^2 | |
| Chitosan/MgO | Reactive blue | 408.16 | 0.0127 | 0.4400 | 0.9544 | 5.55 | 1.090 | 0.9992 | Nga, Thuy Chau and Viet (2020) |
| Chitosan/PVA | Methyl orange | 52.10 | 0.0846 | 0.1912 | 0.9998 | 4.40 | 1.578 | 0.9946 | Habiba, et al. (2017) |
| Chitosan/kaolin clay | Reactive blue | 560.90 | 0.0060 | 0.4167 | 0.9600 | 11.80 | 1.600 | 0.9400 | Jawad, et al. (2020) |
| Chitosan/MWCNT | Direct blue | 29.33 | 0.3860 | 0.3860 | 0.9980 | 10.42 | 3.650 | 0.9660 | Abbasi and Habibi (2016) |
| Chitosan/alumina | Methyl orange | 32.67 | 0.8210 | 0.8210 | 0.9880 | 11.27 | 2.884 | 0.9720 | Zhang, Zhou and Ou (2012) |
| Chitosan/bentonite | Methylene blue | 496.40 | 0.1660 | 0.0197 | 0.9985 | 170.40 | 5.156 | 0.9251 | Liu, et al. (2015) |
| Chitosan/ γ-Fe₂O₃ | Methyl orange | 29.59 | 0.1340 | 0.1340 | 0.9980 | 5.23 | 2.163 | 0.9930 | Zhu, et al. (2010) |

For the comparison of maximum biosorption capacity values, chitosan/kaolin clay composite possessed the highest maximum biosorption capacity value of 560.90 mg/g among the chitosan composites listed in Table 4.8. The availability of –OH, silanol, and aluminol function groups on the surface chitosan/kaolin clay composite was attributed by incorporating kaolin clay (Jawad and Abdulhameed, 2020b). These additional surface functional groups corresponded to cellulose served as adsorption sites to interact electrostatically with the dye molecules that could maximise the biosorption capacity in order to reduce the dye concentration in the solution. The rough and irregular surface of chitosan/kaolin clay composite also helped to promote the biosorption of dyes.

In contrast, chitosan/zeolite composite exhibited the lowest maximum biosorption capacity value of 24.51 mg/g for the removal of methylene blue dyes as compared to the other chitosan composites. As suggested by the Freundlich isotherm model, the biosorption of methylene dyes occurred on the heterogeneous surface of chitosan/zeolite composite. The removal of methylene blue was dominated by the physisorption process rather than the chemisorption process. Hence, the weak intermolecular interaction between the biosorbent and dye molecules as well as between the dye molecules might be broken easily. This might be attributed to the collision between dye molecules as the dye concentration and temperature increased (Xie, et al., 2013). Consequently, the dye molecules were desorbed from the chitosan/zeolite surface and remained in the aqueous solution, resulting in lower adsorption capacity.

4.4 Biosorption Thermodynamics

Thermodynamic studies are usually carried out to investigate the effect of temperature on the dye biosorption process. Besides, the studies also provide detailed insight information on the feasibility, spontaneity and nature of the biosorption process as well as the orderliness of dyes molecules at the solid-liquid interface (Shazwani, et al., 2017). This information can be obtained by determining the thermodynamic parameters such as Gibb's free energy change (ΔG° in kJ/mol), enthalpy change (ΔH° in kJ/mol) and entropy change (ΔS° in J/(mol·K)). The corresponding thermodynamic parameters can be computed by

using the mathematical formulas from Equation 4.9 to Equation 4.11 (Habiba, et al., 2017; Jawad, et al., 2019; Hussain, et al., 2021).

$$K_c = \frac{C_s}{C_{e,m}} \quad (4.9)$$

$$\Delta G^\circ = -RT \ln K_c \quad (4.10)$$

$$\ln K_c = \frac{\Delta S^\circ}{R} - \frac{\Delta H^\circ}{RT} \quad (4.11)$$

Where

C_s = equilibrium concentration of dyes remaining in aqueous solution, mg/L

$C_{e,m}$ = mass of dyes molecules adsorbed per unit mass of chitosan composite at equilibrium, mg/g

R = gas constant (8.314 J/(mol·K))

T = absolute temperature, K

For instance, Gibb's free energy change value is calculated by substituting Equation 4.9 into Equation 4.10 once the equilibrium constant (K_c) has been determined. Next, Equation 4.11 shows the van't Hott equation that can be used to calculate the energy change of the biosorption process. The value of enthalpy change and entropy change can be obtained from the slope and intercept of the graph by plotting $\ln K_c$ against $1/T$.

The thermodynamic parameters for the biosorption of dyes using various chitosan composite were collected from different literature and summarised in Table 4.9 to carry out the thermodynamic studies. The enthalpy change is generally utilised to evaluate whether the nature of biosorption is an exothermic or endothermic process. The biosorption of dyes is an exothermic process if the measured enthalpy change is negative value; otherwise, it is an endothermic process (Madala, Kumar and Vudagandla, 2013).

Table 4.9: Thermodynamic Parameters for Biosorption of Dyes Using Various Type of Chitosan Composites.

| Chitosan Composites | Type of Dyes | K_c | ΔG° (kJ/mol) | ΔH° (kJ/mol) | ΔS° (J/K/mol) | T (K) | References |
|---|---------------------|-------------------------|---|---|--|---------------------------|--------------------------------|
| Chitosan/quartzite | Reactive black | 4.943×10^4 | -25.88 | 21.76 | 166.50 | 288 | Dehghani, et al. (2017) |
| Chitosan/activated carbon | Indigo carmine | 1.090×10^4 | -23.42 | 10.66 | 112.40 | 303 | Wang, et al. (2018) |
| Chitosan/cellulose | Congo red | 7.899 | -5.209 | 86.25 | 300.90 | 303 | Kamal, et al. (2017) |
| Chitosan/MgO | Reactive blue | 7.956×10^3 | -21.73 | 14.56 | 0.1250 | 291 | Nga, Thuy Chau and Viet (2020) |
| Chitosan/PVA | Eosin yellow | 7.743 | -5.156 | -7.486 | -7.716 | 303 | Habiba, et al. (2017) |
| Chitosan/zeolite | Methyl orange | 2.730 | -2.530 | 7.179 | 34.3048 | 283 | Hussain, et al. (2021) |
| Crosslinked chitosan epichlorohydrin | Reactive red | 2.593 | -2.400 | 27.7 | 0.0990 | 303 | Jawad, et al. (2019) |
| Chitosan/kaolin clay | Reactive blue | 6.063 | -4.540 | 4.810 | 0.4300 | 303 | Jawad, et al. (2020) |
| Chitosan/alumina | Methyl orange | 5.335 | -4.148 | -10.54 | -21.59 | 298 | Zhang, Zhou and Ou (2012) |
| Chitosan/bentonite | Amido black | 1.116 | -0.2670 | 15.78 | 0.0547 | 293 | Liu, et al. (2015) |
| Chitosan/γ-Fe₂O₃ | Methyl orange | 1.939 | -1.762 | -17.41 | -48.89 | 320 | Zhu, et al. (2010) |

Next, the biosorption process is considered favourable and spontaneous when the obtained Gibb's free energy change is in negative magnitude. Besides, Gibb's free energy change is also helpful in determining the biosorption type. If the value of Gibb's free energy change lies between -20 kJ/mol and 0 kJ/mol, this indicates the type of biosorption is physisorption. However, if the Gibb's free energy change value is within the range of -80 kJ/mol to -400 kJ/mol, the biosorption of dyes involves chemisorption (Kausar, et al., 2019). Lastly, the orderliness at the solid-liquid interface increases with the increasing entropy change value.

Based on the results as shown in Table 4.9, it was observed that all the biosorption processes using various chitosan composites had the negative value of Gibb's free energy change, reflecting that the biosorption processes were feasible and spontaneous at the low temperature range between 288 and 320 K. In addition, most of the dye biosorption processes was physisorption type since their Gibb's free energy change values were within the range of -20 to 0 kJ/mol. The Gibb's free energy change values of chitosan/quartzite, chitosan/activated-carbon and chitosan/MgO composites were -25.88, -23.42 and -21.73 kJ/mol, respectively, which were in the range of -20 and -80 kJ/mol. These values indicated that the physical adsorption was influenced by certain chemical effects and implied that ion exchange might occur during the biosorption process (Erenturk and Kaygun, 2017; Tzereme et al., 2019).

Moreover, most of the biosorption processes with a positive value of enthalpy change was endothermic that required input energy supplied to the process. The endothermic nature of dye biosorption might be attributed to the dehydration process, where additional energy was required to remove the water molecules adsorbed on the surface of chitosan composite. Meanwhile, the desorption of water molecules could provide a larger surface area for the biosorption of dyes on the chitosan composite surface (Dehghani, et al., 2017). Among the chitosan composite, chitosan/cellulose had the highest positive enthalpy change value due to the membrane layer of cellulose entrapped with a high amount of water molecules, thereby increasing the energy for the removal of water molecules.

However, chitosan/PVA, chitosan/alumina and chitosan/ γ -Fe₂O₃ composites used as the biosorbents for the dye removal demonstrated a different finding with a negative enthalpy change value. The finding suggested that the biosorption process was exothermic, where the dye molecules interacted with the surface functional groups of chitosan composites through electrostatic attraction, hydrogen bonding and weak intermolecular interaction. Consequently, the surface energy of chitosan composite was reduced and the output energy was released to the surrounding (Zhang, Zhou and Ou, 2012).

Furthermore, the biosorption process with a positive magnitude of entropy change reflected that the dye molecules had a good interaction with the chitosan composite. Consequently, this resulted in an increase in the irregularity of dye molecules at the solid-liquid interface. Conversely, the irregularity of dye molecules decreased when a negative entropy change was obtained (Zhu, et al., 2010; Liu, et al., 2015).

CHAPTER 5

CONCLUSIONS AND RECOMMENDATIONS

5.1 Conclusions

Based on the SEM micrographs, the chitosan composites had an irregular and rough surface as compared to pure chitosan. After the biosorption of organic dyes, the rough surface of chitosan composite was transformed to a smooth surface. For the EDX analysis, it proved that the chitosan composites had been successfully synthesised with the presence of additional elemental composition which could not be found in pure chitosan. The existence of S in the chitosan composite further proved that the dye molecules were successfully adsorbed on the composite surface. Besides, the chitosan composites also possessed a higher BET specific surface area ($> 1.81 \text{ m}^2/\text{g}$) than pure chitosan ($> 0.141 \text{ m}^2/\text{g}$). In addition, the presence of additional functional groups on the chitosan surface as detected in the FTIR spectra confirmed that reinforcement material was successfully added to the chitosan matrix. In the XRD spectra, the chitosan composites exhibited lower peak intensity and became more amorphous than pure chitosan. Next, the TGA results showed that the chitosan composites possessed higher thermal stability and lower weight loss ($< 40 \%$) than pure chitosan during the thermal process.

For the kinetic and isotherm studies, most of the chitosan composites were well fitted to PSO kinetic model and Langmuir isotherm model with a high R^2 value. This indicated that monolayer chemisorption of organic dyes occurred on the homogenous surface of chitosan composites. However, except for chitosan/quartzite, chitosan/MgO and chitosan/zeolite composites, their biosorption processes occurred on the heterogeneous biosorbent surfaces as suggested by the Freundlich isotherm model. This might be due to the presence of impurities that were adsorbed on the chitosan composites during the modification of pure chitosan. The impurities on the chitosan composite surface would result in different level of binding energy required for the biosorption of organic dyes. Next, the thermodynamic results indicated that all the dye removal processes using various chitosan composites were feasible and

spontaneous. Moreover, most of the biosorption processes were endothermic in nature except for chitosan/PVA, chitosan/alumina and chitosan/ γ -Fe₂O₃.

As a conclusion, the research objectives were achieved where chitosan as a biopolymer could be modified to synthesise chitosan composite by incorporating with the reinforcement materials. Furthermore, chitosan composites exhibited better characteristics in terms of morphological properties, pore volume, pore size, functional groups, crystallinity and thermal stability as compared to pure chitosan. Therefore, the incorporation of reinforcement materials in the chitosan matrix has greatly improved the physicochemical properties of chitosan. Most of the biosorption processes were endothermic in nature. The process was followed by PSO kinetic model and Langmuir isotherm model. Chitosan composites have been proved to be a promising biosorbent for the removal of organic dyes.

5.2 Recommendations for Future Work

In this study, the data collected from various journals was found to be slightly different. This was due to the fact that the researchers conducted the experiments under different operating conditions. Furthermore, there was limited published data to fully demonstrate the effectiveness of chitosan composites for the removal of organic dyes. In order to increase the accuracy and reliability of the findings, there are some recommendations that can be made for future study.

Firstly, the effect of the reinforcement material ratio added to the pure chitosan matrix should be studied to determine the effectiveness of chitosan composites for the removal of organic dyes. Besides, regeneration studies on various chitosan composite can be performed to determine their recyclability for the removal of organic dyes. In order to compare the results effectively, the characterisation analysis and dye biosorption process for various chitosan composites should be carried out under the same operating conditions. Finally, it is suggested that this review study can be turned into a practical experimental study to validate the reliability of the data obtained from the journals.

REFERENCES

- Abbasi, M. and Habibi, M.M., 2016. Optimization and characterization of Direct Blue 71 removal using nanocomposite of Chitosan-MWCNTs: Central composite design modeling. *Journal of the Taiwan Institute of Chemical Engineers*, 142(4), pp.98-104.
- Abdel Maksoud, M.I.A., Elgarahy, A.M., Farrell, C., Al-Muhtaseb, A.H., Rooney, D.W. and Osman, A.I., 2020. Insight on water remediation application using magnetic nanomaterials and biosorbents. *Coordination Chemistry Reviews*, 403, pp.1–34.
- Abdel-Fatah, M.A., 2018. Nanofiltration systems and applications in wastewater treatment: Review article. *Ain Shams Engineering Journal*, 9(4), pp.3077–3092.
- Abdurrahman, F.B., Akter, M. and Abedin, M.Z., 2013. Dyes removal from textile wastewater using orange peels. *International Journal of Scientific & Technology Research*, 2(9), pp.47–50.
- Abitbol, T., Rivkin, A., Cao, Y., Nevo, Y., Abraham, E., Ben-Shalom, T., Lapidot, S. and Shoseyov, O., 2016. Nanocellulose, a tiny fiber with huge applications. *Current Opinion in Biotechnology*, 39(I), pp.76–88.
- Adewuyi, A., 2020. Chemically modified biosorbents and their role in the removal of emerging pharmaceutical waste in the water system. *Water (Switzerland)*, 12(6), pp.1–31.
- Agarwal, A. and Vaishali, A., 2017. Chitosan based adsorbent: A remedy to handle industrial waste water. *The International Journal of Engineering and Science*, 6(9), pp.34–49.
- Ahmad, T. and Danish, M., 2018. Prospects of banana waste utilisation in wastewater treatment: a review. *Journal of Environmental Management*, 206(9), pp.330–348.
- Akhtar, J., Amin, N.A.S. and Shahzad, K., 2016. A review on removal of pharmaceuticals from water by adsorption. *Desalination and Water Treatment*, 57(27), pp.12842–12860.
- Albadarin, A.B., Collins, M.N., Naushad, M., Shirazian, S., Walker, G. and Mangwandi, C., 2017. Activated lignin-chitosan extruded blends for efficient adsorption of methylene blue. *Chemical Engineering Journal*, 307(3), pp.264–272.
- Al-Manhel, A.J., Al-Hilphy, A.R.S. and Niamah, A.K., 2018. Extraction of chitosan, characterisation and its use for water purification. *Journal of the Saudi Society of Agricultural Sciences*, 17(2), pp.186–190.

Anitha, T., Kumar, S.P. and Kumar, S.K., 2016. Synthesis of nano-sized chitosan blended polyvinyl alcohol for the removal of Eosin Yellow dye from aqueous solution. *Journal of Water Process Engineering*, 13, pp.127–136.

Arafat, A., Samad, S.A., Huq, D., Moniruzzaman, M. and Masum, S.M., 2015. Textile dye removal from wastewater effluents using chitosan-ZnO nanocomposite. *Journal of Textile Science & Engineering*, 5(3), pp.5–8.

Ariyanti, D., Maillot, M. and Gao, W., 2018. Photo-assisted degradation of dyes in a binary system using TiO₂ under simulated solar radiation. *Journal of Environmental Chemical Engineering*, 6(1), pp.539–548.

Auta, M. and Hameed, B.H., 2013. Coalesced chitosan activated carbon composite for batch and fixed-bed adsorption of cationic and anionic dyes. *Colloids and Surfaces B: Biointerfaces*, 105(5), pp.199–206.

Azari, A., Nabizadeh, R., Nasser, S., Mahvi, A.H. and Mesdaghinia, A.R., 2020. Comprehensive systematic review and meta-analysis of dyes adsorption by carbon-based adsorbent materials: Classification and analysis of last decade studies. *Chemosphere*, 250(5), pp.126–135.

Azari, A., Noorisepehr, M., Dehganifard, E., Karimyan, K., Hashemi, S.Y., Kalhori, E.M., Norouzi, R., Agarwal, S. and Gupta, V.K., 2019. Experimental design, modeling and mechanism of cationic dyes biosorption on to magnetic chitosan-lutaraldehyde composite. *International Journal of Biological Macromolecules*, 131, pp.633–645.

Bahalkeh, F., Habibi juybari, M., Zafar Mehrabian, R. and Ebadi, M., 2020. Removal of Brilliant Red dye (Brilliant Red E-4BA) from wastewater using novel Chitosan/SBA-15 nanofiber. *International Journal of Biological Macromolecules*, 164(7), pp.818–825.

Bahrudin, N.N., Nawi, M.A. and Sabar, S., 2019. Immobilized chitosan-montmorillonite composite adsorbent and its photocatalytic regeneration for the removal of methyl orange. *Reaction Kinetics, Mechanisms and Catalysis*, 126(2), pp.1135–1153.

Banerjee, S., Paira, T.K. and Mandal, T.K., 2014. Surface confined atom transfer radical polymerization: Access to custom library of polymer-based hybrid materials for speciality applications. *Polymer Chemistry*, 5(14), pp.4153–4167.

Bartolomeu, M., Neves, M.G.P.M.S., Faustino, M.A.F. and Almeida, A., 2018. Wastewater chemical contaminants: remediation by advanced oxidation processes. *Photochemical and Photobiological Sciences*, 17(11), pp.1573–1598.

Bazan, A., Nowicki, P., Pólrolniczak, P. and Pietrzak, R., 2016. Thermal analysis of activated carbon obtained from residue after supercritical extraction of hops. *Journal of Thermal Analysis and Calorimetry*, 125(3), pp.1199–1204.

Berradi, M., Hsissou, R., Khudhair, M., Assouag, M., Cherkaoui, O., El Bachiri, A. and El Harfi, A., 2019. Textile finishing dyes and their impact on aquatic environs. *Heliyon*, 5(11), pp.1–11.

Bidaisee, S., 2018. The Importance of clean water. *Biomedical Journal of Scientific & Technical Research*, 8(5), pp.1–4.

Cao, Y.L., Pan, Z.H., Shi, Q.X. and Yu, J.Y., 2018. Modification of chitin with high adsorption capacity for methylene blue removal. *International Journal of Biological Macromolecules*, 114(8), pp.392–399.

Chen, Y., Xu, Z., Smith, C. and Sankar, J., 2014. Recent advances on the development of magnesium alloys for biodegradable implants. *Acta Biomaterialia*, 10(11), pp.4561–4573.

Choudhury, A.K.R., 2016. *Textile preparation and dyeing*. New Hampshire: Science Publishers.

Coura, J.C., Profeti, D. and Profeti, L.P.R., 2020. Eco-friendly chitosan/quartzite composite as adsorbent for dye removal. *Materials Chemistry and Physics*, 256(7), pp.112–123.

Crini, G. and Lichtfouse, E., 2019. Advantages and disadvantages of techniques used for wastewater treatment. *Environmental Chemistry Letters*, 17(1), pp.145–155.

Crini, G., Torri, G., Lichtfouse, E., Kyzas, G.Z., Wilson, L.D. and Morin-Crini, N., 2019. Dye removal by biosorption using cross-linked chitosan-based hydrogels. *Environmental Chemistry Letters*, 17(4), pp.1645–1666.

Danish, M. and Ahmad, T., 2018. A review on utilization of wood biomass as a sustainable precursor for activated carbon production and application. *Renewable and Sustainable Energy Reviews*, 87(2), pp.1–21.

Debnath, S., Parashar, K. and Pillay, K., 2017. Ultrasound assisted adsorptive removal of hazardous dye Safranin O from aqueous solution using crosslinked graphene oxide-chitosan composite and optimization by response surface methodology (RSM) approach. *Carbohydrate Polymers*, 175, pp.509–517.

Dehghani, M.H., Dehghan, A., Alidadi, H., Dolatabadi, M., Mehrabpour, M. and Converti, A., 2017. Removal of methylene blue dye from aqueous solutions by a new chitosan/zeolite composite from shrimp waste: kinetic and equilibrium study. *Korean Journal of Chemical Engineering*, 34(6), pp.1699–1707.

Department of Environment, 2017. *Kualiti air sungai river water quality*. [online] Available at: <https://www.doe.gov.my/portalv1/wp-content/uploads/2018/09/iv_EQR2016.pdf%0Aenviro.doe.gov.my/ekmc/wp-content/uploads/2017/09/3_EQR2016_Layout_Bab-2.pdf> [Accessed 18 August 2020].

- Díez-Pascual, A.M., 2019. Synthesis and applications of biopolymer composites. *International Journal of Molecular Sciences*, 20(9), pp.97–105.
- Dotto, G.L., Rodrigues, F.K., Tanabe, E.H., Fröhlich, R., Bertuol, D.A., Martins, T.R. and Foletto, E.L., 2016. Development of chitosan/bentonite hybrid composite to remove hazardous anionic and cationic dyes from colored effluents. *Journal of Environmental Chemical Engineering*, 4(3), pp.3230–3239.
- Elanchezhian, S.S.D., Muthu Prabhu, S. and Meenakshi, S., 2018. Treatment of emulsified oil using biopolymer assisted materials. *Polymer Composites*, 39, pp.261–270.
- Erenturk, S.A. and Kaygun, A.K., 2017. Removal of 226Ra from aqueous media and its thermodynamics and kinetics. *Journal of Radioanalytical and Nuclear Chemistry*, 311(2), pp.1227–1233.
- Fan, L., Luo, C., Sun, M., Qiu, H. and Li, X., 2013. Synthesis of magnetic β -cyclodextrin-chitosan/graphene oxide as nanoadsorbent and its application in dye adsorption and removal. *Colloids and Surfaces B: Biointerfaces*, 103(5), pp.601–607.
- Farias, P.V.S., Aragão, D.C., Farias, M. V., Correia, L.M., Carvalho, T. V., Aguiar, J.E. and Vieira, R.S., 2015. Natural and cross-linked chitosan spheres as adsorbents for diesel oil removal. *Adsorption Science and Technology*, 33(9), pp.783–792.
- Fatombi, J.K., Idohou, E.A., Osseni, S.A., Agani, I., Neumeyer, D., Verelst, M., Mauricot, R. and Aminou, T., 2019. Adsorption of Indigo carmine from aqueous solution by chitosan and chitosan/activated carbon composite: Kinetics, isotherms and thermodynamics studies. *Fibers and Polymers*, 20(9), pp.1820–1832.
- Fomina, M. and Gadd, G.M., 2014. Biosorption: current perspectives on concept, definition and application. *Bioresource Technology*, 160(1), pp.3–14.
- Galadima, A. and Muraza, O., 2020. Waste materials for production of biodiesel catalysts: Technological status and prospects. *Journal of Cleaner Production*, 263, pp.121–127.
- Gautam, R.K., Mudhoo, A., Lofrano, G. and Chattopadhyaya, M.C., 2014. Biomass-derived biosorbents for metal ions sequestration: adsorbent modification and activation methods and adsorbent regeneration. *Journal of Environmental Chemical Engineering*, 71(2), pp.239–259.
- Ghormade, V., Pathan, E.K. and Deshpande, M. V., 2017. Can fungi compete with marine sources for chitosan production? *International Journal of Biological Macromolecules*, 104, pp.1415–1421.
- Gu, F., Geng, J., Li, M., Chang, J. and Cui, Y., 2019. Synthesis of Chitosan-ignosulfonate composite as an adsorbent for dyes and metal ions removal from wastewater. *ACS Omega*, 4(25), pp.21421–21430.

- Habiba, U., Siddique, T.A., Talebian, S., Lee, J.J.L., Salleh, A., Ang, B.C. and Afifi, A.M., 2017. Effect of deacetylation on property of electrospun chitosan/PVA nanofibrous membrane and removal of methyl orange, Fe(III) and Cr(VI) ions. *Carbohydrate Polymers*, 177, pp.32–39.
- Han, D., Yan, L., Chen, W. and Li, W., 2011. Preparation of chitosan/graphene oxide composite film with enhanced mechanical strength in the wet state. *Carbohydrate Polymers*, 83(2), pp.653–658.
- Hansen, K.M.S., Spiliotopoulou, A., Chhetri, R.K., Escolà Casas, M., Bester, K. and Andersen, H.R., 2016. Ozonation for source treatment of pharmaceuticals in hospital wastewater - Ozone lifetime and required ozone dose. *Chemical Engineering Journal*, 290(4), pp.507–514.
- Hassan, H., Salama, A., El-ziaty, A.K. and El-Sakhawy, M., 2019. New chitosan/silica/zinc oxide nanocomposite as adsorbent for dye removal. *International Journal of Biological Macromolecules*, 131, pp.520–526.
- Hernández, N., Williams, R.C. and Cochran, E.W., 2014. The battle for the ‘green’ polymer. Different approaches for biopolymer synthesis: Bioadvantaged vs. bioreplacement. *Organic and Biomolecular Chemistry*, 12(18), pp.2834–2849.
- Hussain, S., Kamran, M., Ali, S., Shaheen, K., Shah, Z., Suo, H., Khan, Q., Basit, A., Ur, W., Al-ghamdi, Y.O. and Ghani, U., 2021. International Journal of biological macromolecules adsorption, kinetics and thermodynamics studies of methyl orange dye sequestration through chitosan composites films. *International Journal of Biological Macromolecules*, 168(11), pp.383–394.
- Huyen, N.T.M., Trang, P.T.T., Dat, N.M. and Hieu, N.H., 2017. Synthesis of chitosan/graphene oxide nanocomposites for methylene blue adsorption. *AIP Conference Proceedings*, 187(8), pp.1–12.
- Idohou, E.A., Fatombi, J.K., Osseni, S.A., Agani, I., Neumeyer, D., Verelst, M., Mauricot, R. and Aminou, T., 2020. Preparation of activated carbon/chitosan/carica papaya seeds composite for efficient adsorption of cationic dye from aqueous solution. *Surfaces and Interfaces*, 21(8), pp.178–183.
- Jabar, J.M., Odusote, Y.A., Alabi, K.A. and Ahmed, I.B., 2020. Kinetics and mechanisms of congo-red dye removal from aqueous solution using activated Moringa oleifera seed coat as adsorbent. *Applied Water Science*, 10(6), pp.1–11.
- Jacob, J., Haponiuk, J.T., Thomas, S. and Gopi, S., 2018. Biopolymer based nanomaterials in drug delivery systems: A review. *Materials Today Chemistry*, 141(9), pp.43–55.
- Jafri, N., Wong, W.Y., Doshi, V., Yoon, L.W. and Cheah, K.H., 2018. A review on production and characterization of biochars for application in direct carbon fuel cells. *Process Safety and Environmental Protection*, 118(9), pp.152–166.

- Jawad, A.H. and Abdulhameed, A.S., 2020a. Facile synthesis of crosslinked chitosan-tripolyphosphate/kaolin clay composite for decolourization and COD reduction of remazol brilliant blue R dye: Optimization by using response surface methodology. *Colloids and Surfaces A: Physicochemical and Engineering Aspects*, 605(7), pp.114–119.
- Jawad, A.H. and Abdulhameed, A.S., 2020b. Mesoporous Iraqi red kaolin clay as an efficient adsorbent for methylene blue dye: Adsorption kinetic, isotherm and mechanism study. *Surfaces and Interfaces*, 18(6), pp.71–76.
- Jawad, A.H., Abdulhameed, A.S., Malek, N.N.A. and AlOthman, Z.A., 2020. Statistical optimization and modeling for color removal and COD reduction of reactive blue 19 dye by mesoporous chitosan-epichlorohydrin/kaolin clay composite. *International Journal of Biological Macromolecules*, 164, pp.4218–4230.
- Jawad, A.H., Shazwani, N., Mubarak, A. and Sabar, S., 2019. Adsorption and mechanism study for reactive red 120 dye removal by cross-linked chitosan-epichlorohydrin biobeads Adsorption and mechanism study for reactive red 120 dye removal by cross-linked chitosan-epichlorohydrin biobeads, *Composites Part B: Engineering*, 75(10), pp.415–418.
- Jiang, M., Yang, W., Zhang, Z., Yang, Z. and Wang, Y., 2015. Adsorption of three pharmaceuticals on two magnetic ion-exchange resins. *Journal of Environmental Sciences (China)*, 31(2), pp.226–234.
- Joseph, L., Jun, B.M., Flora, J.R.V., Park, C.M. and Yoon, Y., 2019. Removal of heavy metals from water sources in the developing world using low-cost materials: a review. *Chemosphere*, 229, pp.142–159.
- Kamal, M.A., Bibi, S., Bokhari, S.W., Siddique, A.H. and Yasin, T., 2017. Synthesis and adsorptive characteristics of novel chitosan/graphene oxide nanocomposite for dye uptake. *Reactive and Functional Polymers*, 110(5), pp.21–29.
- Kanaujiya, D.K., Paul, T., Sinharoy, A. and Pakshirajan, K., 2019. Biological Treatment processes for the removal of organic micropollutants from wastewater: a review. *Current Pollution Reports*, 5(3), pp.112–128.
- Kaneda, T., Greenbaum, C. and Kline, K., 2020. 2020 World population data sheet shows older populations growing, total fertility rates declining – population reference bureau. [online] Available at: <<https://www.prb.org/2020-world-population-data-sheet/>> [Accessed 18 August 2020].
- Kanmani, P., Aravind, J., Kamaraj, M., Sureshbabu, P. and Karthikeyan, S., 2017. Environmental applications of chitosan and cellulosic biopolymers: A comprehensive outlook. *Bioresource Technology*, 242, pp.295–303.

- Kausar, A., Naeem, K., Tariq, M., Nazli, Z.I.H., Bhatti, H.N., Jubeen, F., Nazir, A. and Iqbal, M., 2019. Preparation and characterization of chitosan/clay composite for direct Rose FRN dye removal from aqueous media: Comparison of linear and non-linear regression methods. *Journal of Materials Research and Technology*, 8(1), pp.1161–1174.
- Khademian, E., Salehi, E., Sanaeepur, H., Galiano, F. and Figoli, A., 2020. A systematic review on carbohydrate biopolymers for adsorptive remediation of copper ions from aqueous environments-part A: classification and modification strategies. *Science of the Total Environment*, 38 (7), pp.1–20.
- Kim, M.H., An, S., Won, K., Kim, H.J. and Lee, S.H., 2012. Entrapment of enzymes into cellulose-biopolymer composite hydrogel beads using biocompatible ionic liquid. *Journal of Molecular Catalysis B: Enzymatic*, 75, pp.68–72.
- Kuilla, T., Bhadra, S., Yao, D., Kim, N.H., Bose, S. and Lee, J.H., 2010. Recent advances in graphene based polymer composites. *Progress in Polymer Science (Oxford)*, 35(11), pp.1350–1375.
- Kumari, S., Rath, P., Sri Hari Kumar, A. and Tiwari, T.N., 2015. Extraction and characterization of chitin and chitosan from fishery waste by chemical method. *Environmental Technology and Innovation*, 98(3), pp.77–85.
- Kyzas, G.Z., Kostoglou, M., Lazaridis, N.K. and Bikiaris, D.N., 2013. N-(2-carboxybenzyl) grafted chitosan as adsorptive agent for simultaneous removal of positively and negatively charged toxic metal ions. *Journal of Hazardous Materials*, 244–245, pp.29–38.
- Lellis, B., Fávoro-Polonio, C.Z., Pamphile, J.A. and Polonio, J.C., 2019. Effects of textile dyes on health and the environment and bioremediation potential of living organisms. *Biotechnivegy Research and Innovation*, 3(2), pp.275–290.
- Li, C., Cui, J., Wang, F., Peng, W. and He, Y., 2016. Adsorption removal of Congo red by epichlorohydrin-modified cross-linked chitosan adsorbent. *Desalination and Water Treatment*, 57(30), pp.14060–14066.
- Li, H. and Huang, D., 2013. Microwave preparation and copper ions adsorption properties of crosslinked chitosan/ZSM molecular sieve composites. *Journal of Applied Polymer Science*, 129(1), pp.86–93.
- Li, J., Jiang, B., Liu, Y., Qiu, C., Hu, J., Qian, G., Guo, W. and Ngo, H.H., 2017. Preparation and adsorption properties of magnetic chitosan composite adsorbent for Cu²⁺ removal. *Journal of Cleaner Production*, 158, pp.51–58.
- Li, X., Li, Y., Zhang, S. and Ye, Z., 2012. Preparation and characterisation of new foam adsorbents of poly(vinyl alcohol)/chitosan composites and their removal for dye and heavy metal from aqueous solution. *Chemical Engineering Journal*, 183, pp.88–97.

- Liu, D., Zhu, Y., Li, Z., Tian, D., Chen, L. and Chen, P., 2013. Chitin nanofibrils for rapid and efficient removal of metal ions from water system. *Carbohydrate Polymers*, 98(1), pp.483–489.
- Liu, Q., Yang, B., Zhang, L. and Huang, R., 2015. Adsorption of an anionic azo dye by cross-linked chitosan/bentonite composite. *International Journal of Biological Macromolecules*, 72, pp.1129–1135.
- Liu, Y., Zheng, Y. and Wang, A., 2010. Enhanced adsorption of Methylene Blue from aqueous solution by chitosan-g-poly (acrylic acid)/vermiculite hydrogel composites. *Journal of Environmental Sciences*, 22(4), pp.486–493.
- Luo, W., Bai, Z. and Zhu, Y., 2018. Fast removal of Co(ii) from aqueous solution using porous carboxymethyl chitosan beads and its adsorption mechanism. *RSC Advances*, 8(24), pp.13370–13387.
- Madala, S., Kumar, S. and Vudagandla, S., 2013. Equilibrium , kinetics and thermodynamics of Cadmium (II) biosorption on to composite chitosan biosorbent. *Arabian Journal of Chemistry*, 75(2), pp.543–550.
- Malaysian Investment Development Authority (MIDA), 2018. *Inspiring technological transformation. Malaysia Investment performance report 2018*. [online] Available at: <https://www.mida.gov.my/home/administrator/system_files/modules/photo/uploads/20190315105335_MIDA_IPR_2018.pdf> [Accessed 18 August 2020].
- Marrakchi, F., Hameed, B.H. and Hummadi, E.H., 2020. Mesoporous biohybrid epichlorohydrin crosslinked chitosan/carbon–clay adsorbent for effective cationic and anionic dyes adsorption. *International Journal of Biological Macromolecules*, 163, pp.1079–1086.
- Massimi, L., Giuliano, A., Astolfi, M.L., Congedo, R., Masotti, A. and Canepari, S., 2018. Efficiency evaluation of food waste materials for the removal of metals and metalloids from complex multi-element solutions. *Materials*, 113, pp.170–183.
- Mbaeze, M.C., Agbazue, V. and Orjioko, N., 2017. Comparative assessment of performance of aluminium sulphate (alum) and ferrous sulphate as coagulants in water treatment. *Modern Chemistry & Applications*, 5(4), pp.1–18.
- Metin, A.Ü., Çiftçi, H. and Alver, E., 2013. Efficient removal of acidic dye using low-cost biocomposite beads. *Industrial and Engineering Chemistry Research*, 52(31), pp.569–581.
- Michalak, I., Chojnacka, K. and Witek-Krowiak, A., 2013. State of the art for the biosorption process - a review. *Applied Biochemistry and Biotechnology*, 170(6), pp.1389–1416.
- Mohammad, A.K.T., Abdulhameed, A.S. and Jawad, A.H., 2019. Box-Behnken design to optimize the synthesis of new crosslinked chitosan-glyoxal/TiO₂ nanocomposite: Methyl orange adsorption and mechanism studies. *International Journal of Biological Macromolecules*, 129, pp.98–109.

- Monteiro, M.R., Kugelmeier, C.L., Pinheiro, R.S., Batalha, M.O. and da Silva César, A., 2018. Glycerol from biodiesel production: Technological paths for sustainability. *Renewable and Sustainable Energy Reviews*, 88(3), pp.109–122.
- Morali, E.K., Uzal, N. and Yetis, U., 2016. Ozonation pre and post-treatment of denim textile mill effluents: Effect of cleaner production measures. *Journal of Cleaner Production*, 137(12), pp.1–9.
- Muinde, V.M., Onyari, J.M., Wamalwa, B. and Wabomba, J.N., 2020. Adsorption of malachite green dye from aqueous solutions using mesoporous chitosan–zinc oxide composite material. *Environmental Chemistry and Ecotoxicology*, 54(2), pp.115–125.
- Nagireddi, S., Katiyar, V. and Uppaluri, R., 2017. Pd(II) adsorption characteristics of glutaraldehyde cross-linked chitosan copolymer resin. *International Journal of Biological Macromolecules*, 94, pp.72–84.
- Nakkeeran, E., Varjani, S.J., Dixit, V. and Kalaiselvi, A., 2018. Synthesis, characterization and application of zinc oxide nanocomposite for dye removal from textile industrial wastewater. *Indian Journal of Experimental Biology*, 56(7), pp.498–503.
- Nešić, A.R., Veličković, S.J. and Antonović, D.G., 2013. Modification of chitosan by zeolite A and adsorption of Bezactive Orange 16 from aqueous solution. *Composites Part B: Engineering*, 53(5), pp.145–151.
- Nga, N.K., Thuy Chau, N.T. and Viet, P.H., 2020. Preparation and characterization of a chitosan/MgO composite for the effective removal of reactive blue 19 dye from aqueous solution. *Journal of Science: Advanced Materials and Devices*, 5(1), pp.65–72.
- Nguyen, N.T., Nguyen, N.T. and Nguyen, V.A., 2020. In situ synthesis and characterization of ZnO/Chitosan nanocomposite as an adsorbent for removal of congo red from aqueous solution. *Advances in Polymer Technology*, 3(1), pp.1–8.
- Niaounakis, M., 2013. *Biopolymers: reuse, recycling and disposal*. 1st ed. Waltham, MA: William Andrew.
- Obiora-Okafo, I.A. and Onukwuli, O.D., 2017. Optimization of Coagulation-Flocculation for Colour Removal From Azo Dye Using Natural Polymers: Response Surface Methodological Approach. *Nigerian Journal of Technology (NIJOTECH)*, 36(2), pp.482–495.
- Onwuegbuzie, A.J. and Frels, R., 2016. Seven steps to a comprehensive literature review. *Journal of Educational Social Studies*, 23(2), pp.48–64.
- Ortiz-Martínez, V.M., Andreo-Martínez, P., García-Martínez, N., Pérez de los Ríos, A., Hernández-Fernández, F.J. and Quesada-Medina, J., 2019. Approach to biodiesel production from microalgae under supercritical conditions by the PRISMA method. *Fuel Processing Technology*, 191(3), pp.211–222.

- Pang, Y. L. and Abdullah, A. Z., 2013. Current status of textile industry wastewater management and research progress in Malaysia: a review. *Clean - Soil, Air, Water*, 41(8), pp. 751–764.
- Perez-Madrugal, M.M., Edo, M.G. and Aleman, C., 2016. ChemInform abstract: Powering the future: application of cellulose-based materials for supercapacitors. *ChemInform*, 47(52), pp.80–88.
- Poli, A., Anzelmo, G., Fiorentino, G., Nicolaus, B., Tommonaro, G. and Di, P., 2011. Polysaccharides from wastes of vegetable industrial processing: new opportunities for their eco-friendly re-use. *Biotechnology of Biopolymers*, 365, pp.33–56.
- Quan, X., Luo, D., Wu, J., Li, R., Cheng, W. and Ge, shuping, 2017. Ozonation of acid red 18 wastewater using O₃/Ca(OH)₂ system in a micro bubble gas-liquid reactor. *Journal of Environmental Chemical Engineering*, 5(1), pp.283–291.
- Quesada, H.B., de Araújo, T.P., Vareschini, D.T., de Barros, M.A.S.D., Gomes, R.G. and Bergamasco, R., 2020. Chitosan, alginate and other macromolecules as activated carbon immobilizing agents: A review on composite adsorbents for the removal of water contaminants. *International Journal of Biological Macromolecules*, 164(6), pp.2535–2549.
- Rafique, A., Mahmood Zia, K., Zuber, M., Tabasum, S. and Rehman, S., 2016. Chitosan functionalized poly(vinyl alcohol) for prospects biomedical and industrial applications: A review. *International Journal of Biological Macromolecules*, 87, pp.141–154.
- Rangabhashiyam, S. and Balasubramanian, P., 2019. Characteristics, performances, equilibrium and kinetic modeling aspects of heavy metal removal using algae. *Bioresource Technology Reports*, 5(8), pp.261–279.
- Rangabhashiyam, S., Anu, N. and Selvaraju, N., 2013. Sequestration of dye from textile industry wastewater using agricultural waste products as adsorbents. *Journal of Environmental Chemical Engineering*, 1(4), pp.629–641.
- Rasheed, T., Bilal, M., Nabeel, F., Adeel, M. and Iqbal, H.M.N., 2019. Environmentally-related contaminants of high concern: potential sources and analytical modalities for detection, quantification, and treatment. *Environment International*, 122(9), pp.52–66.
- Raval, N.P., Shah, P.U. and Shah, N.K., 2016. Adsorptive removal of nickel(II) ions from aqueous environment: A review. *Journal of Environmental Management*, 179, pp.1–20.
- Rekik, R., Kallel, I., Casillas, J. and Alimi, A.M., 2018. Assessing web sites quality: A systematic literature review by text and association rules mining. *International Journal of Information Management*, 38(1), pp.201–216.

- Rezakazemi, M., Ebadi Amooghin, A., Montazer-Rahmati, M.M., Ismail, A.F. and Matsuura, T., 2014. State-of-the-art membrane based CO₂ separation using mixed matrix membranes (MMMs): an overview on current status and future directions. *Progress in Polymer Science*, 39(5), pp.817–861.
- Riyanti, F., Hariani, P.L., Fatma, Yuliasari, N., Said, M. and Ramadiati, T., 2020. Synthesis of chitosan-SiO₂ composite for adsorption methyl dyes from solution. *IOP Conference Series: Materials Science and Engineering*, 857(1), pp.154–162.
- Rocha, L.S., Pereira, D., Sousa, É., Otero, M., Esteves, V.I. and Calisto, V., 2020. Recent advances on the development and application of magnetic activated carbon and char for the removal of pharmaceutical compounds from waters: A review. *Science of the Total Environment*, 718(4), pp.461–473.
- Sadeek, S.A., Negm, N.A., Hefni, H.H.H. and Abdel Wahab, M.M., 2015. Metal adsorption by agricultural biosorbents: adsorption isotherm, kinetic and biosorbents chemical structures. *International Journal of Biological Macromolecules*, 81, pp.400–409.
- Sadeghi-Kiakhani, M., Arami, M. and Gharanjig, K., 2013. Dye removal from colored-textile wastewater using chitosan-PPI dendrimer hybrid as a biopolymer: Optimization, kinetic, and isotherm studies. *Journal of Applied Polymer Science*, 127(4), pp.2607–2619.
- Salam, M.A., Makki, M.S.I. and Abdelaal, M.Y.A., 2011. Preparation and characterisation of multi-walled carbon nanotubes/chitosan nanocomposite and its application for the removal of heavy metals from aqueous solution. *Journal of Alloys and Compounds*, 509(5), pp.2582–2587.
- Salehi, R., Arami, M., Mahmoodi, N.M., Bahrami, H. and Khorramfar, S., 2010. Novel biocompatible composite (chitosan-zinc oxide nanoparticle): Preparation, characterization and dye adsorption properties. *Colloids and Surfaces B: Biointerfaces*, 80(1), pp.86–93.
- Samrot, A. V., Sean, T.C., Kudaiyappan, T., Bisyarah, U., Mirarmandi, A., Faradjeva, E., Abubakar, A., Ali, H.H., Angalene, J.L.A. and Suresh Kumar, S., 2020. Production, characterization and application of nanocarriers made of polysaccharides, proteins, bio-polyesters and other biopolymers: A review. *International Journal of Biological Macromolecules*, 165(2), pp.3088–3105.
- Sanchez-Vazquez, S.A., Hailes, H.C. and Evans, J.R.G., 2013. Hydrophobic polymers from food waste: resources and synthesis. *Polymer Reviews*, 53(4), pp.627–694.
- Sandra, A.C., Azreen, N., Jamil, M., Jabbar, S. and Sakyat, S., 2017. Aerobic and anaerobic sewage biodegradable processes: the gap analysis. *International Journal of Research in Environmental Science*, 3(3), pp.9–19.

- Sanyang, M.L., Sapuan, S.M., Jawaid, M., Ishak, M.R. and Sahari, J., 2016. Effect of sugar palm-derived cellulose reinforcement on the mechanical and water barrier properties of sugar palm starch biocomposite films. *BioResources*, 11(2), pp.4134–4145.
- Saratale, G.D., Jung, M.Y. and Oh, M.K., 2016. Reutilization of green liquor chemicals for pretreatment of whole rice waste biomass and its application to 2,3-butanediol production. *Bioresource Technology*, 205, pp.90–96.
- Sargin, I., Arslan, G. and Kaya, M., 2019. Production of magnetic chitinous microcages from ephippia of zooplankton *Daphnia longispina* and heavy metal removal studies. *Carbohydrate Polymers*, 207(9), pp.200–210.
- Sarode, S., Upadhyay, P., Khosa, M.A., Mak, T., Shakir, A., Song, S. and Ullah, A., 2019. Overview of wastewater treatment methods with special focus on biopolymer chitin-chitosan. *International Journal of Biological Macromolecules*, 121, pp.1086–1100.
- Shazwani, N., Mubarak, A., Jawad, A.H. and Nawawi, W.I., 2017. Equilibrium, kinetic and thermodynamic studies of Reactive Red 120 dye adsorption by chitosan beads from aqueous solution. *Energy, Ecology and Environment*, 2(1), pp.85–93.
- Shukla, S.K., Mishra, A.K., Arotiba, O.A. and Mamba, B.B., 2013. Chitosan-based nanomaterials: A state-of-the-art review. *International Journal of Biological Macromolecules*, 59, pp.46–58.
- Simonin, J.P., 2016. On the comparison of pseudo-first order and pseudo-second order rate laws in the modeling of adsorption kinetics. *Chemical Engineering Journal*, 300(4), pp.254–263.
- Snyder, H., 2019. Literature review as a research methodology: An overview and guidelines. *Journal of Business Research*, 104(8), pp.333–339.
- Stone, J. and Rahimifard, S., 2018. Resilience in agri-food supply chains: a critical analysis of the literature and synthesis of a novel framework. *Supply Chain Management*, 23(3), pp.207–238.
- Sun, X., Peng, B., Ji, Y., Chen, L. and Li, D., 2009. Chitosan(chitin)/cellulose composite biosorbents prepared using ionic liquid for heavy metal ions adsorption. *AIChE Journal*, 55(8), pp.2062–2069.
- Teofilović, V., Pavličević, J., Bera, O., Jovičić, M., Budinski-Simendić, J., Szécsényi, K.M. and Aroguz, A., 2014. The preparation and thermal properties of chitosan/bentonite composite beads. *Hemijska Industrija*, 68(6), pp.653–659.
- Thakur, M.K., Rana, A.K., Liping, Y., Singha, A.S. and Thakur, V.K., 2015. *Surface modification of biopolymers*. Wiley, New York.
- Thakur, V.K., Thakur, M.K. and Gupta, R.K., 2013. Development of functionalised cellulosic biopolymers by graft copolymerisation. *International Journal of Biological Macromolecules*, 62, pp.44–51.

The World Bank, 2014. The Bangladesh responsible sourcing initiative, a new model for green growth. *The Bangladesh Responsible Sourcing Initiative, A New Model For Green Growth*, 1, pp.1–80.

Tomei, M.C., Mosca Angelucci, D. and Daugulis, A.J., 2016. Sequential anaerobic-aerobic decolourisation of a real textile wastewater in a two-phase partitioning bioreactor. *Science of the Total Environment*, 573(1), pp.585–593.

Tran, H. V., Bui, L.T., Dinh, T.T., Le, D.H., Huynh, C.D. and Trinh, A.X., 2017. Graphene oxide/Fe₃O₄/chitosan nanocomposite: A recoverable and recyclable adsorbent for organic dyes removal. Application to methylene blue. *Materials Research Express*, 4(3), pp.401–411.

Travlou, N.A., Kyzas, G.Z., Lazaridis, N.K. and Deliyanni, E.A., 2013. Graphite oxide/chitosan composite for reactive dye removal. *Chemical Engineering Journal*, 217(4), pp.256–265.

Truskewycz, A., Shukla, R. and Ball, A.S., 2016. Iron nanoparticles synthesized using green tea extracts for the fenton-like degradation of concentrated dye mixtures at elevated temperatures. *Journal of Environmental Chemical Engineering*, 4(4), pp.4409–4417.

Tsang, Y.F., Kumar, V., Samadar, P., Yang, Y., Lee, J., Ok, Y.S., Song, H., Kim, K.H., Kwon, E.E. and Jeon, Y.J., 2019. Production of bioplastic through food waste valorization. *Environment International*, 127(1), pp.625–644.

Upadhye, V. B. and Joshi, S. S., 2012. Advances in wastewater treatment - a review. *International Journal of Chemical Sciences and Applications*, 3(2), pp. 2278–6015.

Ventorino, V., Robertiello, A., Cimini, D., Argenzio, O., Schiraldi, C., Montella, S., Faraco, V., Ambrosanio, A., Viscardi, S. and Pepe, O., 2017. Bio-based succinate production from arundo donax hydrolysate with the new natural succinic acid-producing strain *basfia succiniciproducens* BPP7. *Bioenergy Research*, 10(2), pp.488–498.

Víctor-Ortega, M.D., Ochando-Pulido, J.M. and Martínez-Ferez, A., 2017. Impacts of main parameters on the regeneration process efficiency of several ion exchange resins after final purification of olive mill effluent. *Separation and Purification Technology*, 173(6), pp.1–8.

Vidal, R.R.L. and Moraes, J.S., 2019. Removal of organic pollutants from wastewater using chitosan: a literature review. *International Journal of Environmental Science and Technology*, 16(3), pp.1741–1754.

Vijayaraghavan, K., Rangabhashiyam, S., Ashokkumar, T. and Arockiaraj, J., 2017. Assessment of samarium biosorption from aqueous solution by brown macroalga *Turbinaria conoides*. *Journal of the Taiwan Institute of Chemical Engineers*, 74(7), pp.113–120.

- Vinod, A., Sanjay, M.R., Suchart, S. and Jyotishkumar, P., 2020. Renewable and sustainable biobased materials: An assessment on biofibers, biofilms, biopolymers and biocomposites. *Journal of Cleaner Production*, 258(4), pp.124–131.
- Wan Ngah, W.S., Teong, L.C., Wong, C.S. and Hanafiah, M.A.K.M., 2012. Preparation and characterization of chitosan-zeolite composites. *Journal of Applied Polymer Science*, 125(3), pp.2417–2425.
- Wang, J. and Chen, C., 2014. Chitosan-based biosorbents: Modification and application for biosorption of heavy metals and radionuclides. *Bioresource Technology*, 160, pp.129–141.
- Wang, J., Zhou, Q., Song, D., Qi, B., Zhang, Y., Shao, Y. and Shao, Z., 2015. Chitosan–silica composite aerogels: preparation, characterization and Congo red adsorption. *Journal of Sol-Gel Science and Technology*, 76(3), pp.501–509.
- Wang, X., Zhu, C.S., Chen, C.Z., Zhang, H., Wang, D. and Ma, Y.Y., 2013. Recent developments in treatment of chromium-contaminated wastewater by starch-based adsorbents. *Advanced Materials Research*, 781–784, pp.2120–2123.
- Wang, Y., Wang, H., Peng, H., Wang, Z., Wu, J. and Liu, Z., 2018. Dye adsorption from aqueous solution by cellulose/chitosan composite: Equilibrium, kinetics, and thermodynamics. *Fibers and Polymers*, 19(2), pp.340–349.
- Wyasu, G., Gimba, C.E., Agbaji, E.B. and Ndukwe, G.I., 2016. Thermogravimetry(TGA) and DSC of thermal analysis techniques in production of active carbon from lignocellulosic materials. *Pelagia Research Library Advances in Applied Science Research*, 7(2), pp.109–115.
- Xie, J., Li, C., Chi, L. and Wu, D., 2013. Chitosan modified zeolite as a versatile adsorbent for the removal of different pollutants from water. *Fuel*, 103, pp.480–485.
- Yaashikaa, P.R., Kumar, P.S., Varjani, S. and Saravanan, A., 2020. A critical review on the biochar production techniques, characterization, stability and applications for circular bioeconomy. *Biotechnology Reports*, 28(4), pp.5-9.
- Yaseen, D.A. and Scholz, M., 2019. Textile dye wastewater characteristics and constituents of synthetic effluents: a critical review, 137 (3), pp.76–86.
- Younes, B., 2017. Classification, characterization, and the production processes of biopolymers used in the textiles industry. *Journal of the Textile Institute*, 108(5), pp.674–682.
- Zhang, J., Zhou, Q. and Ou, L., 2012. Kinetic, isotherm, and thermodynamic studies of the adsorption of methyl orange from aqueous solution by chitosan/alumina composite. *Journal of Chemical and Engineering Data*, 57(2), pp.412–419.

Zheng, C., Zheng, H., Wang, Y., Sun, Y., An, Y., Liu, H. and Liu, S., 2019. Modified magnetic chitosan microparticles as novel superior adsorbents with huge “force field” for capturing food dyes. *Journal of Hazardous Materials*, 367(8), pp.492–503.

Zhu, H.Y., Jiang, R., Xiao, L. and Li, W., 2010. A novel magnetically separable γ -Fe₂O₃/crosslinked chitosan adsorbent: Preparation, characterization and adsorption application for removal of hazardous azo dye. *Journal of Hazardous Materials*, 179(1–3), pp.251–257.